A phantom based evaluation on the effects of patient breathing motion on Stereotactic Body Radiotherapy treatment volumes

MSc (Med)

University of Cape Town/Medical Physics Department and Equra Health

Nicolene Coetzee

Supervisor: Hester Burger

Co-supervisor: Nanette Joubert

DECLARATION

I, Nicolene Coetzee, do solemnly declare that the entire body of work contained in this research assignment is my own, original work, that I am the sole author thereof (except where explicitly stated otherwise, and noted in acknowledgements), and that it has not previously in its entirety or in part been submitted elsewhere for the purposes of obtaining a qualification. Reproduction and publication of this research by the University of Cape Town will not infringe any third-party rights.

Signed by candidate

Nicolene Coetzee **December 2019**

GNTNIC002

ABSTRACT

Aim:

The aim of the study was to design an upper body phantom to mimic the movement of the lesion inside the lungs during a breathing cycle. Phantom design included an assessment of the motion observed for lung lesions, identification of suitable phantom materials as well as design of a motorized arm to mimic the movements observed inside the lung area of the phantom.

Introduction:

Expansion margins are added to clinical target volumes contoured by Oncologists in order to safeguard against under- or over-treatment of the target volume. They are designed to account for errors during setup, inaccuracies on the linear accelerator, and movement of targets inside the patient. If the margins are too small, there is a risk that the lesion/target may not receive the necessary dose, due to being partially missed. On the other hand, if the margins are too wide, the lesion will be covered, but normal tissue may receive unnecessary dose, resulting in additional side effects to the patient. Assessment of the impact of these margins is not possible in a static phantom and the availability of a low-cost motorized phantom would assist in the validation of these margins.

Method:

Previously treated patients' 4D CT scanning data were used to quantify the amount of movement seen for lesions within the lung. A phantom was then designed and built in an attempt to mimic both patient anatomy and movement. Materials were identified to replicate anatomical shape and densities of various organs in the thorax, as seen on CT scan data. Two treatment planning systems (Monaco, (Elekta) and Eclipse (Varian)) were used to determine the dosimetric characteristics of the materials. This was compared to actual dose as delivered by a linear accelerator (Elekta Synergy).

Results:

Paths were calculated from the breathing cycles during the 4D-CT scan sets and templates designed to mimic these movements. A thorax phantom was built with the appropriate materials suitable and matched densities to replicate a human thorax. Comparing transmission for these materials on a linear accelerator for 6MV and 10MV energy, the deviation from planned versus measured dose varied between 1.67% to 3.32% and 0.45% to 2.30%, respectively for the silicon material and between 0.77% to 3.22% and 0.17% to 2.57% for the 3D printed bone for 6MV and 10MV.

Conclusion:

The measurements done on the linear accelerator matched closely with the calculated values on the treatment planning system for transmission through the materials in the customised phantom.

Various proposals were put forward to mimic the movement of the targets within the lung regions. However, it was not possible to manufacture a mechanically based working model due to the small movements observed (<5mm). It is recommended that a robotic solution be investigated as alternative to mimic these small movements.

Table of Contents

ACKNOWLEDGEMENTS

I would like to thank my supervisor Hester Burger, and co-supervisor Nanette Joubert for their guidance and support.

My special thanks goes to the following people for their valuable contributions, and assistance on this project:

Annemari Groenewald – Equra Health, now UCT/GSH;

David Bullock – 3D printing;

Homecor Cupboards;

Melina Loubser – iThemba Labs;

Robin Hiscock – Medical Physics Mechanical Workshop, Groote Schuur Hospital;

Roopam + Habtamu - Department of Biomedical Engineering, University of Cape Town;

Schnetler&Corbett – Radiology, Panorama Medi-Clinic;

Susan Tovey – Medical Physics Mouldroom, Groote Schuur Hospital.

LIST OF FIGURES

LIST OF TABLES

GLOSSARY

3D-CRT	3-Dimensional Conformal Radiotherapy
4D CT	4-Dimensional Computed Tomography
AAA	Anisotropic Analytical Algorithm
AM	Additive Manufacturing
ASTRO	American Society for Radiology Oncology
BED	Biologically Effective Dose
CBCT	Cone Beam Computed Tomography
CNC	Computer Numerical Control
CT	Computed Tomography
CTV	Clinical Target Volume
DIBH	Deep inspiration breath-hold
DVH	Dose-Volume Histogram
ED	Electron Density
EPI	Electronic Portal Imaging
EUD	Equivalent Uniform Dose
GBBS	Grid Based Boltzmann Solver
gEUD	Generalised Equivalent Uniform Dose
HREC	Human Research Ethics Committee
HU	Hounsfield Unit
GTV	Gross Tumour Volume
IM	Internal Margin
ITV	Internal Target Volume
LBTE	Linear Boltzmann Transport Equation
LPD	Liquid Plastic Deposition
LQ	Linear Quadratic
MC	Monte Carlo
MDF	Medium Density Fibreboard
MIP	Maximum-intensity Projection
MV	Mega Voltage
NTCP	Normal Tissue Complication Probability
NTD	Normalised Total Dose

NSCL	Non-Small Cell Lung
OAR	Organ at Risk
PC	Polycarbonate
PTV	Planning Target Volume
RPM	Real-time Positioning Management System
RTOG	Radiation Therapy Oncology Group
SABR	Stereotactic Ablative Body radiotherapy
SBRT	Stereotactic Body Radiotherapy
SFF	Free Form Fabrication
SLS	Selective Laser Sintering
SM	Set-up margin
SVC	Slow Vital Capacity
TPS	Treatment Planning System
TV	Target Volumes

1 INTRODUCTION

Today lung cancer is still a deadly disease, but the survival rate of patients is increasing. The overall quality of life can also be improved. Although surgery for lung cancer patients is an option, the complications and risks involved in surgery are factors that still need to be considered. Other non-invasive procedures then become far more attractive, for example radiotherapy and, more specifically, modern specialised techniques such as Stereotactic Body Radiotherapy (SBRT).

The treatment of lung cancer with radiotherapy has always been a controversial topic due to highly inhomogeneous densities that need to be considered when calculating dose in these areas. Extreme caution should be taken to select the correct dose algorithms used in a Treatment Planning System (TPS). Another concern is movement during breathing, or the respiratory cycle of a patient. Depending on the location and size of the lesion in the lung, the motion can differ quite significantly. To accurately treat only this lesion and minimise dose exposure to the surrounding lung and organs at risk (OAR), it becomes difficult and complex to perform this type of treatment successfully.

Margins are to safeguard against under- or over-treatment of the target volume that the oncologist has drawn in. They are designed to account for errors during setup, inaccuracies on the linear accelerator, and movement of targets inside the patient. If the margins are too small, there is a risk that the lesion/target may not receive the necessary dose, due to being partially missed. On the other hand, if the margins are too wide, the lesion will be covered, but normal tissue may receive unnecessary dose, resulting in additional side effects for the patient.

Previously treated patients' 4D scanning data will be used to quantify the amount of movement seen for the lesions within the lung. This will be done by evaluating and quantifying the movement of the targets as drawn in for the different 4D-CT scan sets.

The impact of these increased or decreased margins can be evaluated on the treatment planning system to determine the radiobiological impact of the margin choices. It will therefore be possible to determine whether the margins used in clinical practices are optimal or

individualised, or patient specific margins can be used as recommended. This can be dedicated to a future project from this study.

Due to these main risk factors for lung SBRT, the aim of the study is to design an upper body phantom to mimic the movement of the lesion inside the lungs during a breathing cycle. This phantom can then be used to test the impact of different radiotherapy treatment margins used in clinical practice by irradiating the targets on the linear accelerator, while the phantom and target mimic the Clinical Target Volume (CTV) or lesion motion.

The aim of this study is to:

- Determine the movement seen in previously treated patients from the 4D CT scan sets and used during SBRT treatment;
- Design a thorax phantom to mimic tissue characteristics and internal motion of the CTV;
- Compare the customised built phantom in terms of tissue characteristics applicable from the Treatment Planning System (TPS) and on the linear accelerator.

Due to the retrospective patient data that will be used on the phantom, the following is in place for ethical consideration:

- Consent forms from treatment site to use patient data and equipment;
- Ethical application;
- Patient consent form template.

This study is a medical review study and will not influence clinical decision making or treatment in any way.

Figure 1.1 is a flowchart which outlines the workflow of this study and the design and build of the customised phantom to mimic tumour motion in the lung.

Figure 1.1: Flowchart of study

2 Literature Review

2.1 Current status

Today, early detection of cancer, new effective treatment options and improved clinical follow-up after treatment have resulted in the number of cancer survivors increasing world-wide. Even where cancer is not cured, nowadays after diagnosis patients survive for longer periods than before (American Cancer Society Infographics, 2013). However, the outcome of radiotherapy is still lesion and site dependent.

Historically, inoperable stage 1 lung cancer has been a diagnosis with limited treatment options (R. D. Timmerman, 2009). Patients with stage 1 lung cancer are often medically unfit to undergo anaesthetics and as a result surgical removal of their tumours may not be possible. Even if they are fit to undergo the surgery, the post recovery period is a risk to these patients due to general frailty and other comorbidities (Buyyounouski et al., 2010). Traditional radiotherapy approaches based on either 3D conformal techniques or observation without specific cancer therapy (watch and wait approach), resulted in poor tumour control and survival rates. Primary tumour control for medically inoperable patients with early stage lung cancer is 30% to 40%. A high mortality rate (20% to 35% survival rate) is seen with the traditional management of this group of patients (R. Timmerman, 2010). The availability of SBRT can change the prognosis of this group of patients.

Stereotactic Body Radiotherapy is a technique where highly focused radiation fields are aimed with very high precision at small target areas in the body of a patient. 'Precision' refers to agreement between repeated independent measurement results under specific conditions that include, but are not limited to, dosimetric and geometric accuracy. The term 'accuracy' describes the closeness of agreement between a result and the true value. The accuracy is accomplished by combining imaging, simulation, treatment planning and delivery thereof into all phases of the treatment process (Benedict et al., 2010). This form of radiotherapy treatment requires a high level of confidence in terms of the accuracy of the overall treatment delivery process (Benedict et al., 2010).

Internationally, SBRT is now considered a well-established treatment option for inoperable early stage lung cancer with two-year local control rates ranging from 80% to 97% (Modh, 2014). Due to the small fields used during treatment, combined with high geometric precision

during treatment delivery, dose escalation is possible without compromising normal tissue. Although these tumours are typically close to organs at risk (OAR), the rapid dose fall-off inherent in this technique minimises doses to these structures. This is achieved by dose prescriptions in SBRT that are specified at lower isodoses (e.g. 80% or 90% isodose) and with no or small margins for beam penumbra at the target edge. This increases dose heterogeneity within the target compared to conventional therapy. It has been hypothesised that the radio resistant hypoxic cells are located in the central part of the tumour and dose heterogeneity hot spots within the target may be acceptable and possibly even an advantage (Benedict et al., 2010).

Literature (D. R. Timmerman, 2014) indicates an increase in five-year survival outcomes from ten percent (10%) to thirty percent (30%) reported for 3D Conformal Radiotherapy (3D-CRT) (DE, 1992; Sibley, 1998), to 40% five year survival for patients receiving SBRT (R. Timmerman, 2014). This is according to an update of RTOG 0236 published in 2010, where previously the original document of RTOG 0236 indicated only a three-year survival (R. D. Timmerman, 2009). This technique can also be used for patients refusing surgery as well as for metastatic disease, e.g. spine, brain, liver and prostate (Benedict et al., 2010; Buyyounouski et al., 2010).

The technique is technically difficult to implement, however, and various aspects need to be investigated and validated to allow for safe clinical use in the local context. This study focuses on SRS techniques applicable to early stage lung cancer and metastatic lung cancer patients only.

2.2 Classification of target volumes

2.2.1 Volumes and margins

Treatment delivery is dependent on volume and dose and these parameters need to be specified for different purposes such as prescription, recording and reporting. Universally accepted terminology is important to ensure a common language when reporting results from different centres. It is important, therefore, to define the volumes to be treated to the prescribed dose in a clear and concise way, irrespective of the treatment technique used. This leads to concepts such as Gross Tumour Volume (GTV), Clinical Target Volume (CTV) and Planning Target Volume (PTV) (Berthelsen, 2007).

First, to accurately define these different volumes for the purpose of dose escalation, a close relationship is needed between position of volumes and organs in the patient, and position and orientation of beams used during imaging and treatment. This can be achieved by means of three coordinate systems, namely one within the patient, one related to the imaging unit and one related to the treatment unit. To link these three coordinate systems, anatomical reference points or alignment marks are used to relate to the position of the volumes or tissue in the patient. These are then again linked to the coordinate systems of the imaging and treatment machines since the reference points or alignment marks can be defined in both patient and machine coordinates (ICRU 62).

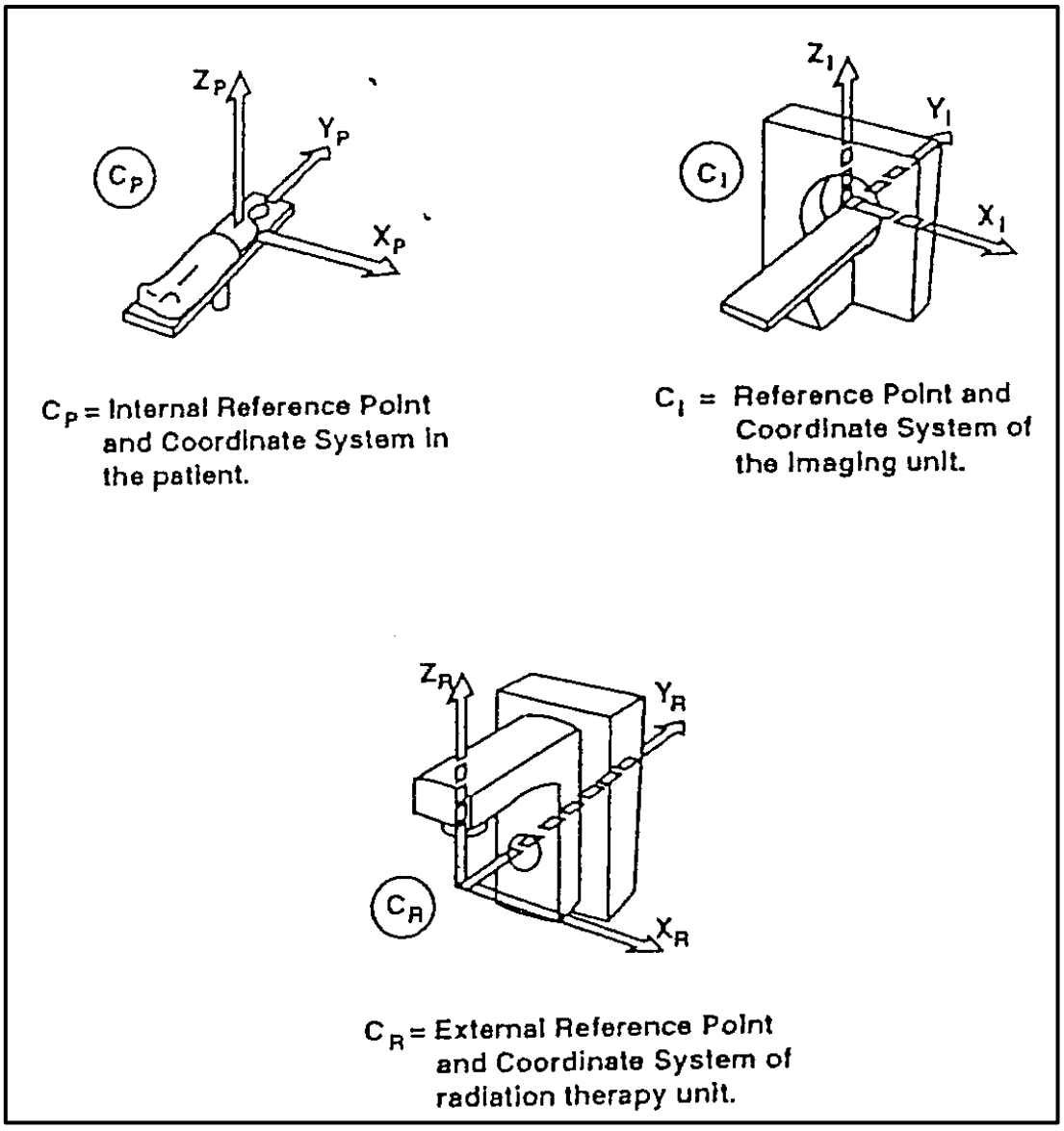

Figure 2.1: A suggested set of coordinate systems

A suggested set of coordinate systems
C_p – related to patient – internal reference point

C_I – related to imaging unit – CT Scanner information
C_R – related to radiation therapy unit – external reference point.
("International Commission on Radiation Units and Measurements. Prescribing, recording, and reporting photon beam therapy (supplement to ICRU report 50). ICRU report 62. Bethesda, MD," 1999)

The reference points can be either internal or external and form the basis to establish the patient coordinate system as well as assist with reproducible alignment of the patient for imaging and treatment. Anatomical landmarks such as bony anatomy may be used for localisation of the GTV or CTV and accurate set-up at the imaging and treatment unit. These landmarks are referred to as internal reference points. External reference points are palpable or visible points on the surface of either the patient or the immobilisation device in use that fits closely to the external body of the patient. The coordinate system for the patient is based on these internal and external reference points for orientation of the system and alignment of the patient (ICRU 62).

Coordinate systems related to imaging and treatment units are defined with respect to the gantry, collimators, radiation and light beams, laser alignment beams and couch-top system (ICRU 62).

The GTV or Gross Tumour Volume is the gross palpable visible/demonstrable extent and location of the malignant growth. ("International Commission on Radiation Units and Measurements. Prescribing, recording, and reporting photon beam therapy (supplement to ICRU report 50). ICRU report 62. Bethesda, MD," 1999)

The tissue volume that contains a GTV and/or demonstrable tumour and/or areas of suspected subclinical microscopic malignant disease is defined as the Clinical Target Volume (CTV). ("International Commission on Radiation Units and Measurements. Prescribing, recording, and reporting photon beam therapy (supplement to ICRU report 50). ICRU report 62. Bethesda, MD," 1999) CTV is referred to as the volume that should receive the prescribed dose and be treated adequately to achieve cure or palliation; the aim of therapy.

Unfortunately, the CTV may not be exactly in the same position on a day by day basis as a result of geometric uncertainties. These geometric uncertainties may come from three sources (ICRU 62):

1. Patient set-up variation;
2. Organ motion and deformation; and
3. Machine related errors.

In 3D Conformal Radiotherapy Treatment (3D-CRT) the CTV should be expanded with a 3D margin to create the Planning Target Volume (PTV) to compensate for the geometric uncertainties defined above. The planned dose to the PTV will then be representative of the real dose to the CTV and the heterogeneity in dose delivery should be kept within 95% to 107% for 3D-CRT (Stroom & Heijmen, 2002).

2.2.2 Motion in lung lesions

SBRT is now emerging as a state-of-the-art treatment for lung cancer patients and may even challenge instances where operable surgery is an option (Baumann et al., 2009). Due to the high doses delivered to the target, the margins associated with these treatments are crucial (R. W. Underberg et al., 2004). Higher radiation dose is associated with better failure-free and overall survival. However healthy lung tissue, the heart and oesophagus are dose-limiting organs. Increasing the dose without reducing the irradiated volume results in an increase of the mean lung dose which leads to higher probability of radiation pneumonitis. This also brings forth an increase in dose to OARs (Marks et al., 2010). To enable safe dose escalation, tumour volumes (TV) and the associated irradiated volumes of normal tissue should be minimised (Caldwell, 2003; Wolthaus et al., 2008)

To compensate for expected physiological movements and changes in shape, size and position of the CTV during treatment, a margin must be added. This is referred to as the Internal Margin (IM). The IM is intended to compensate for all movements and variations in position, size and shape of organs and surrounding tissue adjacent to the CTV. This is an asymmetrical expansion of the CTV, therefore should be expanded with a 3D margin. These internal variations can be due to respiration, bladder filling, rectal filling, heartbeat, bowel movements, to name but a few. They either cannot be controlled or have limited control (in terms of, for example 'bladder fill protocols') and do not depend on external uncertainty in beam geometry but could be influenced by variation in day-to-day patient setup (ICRU 62). This volume, after expansion with the 3D margin, IM, is defined as the Internal Target Volume (ITV), which is considered as the intermediate volume (Stroom & Heijmen, 2002). The main contributors to this margin in thoracic tumours are respiratory and cardiovascular motions. The degree and direction of

movements are dependent on the location of the tumour in the lung and can be visualised where 4DCT are available. Tumours closer to the diaphragm and heart will have bigger movement than those fixated to a structure or OAR (Caldwell, 2003).

Variations or uncertainties in the reproducibility of patient positioning and inaccuracies in alignment of beam positioning during planning and throughout treatment are accounted for with a set-up margin (SM) (Berthelsen, 2007). Uncertainties may vary on different anatomical directions and the margins then depend on selection of beam geometries. Factors such as variations in patient positioning, lack of reproducibility of equipment (for example sagging of gantry, etc.) and human factors can influence these inaccuracies. These may even vary from machine to machine (Berthelsen, 2007). With the use of a 2D set-up margin (SM) it can become quite complicated to incorporate this margin with awkward gantry and/or couch angles. Instead the ITV is expanded with a 3D SM to arrive at the PTV then to be used for plan design (Stroom & Heijmen, 2002).

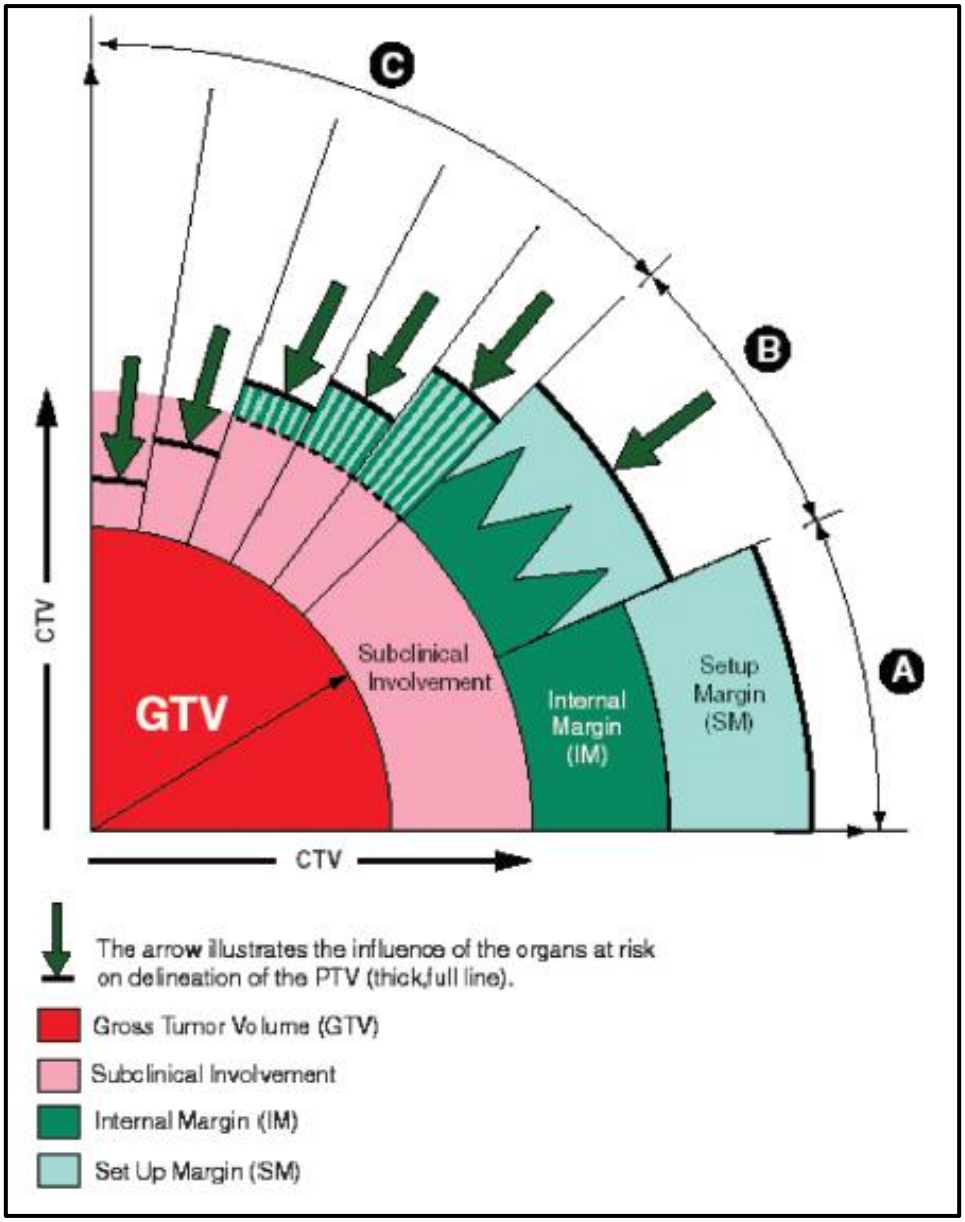

Figure 2.2: Description of margins
(Berthelsen, 2007)

Figure 2.2 depicts three different clinical scenarios. In scenario A a margin is added to take into account potential subclinical invasion around the GTV. This margin and the GTV is defined as the CTV. In External Beam Radiation Therapy (EBRT) all uncertainties and geometrical variations need to be considered to ensure that the CTV receives the prescribed dose. This is done with appropriate/additional margins. As previously discussed for variations in position and/or shape and size of the CTV, an IM is added which creates the ITV. The SM accounts for variations and/or uncertainties in patient-beam positioning. Therefore CTV+IM+SM = PTV on which beam size and arrangement are based (Berthelsen, 2007).

This linear addition of margins can lead to an excessively large PTV that will include OAR and normal tissue and is not compatible with tolerance doses as depicted in Scenario A (Berthelsen, 2007). When calculating the SM to determine an appropriate PTV, all deviations from the planned irradiation geometry during a treatment session should be taken into account. These can be due to random or systematic errors. Random errors are defined as fraction-to-fraction variations around the mean deviation in the measurement/treatment, whereas systematic errors occur when the mean irradiation geometry in the fractionated treatment differs/deviates from the geometry in the treatment plan (Stroom & Heijmen, 2002).

All these errors cannot be added linearly as this will lead to an excessively large PTV and would be incompatible with the tolerances of surrounding tissues, as mentioned above. Therefore, an alternative is to use the root-sum-of-squares of the set-up error and the organ motion:

$$\sigma_{tot} = \sqrt{(\sigma_{int}^2 + \sigma_{ext}^2)}$$ (Stroom & Heijmen, 2002).

Two separate coordinate systems and reference points are used in clinical practice and that was the argument to introduce ITV and SM. Both internal movement and set-up variation are measured with respect to bony anatomy. The effect of organ motion and set-up error (similar size and direction) is basically equal on the dose in the CTV. It is therefore assumed that the internal and external uncertainties are uncorrelated. These uncertainties are characterized by the overall distribution of systematic errors (set-up) $\sum_{tot} = \sqrt{(\sum_{int}^2 + \sum_{ext}^2)}$, and random errors (internal movement) $\sigma_{tot} = \sqrt{(\sigma_{int}^2 + \sigma_{ext}^2)}$. Any combination of $\sum_{int}$ and $\sum_{ext}$ are equivalent with respect to the planning margin. The important parameters for calculating margins are $\sum_{tot}$ and σ_{tot}, which reduces the need for separation of ITV and SM in this scenario. This leads to a standard deviation, $SD_{tot} = \sqrt{(\sum^2 + \sigma^2)}$, which then should be used for margin calculation. (Stroom & Heijmen, 2002)

This adaption leads to scenario B in the figure above (Berthelsen, 2007).

In the majority of cases, a ‘global’ safety margin is accepted, but in some cases the close proximity of an OAR reduces the width of this safety margin. This is shown in scenario C. Also, to keep in mind is that the subclinical invasion may decrease with distance from the GTV, which could depict a reduction in margin and still be compatible with chances for cure. Safety

margins vary with the angle at which one looks at the PTV. If an adequate dose cannot be given to the whole GTV, the treatment aim shifts from radical to palliative (Berthelsen, 2007).

These margins (IM+SM) are the defining margins to account for the combined effect of errors during setup and inaccuracies on the linear accelerator, as well as movement of targets inside the patient, as described above (IRCU 62). The impact of the target movement as well as the inaccuracies in treatment delivery need to be defined for the specific patient and the specific clinic where the radiation is being delivered to accurately calculate the required margins.

Depending on the clinical situation, patient condition and site of CTV and the chosen treatment technique, as shown below in Figure 2.3, the PTV could be very similar to the CTV (small skin lesions) or much larger (lung tumours).

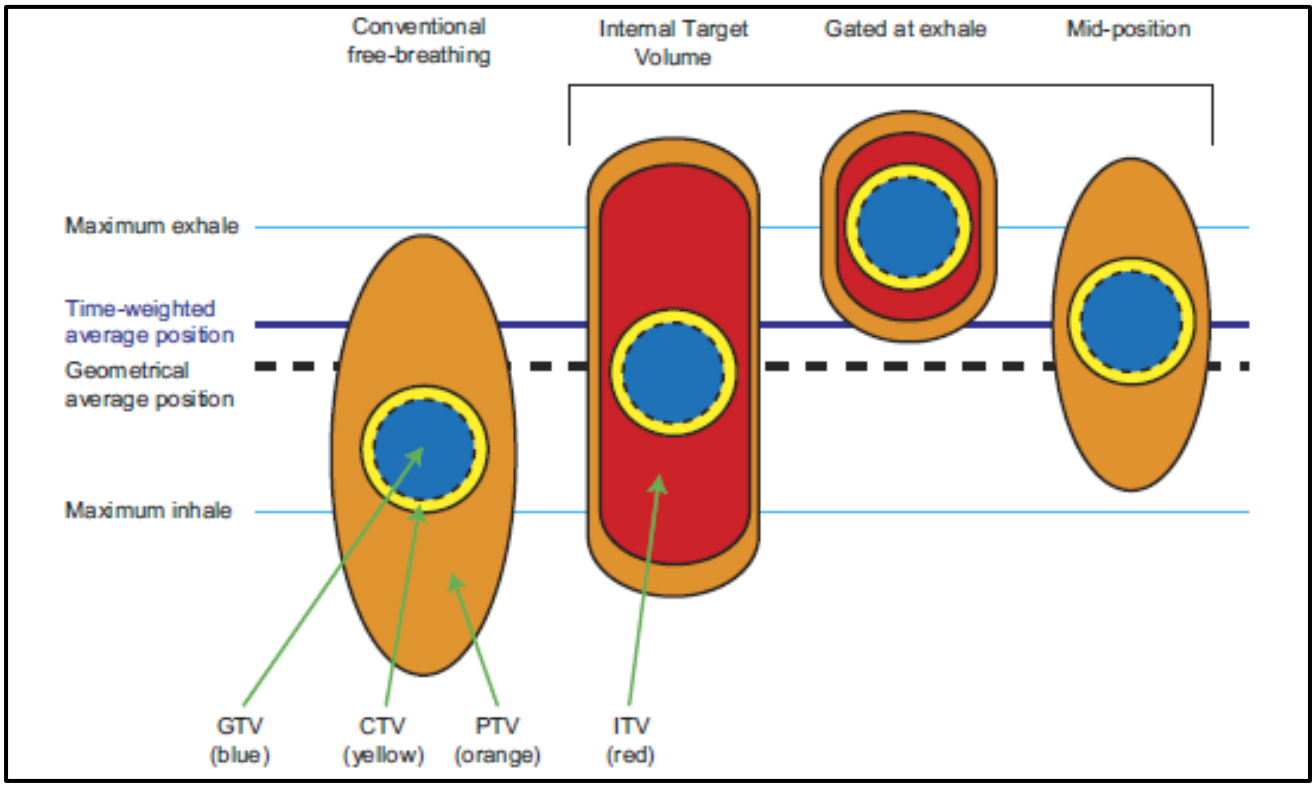

Figure 2.3: Diagram of different treatment-planning concepts

(Wolthaus et al., 2008)

Conventional free-breathing; internal target volume (ITV); gating at exhale and mid-position. Gross Tumor Volume – GTV; Clinical Target Volume (CTV); Planning Target Volume (PTV).

Static CT is only a ‘snapshot’ of the mobile CTV which can be some distance away from the mean position of the moving tumour. The symmetric ‘population based’ margins used historically may introduce systematic errors or even geographic miss of the tumour in the plan (Caldwell, 2003). Individualised margins are now proposed as more appropriate for lung tumours as opposed to the historic standard ‘population based’ margins (R. W. Underberg et al., 2004).

As mentioned before, stereotactic radiotherapy relies heavily on tight margins and steep dose gradients to reduce dose impact on organs at risk. Although the definitions of volumes as mentioned in above discussions are still applicable to stereotactic radiotherapy, the methods used to generate the various volumes in stereotactic radiosurgery can differ from those applied to 3D conventional radiotherapy. For example, the calculation of the set-up margin for PTV in a single fraction treatment with steep dose gradient may not be relevant to the common formalism used (IRCU 62).
In lung tumours located in the lower lung, IM due to respiratory motion can overshadow the required SM.

- When the patient breathes freely during the entire process of treatment, tumour motion needs to be quantified for treatment planning. Contouring on co-registered prospectively binned inspiratory and expiratory 3D CT or on a maximum-intensity projection (MIP) CT scan (from a retrospectively binned 4D CT dataset) can be used to determine the ITV for tumours associated with respiratory motion.
- With breath hold or respiratory gating, the IM will need to account for uncertainties in reproducing the breath hold and residual motion.
- During direct tumour chasing or tumour tracking the IM will need to account for variations in the correlation of internal and external markers or fiducials or movement of the tumour in relation to the implanted fiducials.
- Deformation and rotation of the tumour are included in the IM, but these components can be very small.

It should always be remembered that IM and SM are tools to ensure coverage of the CTV. (IRCU 62).

As radiotherapy treatment machine technology improves in terms of mechanics and quality assurance, target contouring or delineation of volumes account for a larger part of the treatment

uncertainties. Identifying normal tissue as tumour and vice versa can lead to significant impact on radiobiological doses to the patient with regard to either under dosing of the tumour when the tumour is contoured as normal tissue and overdosing of normal tissue if normal tissue was identified as tumour. Adding margins to compensate for these possible variations in target contouring is not the solution. Establishing appropriate target volumes must be evaluated on a technique-specific basis taking into account the radiobiological response of both the specific tumour as well as the critical structures in the immediate vicinity (IRCU 62).

2.2.3 Acquisition of target volumes

In most RT treatment planning departments CT scans are acquired during quiet respiration. The assumption is made that during daily treatments, the position of the target will correspond to these CT scans. However, the short sampling times of modern CT scanners relative to the breathing cycle may result in an inaccurate 3D target volume generated for treatment planning purposes. This happens if the breathing cycle captured during the CT scanning acquisition does not correspond to the breathing cycle during treatment (Lagerwaard et al., 2001).

Approaches available to determine more accurate target volumes and individualised margins are 'slow' CT scans (Lagerwaard et al., 2001), deep inspiration and breath-hold CT scans (Hanley et al., 1999) or 4D or respiration-correlated CT scans (R. W. Underberg et al., 2004).

These technologies/approaches will be discussed in more detail in Section 2.4.

2.3 Radiobiological dose response modelling

Achieving local tumour control is directly related to the radiation dose that can be delivered to the cancer cells, but is limited by the dose that can be tolerated by the surrounding normal tissue and critical structures or OARs close to the tumour. For some structures such as lungs, the dose that can be tolerated depends on the volume of normal tissue (lung) that is included in the treatment field. With advanced 3D conformal techniques, careful target definition and delivery allows dose escalation due to the fact that the volume of normal tissue included in the field can be decreased through careful planning (Barnes et al., 2001). Radiobiological models allow quantification of the risk of developing side effects based on the doses associated with a specific plan. For example, development of grade 2 or higher pneumonitis has been shown to be dependent on the percentage of total lung receiving 20Gy in 3D conformal therapy (V20).

A tight margin is therefore desirable to reduce the dose to surrounding tissue but must not result in under dosing the tumour via geographic miss (Barnes et al., 2001). Radiobiological modelling or dose-response modelling, therefore, can be used to determine appropriate margins as discussed above (Stroom & Heijmen, 2002).

Dose-response modelling is a way to estimate risk to critical anatomical structures as a function of:

1. Dose;
2. Fractionation;
3. Volume;
4. Endpoint
5. Follow-up time
6. Estimated risk of the endpoint occurring within the follow-up time. (Asbell, Grimm, Xue, Chew, & LaCouture, 2016).

In 3D conformal radiotherapy these dose tolerance limits evolved from Emami (Emami, 1991) to Quantitative Analyses of Normal Tissue Effects in the Clinic (QUANTEC) which is currently considered the most accurate method to assess normal tissue complication probability (NTCP) for conventional fractionation (Marks et al., 2010). In terms of Stereotactic Ablative Body radiotherapy (SABR) or Stereotactic Body Radiotherapy (SBRT) dose-tolerance guidelines are extremely rare and published data sparsely available (Asbell et al., 2016).

Three studies of SBRT patients with early stage lung cancer who received Biological Effective Doses (BED) of $100Gy_{10}$ or more, where Gy_x denotes $x=\alpha/\beta$ in the linear quadratic model reported five-year survival rates ranging from 30% to 83%. This demonstrates that significant local control and survival advantage can be achieved when a BED of $100Gy_{10}$ or more is delivered (Srivastava, 2013).

The Biological Effective Dose (BED) is a characteristic dose value that facilitates comparisons between the effects of different dose-fractionation schemes. The definition of BED is expressed as the total dose delivered in an infinite number of infinitesimal small dose fractions that has the same biologic effect as the dose-fractionation scheme in question. Completed repair of sublethal damage between fractions is assumed (Park, Papiez, Zhang, Story, & Timmerman, 2008).

Conversion of dose to BEDs has its own challenges as there are so many methods to convert these doses (Asbell et al., 2016).

One method of calculating BED makes use of the Linear Quadratic theory. In this case the numerical value of BED is expressed in terms of the α and β values of the Linear Quadratic (LQ) model:

Natural log of S (surviving proportion)

$$\ln S = -\alpha * d - \beta * d^2 \quad \text{(LQ equation)}$$

where d is the dose and α and β are expansion parameters; α is the slope of the survival curve at the limit $d \rightarrow 0$, and β is the parameter determining the relative contribution from the quadratic component. (Park et al., 2008)

$$BED = D*(1 + {}^{d}/_{\alpha/\beta})$$

where D is the total dose delivered in n fractions of size d (Park et al., 2008).

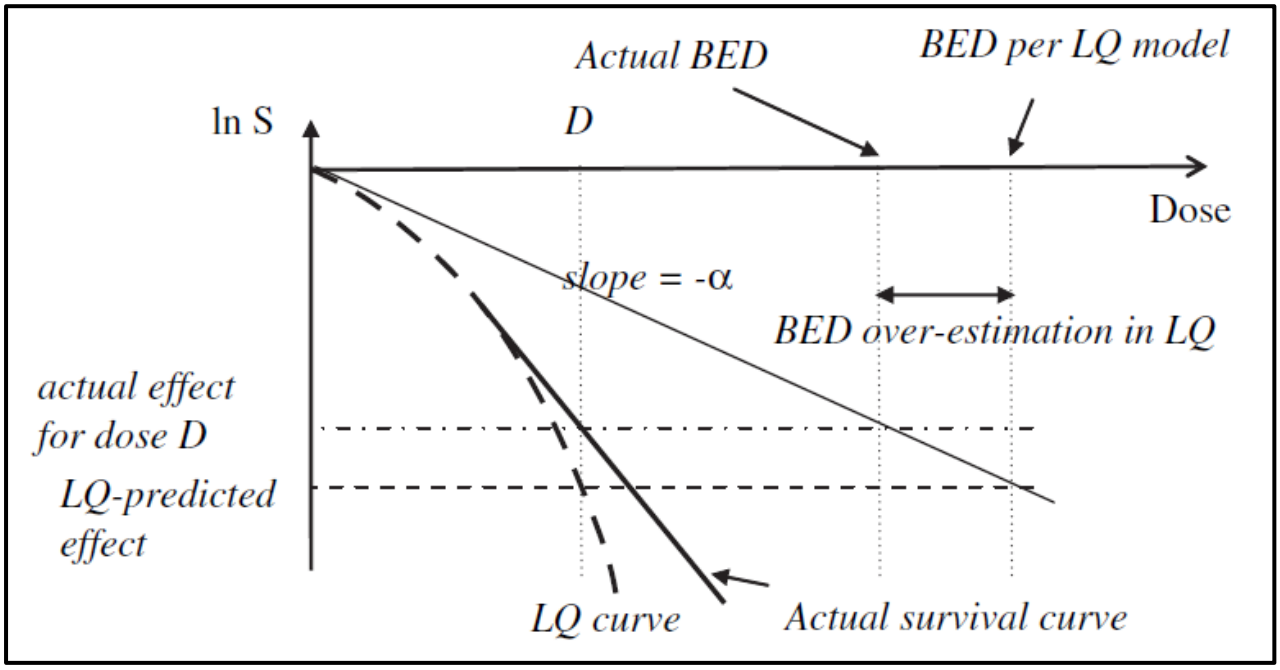

Figure 2.4: Actual Biological Effective Dose (BED) is over-estimated when expressed through the linear quadratic (LG) model parameters
(Park et al., 2008)

Actual BED is over-estimated when expressed through the LQ model parameters.

This formulation of the LQ model is applicable to dose ranges below the commonly used ablative doses in SBRT. This model predicts a continuous downward bending curve in the high-dose region as depicted in Figure 2.4. An overestimation of radiation is therefore predicted in this LQ model in the high-dose range (Park et al., 2008).

An alternative description of clonogenic survival as a function of radiation dose is based on the multitarget model. This model is valuable in the high-dose range as shown in Figure 2.5. A universal survival curve model was constructed from the LQ model survival curve for the low-dose range and the multitarget model asymptote for high-dose range (Park et al., 2008).

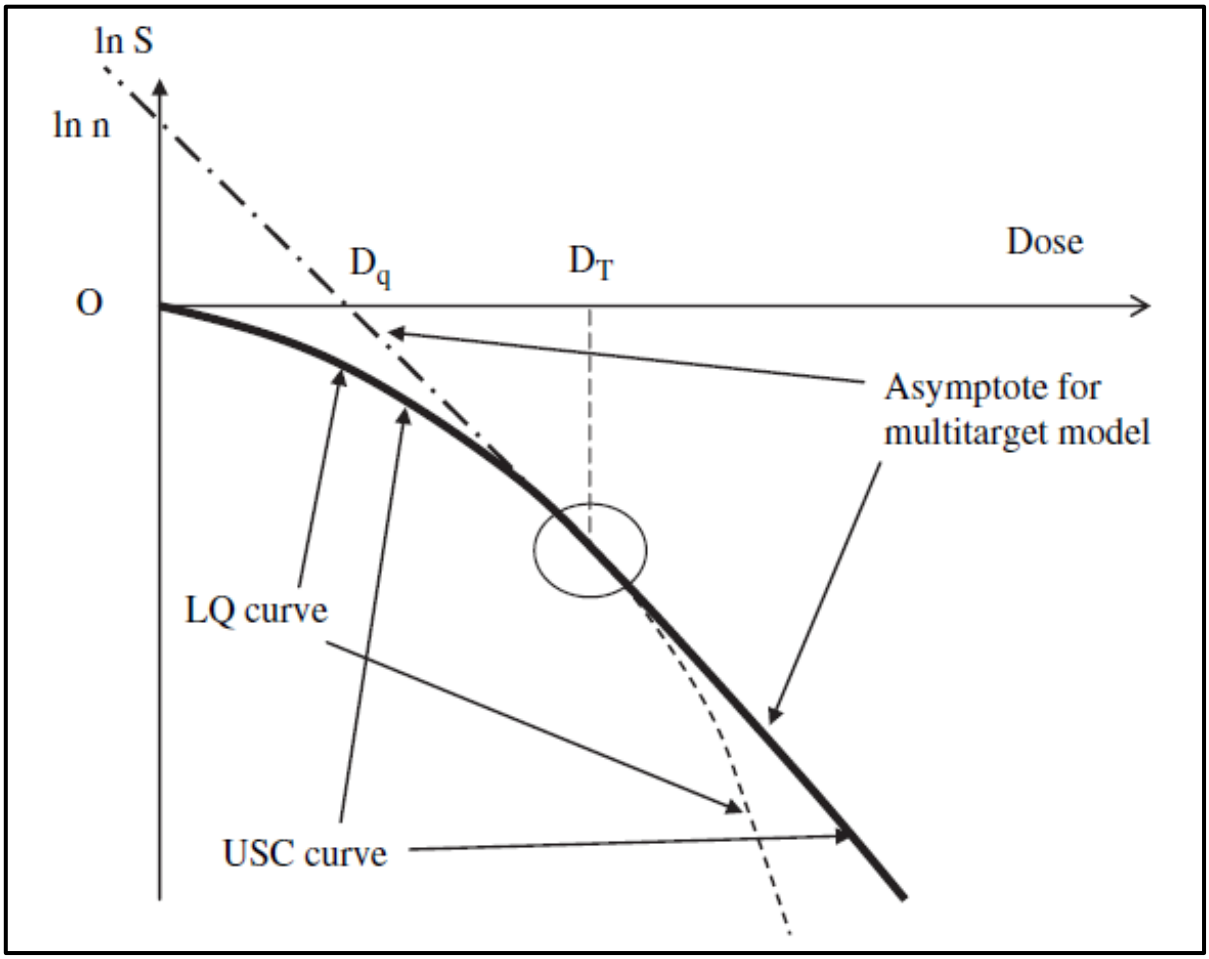

Figure 2.5: The dose range at which the LQ and multitarget model is valid on the Universal Survival Curve (USC)
(Park et al., 2008)

The dose range at which the LQ and multitarget model is valid on the USC. Below transition dose D_T, USC is identical to LQ and above D_T, USC is identical with terminal linear portion of multitarget model.

With conventional dose tolerance limits, Emami's method organised the same percentage volumes (⅓, ⅔,3/3) for most critical structures throughout the body for these limits and partitioned/divided it into two risk levels (5% and 50%). Emami's dose tolerance limit table therefore consisted of six values for each critical structure, three values for low risk (5%) and three values for high risk (50%) doses by volume. See part of Table 2.1 below (Emami, 1991).

Organ	TD 5/5 Volume			TD 50/5 Volume			Selected endpoint
	1/3	2/3	3/3	1/3	2/3	3/3	
Kidney I	5000	3000*	2300		4000*	2800	Clinical nephritis
Kidney II							
Bladder	N/A	8000	6500	N/A	8500	8000	Symptomatic bladder contracture and volume loss
Bone:							
Femoral Head I and II	—	—	5200	—	—	6500	Necrosis
T-M joint mandible	6500	6000	6000	7700	7200	7200	Marked limitation of joint function
Rib cage	5000	—	—	6500	—	—	Pathologic fracture
Skin	10 cm² / —	30 cm² / —	100 cm² / 5000	10 cm² / —	30 cm² / —	100 cm² / 6500	Telangiectasia
	7000	6000	5500	—	—	7000	Necrosis Ulceration
Brain	6000	5000	4500	7500	6500	6000	Necrosis Infarction
Brain stem	6000	5300	5000	—	—	6500	Necrosis Infarction
Optic nerve I & II	No partial volume		5000	—	—	6500	Blindness
Chiasma	No partial volume		5000	No partial volume		6500	Blindness
Spinal cord	3 cm / 5000	10 cm / 5000	20 cm / 4700	3 cm / 7000	10 cm / 7000	20 cm / —	Myelitis necrosis
Cauda equina	No volume effect		6000	No volume effect		7500	Clinically apparent nerve damage
Brachial plexus	6200	6100	6000	7700	7600	7500	Clinically apparent nerve damage

Table 2.1: Normal tissue tolerance to therapeutic irradiation
(Emami, 1991)

For SBRT a similar unified format was needed. Because of the strong dependency on fractionation and the fact that the volumes are vastly different from those seen in conventional fractionation for SBRT, five rows were needed according to number of fractions (fraction 1-5). However, the true statistical risk is still unknown for most published SBRT dose tolerance limit (Srivastava, 2013).

An additional parameter that needs to be included from the most common published SBRT dose tolerance limits is the maximum point dose (i.e. zero volume). For the ablative doses of SBRT only small volumes are tolerable to these doses (Srivastava, 2013). Grimm et al. (2011) performed an extensive review of literature to compare dose limits utilised and reported in existing publications. This was an initial step closer to the goal of having a comprehensive set of SBRT normal organ dose tolerance limits. From this extensive review a similar unified format could be established (Srivastava, 2013).

	Low Risk Limits					High Risk Limits				
	50% Vol Limit (Gy)	10% Vol Limit (Gy)	10.0cc Limit (Gy)	1.0cc Limit (Gy)	Max Limit (Gy)	50% Vol Limit (Gy)	10% Vol Limit (Gy)	10.0cc Limit (Gy)	1.0cc Limit (Gy)	Max Limit (Gy)
1fx:	4.0	5.0	23.0	28.0	36.0	6.0	15.0	31.0	32.2	37.0
2fx:	7.0	10.0	27.0	32.0	40.0	12.0	22.0	35.0	36.2	41.0
3fx:	10.0	15.0	31.0	36.0	44.0	18.0	29.0	39.0	40.2	45.0
4fx:	13.0	19.0	35.0	40.0	49.0	22.0	35.0	43.0	44.2	50.0
5fx:	15.0	22.0	39.0	43.9	51.5	25.0	40.0	47.0	48.1	52.5

Table 2.2: Low and High Risk Limits for aortic toxicity
(Srivastava, 2013)

As described in the paragraph and shown in Table 2.2, the unified dose tolerance format for SBRT consists of five rows, one for each fractionation (1-5); two risk groups (columns) namely one for low-risk and one for high-risk; and then five columns within each of these risk groups, for each of the five dose-descriptor points or volume vs dose limits. These include 50% volume, 10% volume, the two most common cubic centimetre (cc) absolute volumes (Grimm, 2011), of which the one is 1cc and the maximum point dose (Srivastava, 2013).

A well-defined dose-tolerance limit (human dose tolerance to radiation) must specify at least the following:

1. Dose;
2. Fractionation;
3. Volume;
4. Endpoint;
5. Follow-up time;
6. Estimated risk of the endpoint occurring within the follow-up time.
   (Asbell et al., 2016).

To keep this relationship between dose tolerance limits and their respective risks as simple as possible, simple graphs of the dose tolerance limits as a function of the number of fractions were made. This led to the creation of the dose-volume histogram (DVH) Risk Map (Asbell et al., 2016; Srivastava, 2013).

In the Dose-Volume Histogram (DVH) Risk Map only pure physical dose is used to plot these limits on a linear scale. The Timmerman 2008 limits (R. D. Timmerman, 2008) are related by straight lines (Asbell et al., 2016). From the universal survival curve (USC) this potential linear expression of BED at high dose per fraction can be seen and was explained in the above paragraphs. The USC is one of the many models that have been proposed as alternatives to the LQ model for biological equivalence (Asbell et al., 2016).

The DVH Risk Map consists of dose on the y-axis, each subplot is for a specific volume, and the x-axis, the number of fractions for each subplot. Inverse power law, effective volume (V_{eff}), effective dose (D_{eff}) or Equivalent Uniform Dose (EUD) are some of the dose-volume metrics that combine dose and volume. A dose-tolerance limit can be specified by any of these metrics and in turn can be used as one of the five subplots in the DVH Risk Map (Asbell et al., 2016).

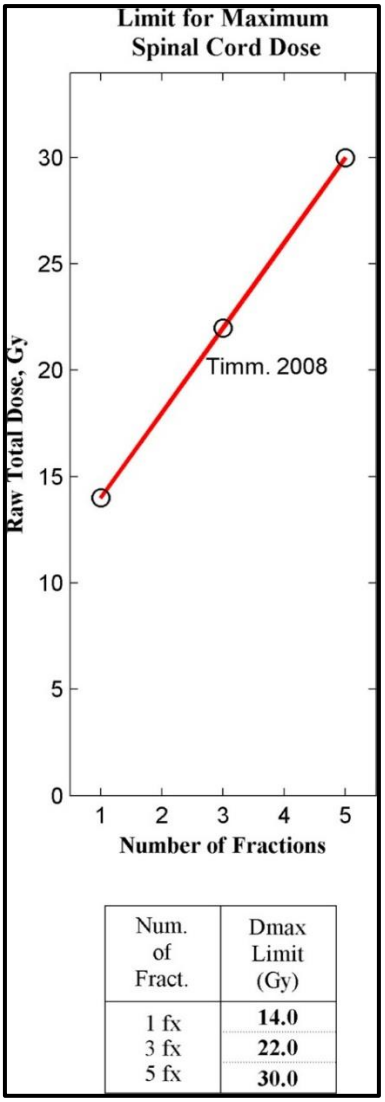

Figure 2.6: Simplified DVH risk map for Spinal Cord
(Asbell et al., 2016)

DVH Risk Map for spinal cord, D_{max} limits for 1, 3 and 5 fractions (R. D. Timmerman, 2008). The USC is linear at high dose per fraction.

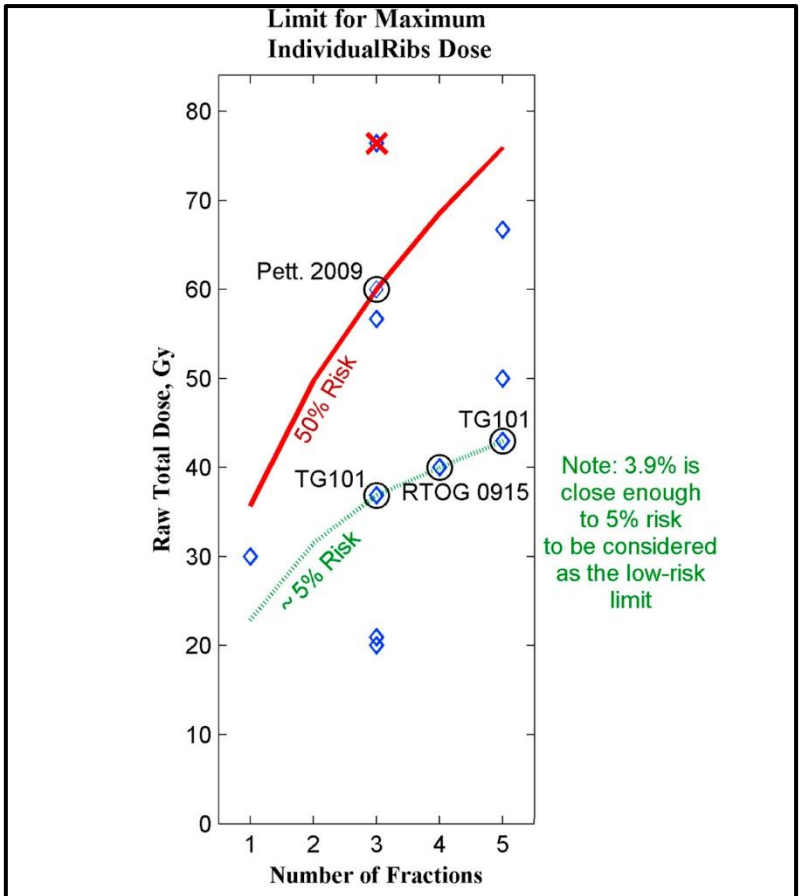

	Low-Risk Limit (~5%)	High-Risk Limit (~50%)
Number Of Fractions	Dmax Limit (Gy)	Dmax Limit (Gy)
3 fx	36.9 Gy (ref 41), 4.5% Risk	60 Gy (ref 58), 49.9% Risk
4 fx	40.0 Gy (ref 39), 3.9% Risk	
5 fx	43.0 Gy (ref 41)	

Figure 2.7: DVH risk map for rib maximum point dose, D_{max}

(Asbell et al., 2016)

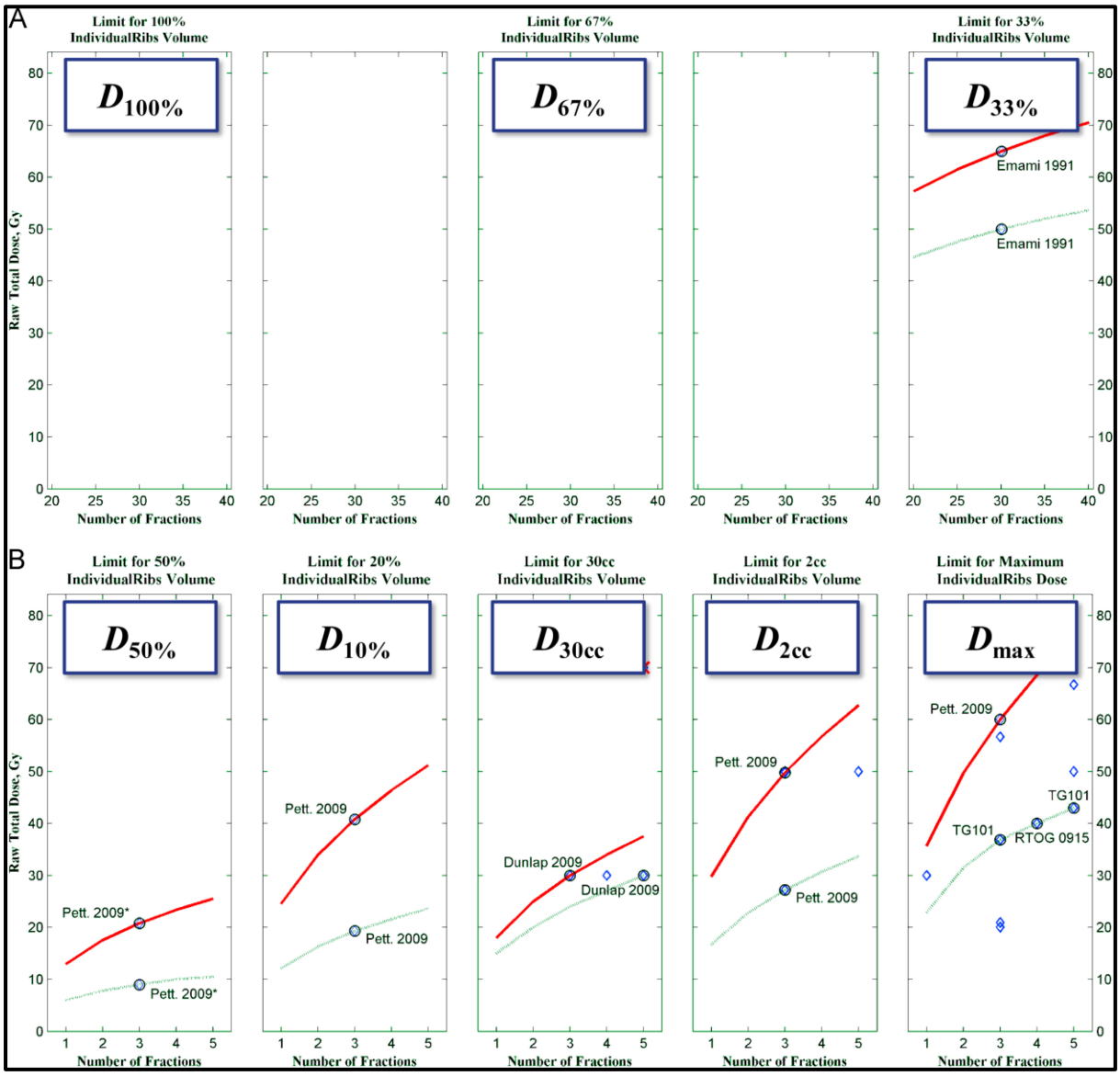

Figure 2.8: DVH risk map

(Asbell et al., 2016)

DVH Risk Map as a function of volume for (A) Conventional fractionation and (B) SBRT.

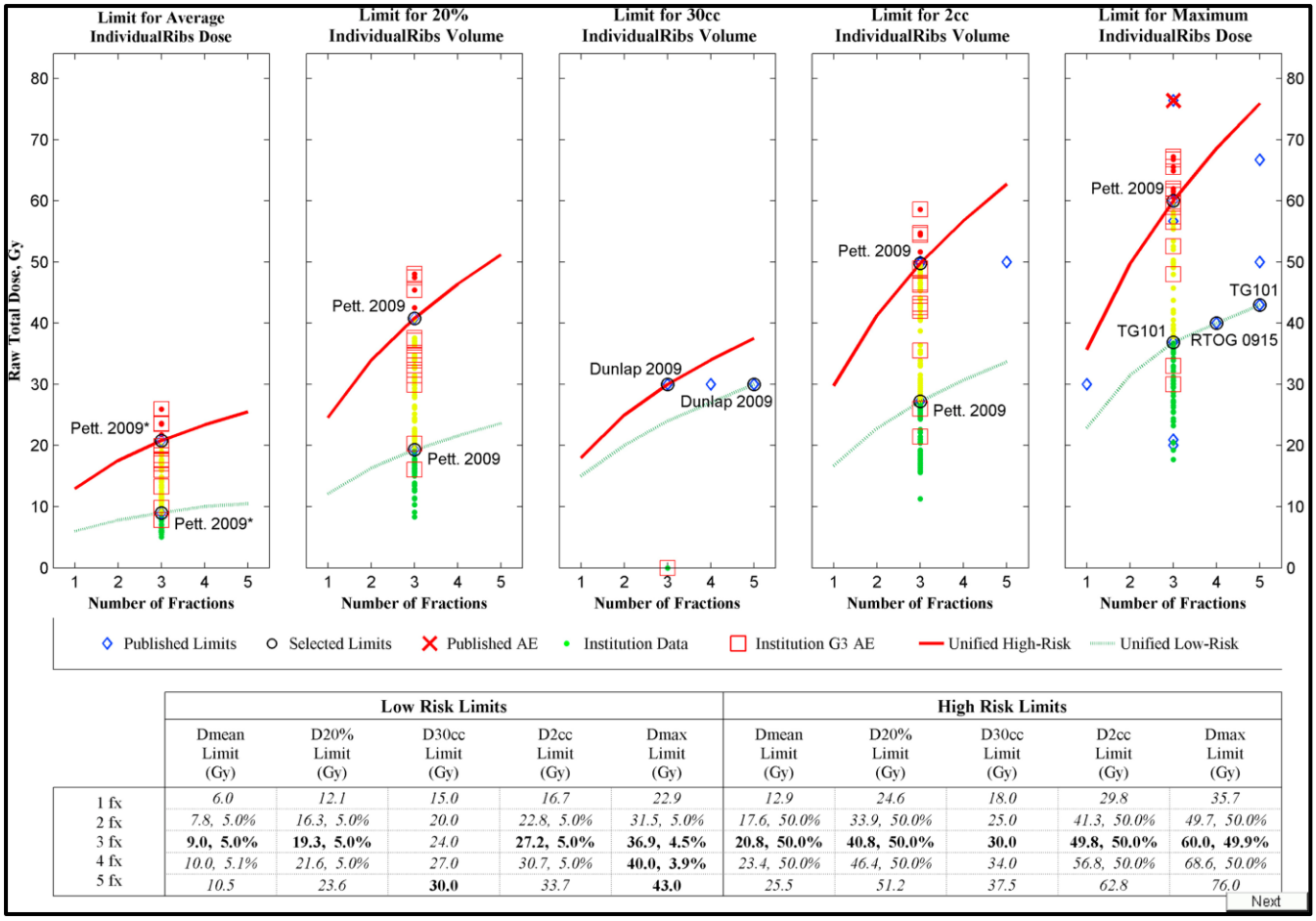

	Low Risk Limits					High Risk Limits				
	Dmean Limit (Gy)	D20% Limit (Gy)	D30cc Limit (Gy)	D2cc Limit (Gy)	Dmax Limit (Gy)	Dmean Limit (Gy)	D20% Limit (Gy)	D30cc Limit (Gy)	D2cc Limit (Gy)	Dmax Limit (Gy)
1 fx	*6.0*	*12.1*	*15.0*	*16.7*	*22.9*	*12.9*	*24.6*	*18.0*	*29.8*	*35.7*
2 fx	*7.8, 5.0%*	*16.3, 5.0%*	*20.0*	*22.8, 5.0%*	*31.5, 5.0%*	*17.6, 50.0%*	*33.9, 50.0%*	*25.0*	*41.3, 50.0%*	*49.7, 50.0%*
3 fx	**9.0, 5.0%**	**19.3, 5.0%**	*24.0*	**27.2, 5.0%**	**36.9, 4.5%**	**20.8, 50.0%**	**40.8, 50.0%**	**30.0**	**49.8, 50.0%**	**60.0, 49.9%**
4 fx	*10.0, 5.1%*	*21.6, 5.0%*	*27.0*	*30.7, 5.0%*	**40.0, 3.9%**	*23.4, 50.0%*	*46.4, 50.0%*	*34.0*	*56.8, 50.0%*	*68.6, 50.0%*
5 fx	*10.5*	*23.6*	**30.0**	*33.7*	**43.0**	*25.5*	*51.2*	*37.5*	*62.8*	*76.0*

Figure 2.9: Full DVH risk map for ribs
(Asbell et al., 2016)

In SBRT, absolute volume is more important, particularly small absolute volumes like 1cc or 0.1cc. In addition to $D_{50\%}$, $D_{10\%}$ and D_{max} another two absolute volumes are provided for DVH Risk Maps dose-tolerance limits depending and chosen specific to each anatomical structure (Asbell et al., 2016).

Final treatment volumes are highly dependent on margins added to the CTV, and any increase in margin will increase volume of normal tissue receiving radiation. The likelihood of treatment-related toxicity can therefore be limited by defining individualised target volumes more accurately, especially when working with highly mobile tumours (R. W. Underberg et al., 2004). Lung volume in the high-dose region is a dose-limiting factor for lung carcinoma treatments. Reduction in treatment margins could, in principle, allow for increased dose to the CTV for the same NTCP (Hanley et al., 1999).

2.4 Acquisition techniques

2.4.1 Slow CT scans

'Slow' CT scans are performed at a rotation of 4s (Lagerwaard et al., 2001), whereas the latest technology has a rotation time of 0.28s ("Siemens Somatom,"). A single 'slow' rotation should correlate to one breathing cycle of the patient to include all target motion during a respiratory cycle. A 'slow' CT scan is limited to the region of interest and therefore the time required to complete a scan is comparable to that of a complete planning CT scan. The radiation exposure arising from this 'slow' scan was calculated between 20% and 25% of that of a standard planning CT scan (Lagerwaard et al., 2001).

In another study it was also concluded that although the 'slow' CT scan reduces the ITV, delineation of the lesion becomes much more difficult. This is due to the blurring or 'smeared out' effect of the lesion at the edges. Another concern is when the lesion is in close proximity of OAR's, definite edges are hard to recognise and is sometimes difficult to distinguish tumour from infiltrate. In this study the CTV coverage analysis suggests an underdosage should the 'slow' CT scan be used for delineation of the lesion. (Bosmans et al., 2006)

2.4.2 Deep inspiration breath-hold technique

Deep inspiration breath-hold (DIBH) reduces lung density by increasing lung volume, and it immobilises lung tumours and therefore allows reduction in margins. The reduced lung density relative to the tumour in the high-dose region can reduce the amount of normal lung tissue irradiated, thus reducing morbidity (Hanley et al., 1999). With high energy photon beams secondary electrons produced by Compton interaction of the photons (Ekstrand & Barnes, 1990) set in motion are capable of penetrating to an average depth characterised by the measured depth of maximum dose for these beams. Lateral scatter of electrons out of the beam is known to reduce dose near the beam edge for all megavoltage photon beams (White, Zwicker, & Huang, 1996). This is because the electrons scatter laterally as well as moving in a forward direction with the beam; therefore electrons travel outside the geometric boundaries of the radiation field (Ekstrand & Barnes, 1990). The reduced lung density in the beam path further compromises lateral electron equilibrium by allowing even greater electron travel. This could result in loss of electronic equilibrium along the central axis near the lung/soft tissue boundary (White et al., 1996). This may result in an increase in penumbra and deterioration in the flatness of the beam (Ekstrand & Barnes, 1990).

Penumbra is defined as the rapid decrease of dose at the edge of the radiation beam. This is usually defined as the distance or space between the 20% and 80% isodose lines of the central axis dose value. There is a dramatic increase in penumbra with increased photon energy when density decreases. A way to measure the lack of flatness in the beam is to determine the distance between the 50% and 90% dose levels. This is then defined as the 'beam fringe' to distinguish it from beam penumbra. The fringe is significant in the sense that it represents the minimal margin that is needed around the tumour to ensure that the tumour receives at least 90% of the dose on the central axis (Ekstrand & Barnes, 1990). The assumption can be made that increased penumbra is inversely proportional to density. The DIBH technique could, on average, expect to increase the 50%-90% beam fringe by 1.5mm, which has little dosimetric significance compared to the margins applied for other treatment uncertainties, e.g. set-up and residual organ motion (Hanley et al., 1999).

The technique involving coaching of the patient to ensure and reproduce deep inspiration level throughout planning and treatment delivery is called a DIBH technique which involves a modified version of the slow vital capacity (SVC) manoeuvre.

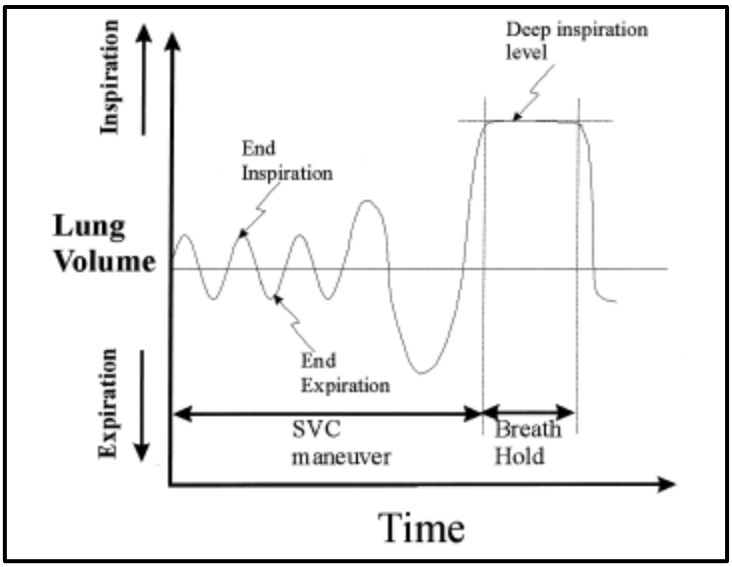

Figure 2.10: Modified SVC manoeuvre
(Hanley et al., 1999)

This DIBH manoeuvre begins with the patient in quiet respiration, followed by one slow deep inspiration and one deep expiration, then another slow deep inspiration to maximum level and then breath-hold. A spirometer monitors the patient's respiration level. The patient breathes

through a mouthpiece, a nose-clip is used to prevent nose breathing. The spirometer measures the volume of inhaled and exhaled air and is recorded as a function of time. CT slices are acquired during the breath-hold period only. The breath-hold scans are acquired using three to four segments of which each segment consist of 10 to 13 second breath-hold (Hanley et al., 1999).

These two properties, namely target immobilisation and expanded lung volume from the DIBH technique, can potentially be beneficial to lung carcinoma treatments and potentially allow for dose escalation (Hanley et al., 1999).

2.4.3 4D CT scans

With the use of 4D or respiration-correlated CT scans, this technique entails retrospective gating, the respiratory waveform is synchronously recorded during CT acquisition, and multiple CT slices are acquired at each table position for at least the duration of one full respiratory cycle. This yields CT datasets for 10 phase bins of the respiratory cycle (R. W. Underberg et al., 2004).

In a 4DCT scan, spatial and temporal information on shape and mobility are acquired synchronously in a single investigation. The breathing pattern can be recorded either with a Real-time Positioning Management System (RPM) (Slotman, Lagerwaard, & Senan, 2006) or with the use of a Respiratory Gating System (Solutions).

2.4.3.1 Real-time Positioning Management System (RPM)

The respiratory breathing signals are recorded using infrared-reflecting markers on the upper abdomen of the patient during free breathing. The markers are illuminated by infrared-emitting diodes surrounding a camera. The motion of these markers is captured at a frequency of 25 frames per second. The respiratory signal is recorded in synchronisation with the x-ray ‘on’ signal from the CT scanner. A single 4DCT scan is relatively simple and poses no problem for patients with poor pulmonary function. Although the radiation exposure from a 4DCT scan is approximately six times higher than a conventional helical CT scan, the additional dose associated with the 4D scan can be justified with the smaller volumes generated from the 4DCT scan in comparison with the standard PTV (Slotman et al., 2006).

2.4.3.2 Respiratory Gating System – Anzai

There are two types of respiratory sensors available:

- Load Cell Sensor (Patient contact type);
- Laser Sensor (Non-Patient contact type).

The first sensor mentioned detects pressure by using strain gauge bridge circuit. The pressure detecting part is used with a belt and the motion of the body surface (pressure change at the abdomen) is displayed as a respiratory waveform.
The second sensor measures the reflection of laser light (infrared). Laser light is spotted on the patient's skin and the motion of the body surface (displacement of distance to the sensor) is displayed as a respiratory waveform (Solutions).

After the 4D datasets have been acquired, the datasets are sorted in 10 phase bins within the respiratory cycle. Registration is made based on nearest neighbour criterion, where at each slice location the image is selected so that its phase is closest to each phase bin. These volumetric datasets are a representation of the 10 phases of respiration (bins).

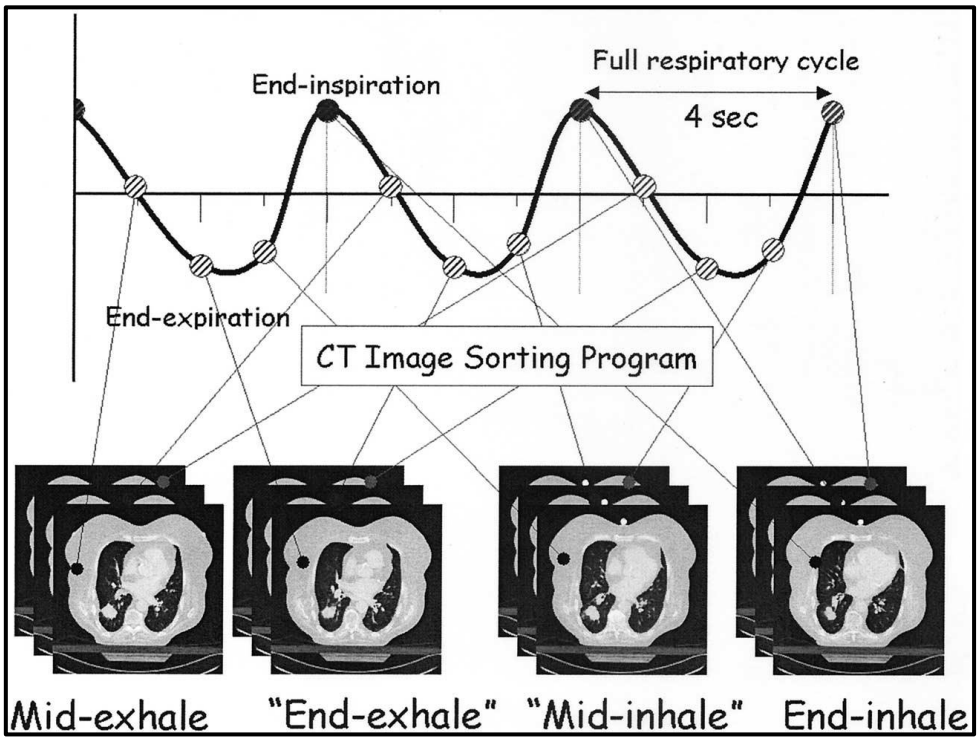

Figure 2.11: Overview of respiratory phase 'bin' generation from 4D CT data
(R. W. Underberg et al., 2004)

For this study, 4D CT data sets with the Anzai Respiratory Gating system with the Load Cell Sensor, were used to extract the motion of the target in the lungs as this was available in the clinic.

2.5 Commercially available motion phantoms

Several radiotherapy motion phantoms are available commercially. The QUASAR™ Respiratory Motion Phantom is a programmable state-of-the-art breathing simulator for conducting quality assurance testing on radiotherapy systems developed by Modus QA ("Quasar Phantom,").

Figure 2.12: Commercially available Quasar Phantom
("Quasar Phantom,")

The software application downloads patient respiratory waveforms to the phantom, simulating the breathing function. The body of the phantom is made from acrylic with two openings with acrylic, cedar and hollow inserts available.

This respiratory motion phantom is regularly used to simulate patient breathing patterns to check image quality and accuracy for 4D CBCT systems (Lee et al., 2015) and checking of consistency of contouring or delineation of volumes with the different contouring tools available across multiple treatment planning systems (Pogson et al., 2015). One of the main aims of this phantom is to implement quality assurance of motion management in a radiotherapy department. In an Australian Research Institute this phantom was modified to simulate more realistic patient motion by replacing the DC motor by a stepper motor. A separate motion platform was also designed to accommodate a variety of surrogate marker systems and to allow reproducing motion in more directions. This upgraded motion phantom

was found to be useful in terms of simulating patient motion and test patterns to aid in quality assurance of motion management. (Dunn et al., 2012)

RS-1500 Dynamic Dan breathable phantom from Oprax Medical International is a complex plastic simulation of a humanoid torso including lungs, ribcage/chest-wall bone, skin and sub-dermis, and an independently movable tumour within one of the lung volumes ("Dynamic Dan,").

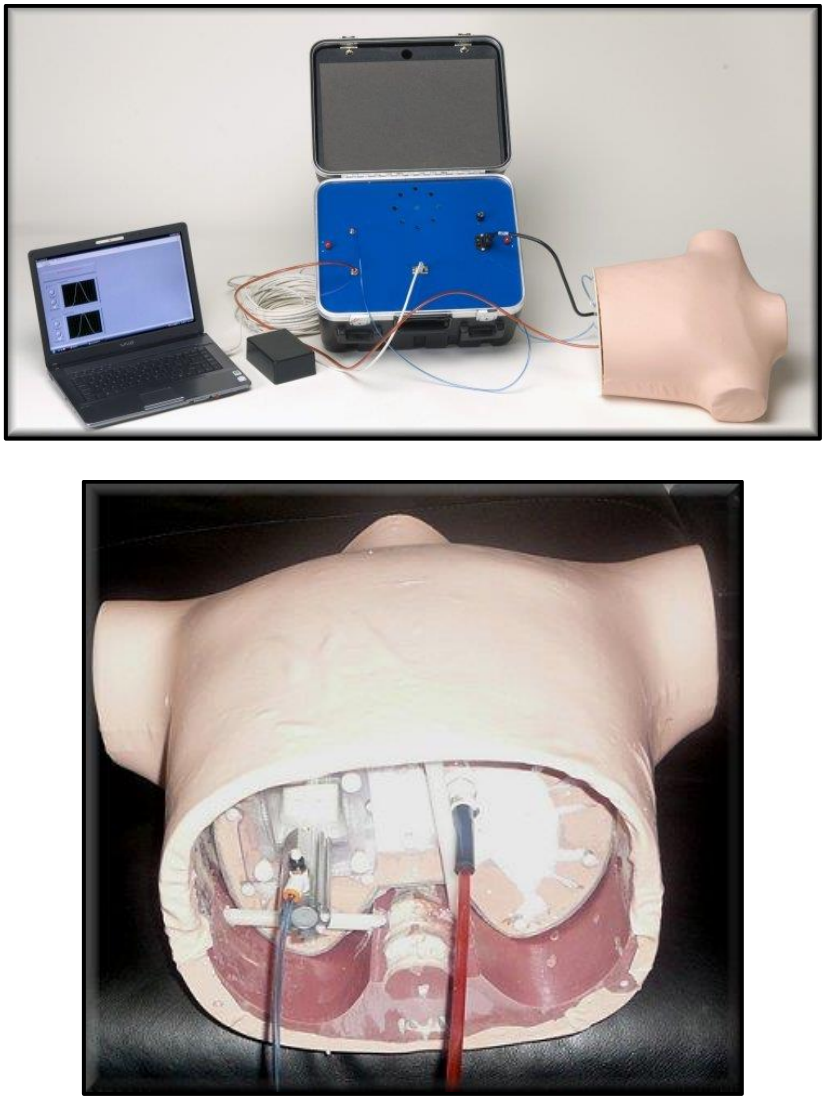

Figure 2.13: Dynamic Dan. Complex breathable phantom from Oprax Medical International

("Dynamic Dan,")

The programmed application can replicate humanoid lung function.

However, these phantoms are extremely expensive and therefore not cost effective or readily available in a third world country. A non-commercial locally designed phantom was therefore investigated as an alternative to the high cost commercial phantoms.

2.6 Customised dosimetry phantom

A suitable phantom to mimic this movement and accurately determine if the margins are adequate or not, is extremely costly. It is also not fulfilling the true aim to determine if certain margins are used correctly for a specific patient and location of a lesion in the lung (R. W. Underberg et al., 2004). Different motion phantoms are on the market which include, but are not limited to, QUASAR^{TM} Respiratory Motion Phantom as shown and discussed previously. The phantom is made of acrylic, which is not tissue equivalent, especially when measuring in different mediums such as lung. This is important for dosimetric considerations (Akhlaghi, Hakimabad, & Motavalli, 2015). Although it can be set to different breathing cycles, bpm (breath per minute), the actual movement of the target within the lung is dependent on size and location in the lung (R. W. Underberg et al., 2004; Wolthaus et al., 2008). For customised build phantoms, proper materials and densities must be found. This includes matching on CT scans (relative electron density) (Steidl et al., 2012) as well as measurements on the linear accelerator with MV photon beams.

As mentioned before, there are commercialised phantoms that mimic movement, but not as per original patient dataset. By this statement it is meant that directly from the 4D CT scanner, the exact breathing cycle are not imported into the phantom, but a breathing cycle is mimicked. Movement differs in different sections of the lung, and in breathing cycles, which is dependent on each patient dataset (Wolthaus et al., 2008). Trajectory of the tumour motion due to respiration can be determined from the 4D CT patient dataset. The position of the tumour can be shown relative to phase zero of the 10 phases within the dataset, as reconstructed during the 4D CT scan. Data can be derived for left-right (LR), cranio-caudal (CC) and anterior-posterior (AP) directions to form a 3D trajectory or path.

From published data this is as follows:

	Tumour Motion (mm)		
	LR	CC	AP
Upper Thorax	1.7 (1.3)	3.7 (2.8)	3.1 (2.5)
Lower Thorax	2.3 (1.3)	11.6 (4.8)	3.1 (2.0)
Total	1.9 (1.3)	7.2 (5.5)	3.1 (2.3)

Table 2.3: Tumour in 3D for 45 patients (whole patient group) in position in thorax (Wolthaus et al., 2008)

Values are mean (SD)

Proper materials and their respective densities must be found to build a customised phantom that will fulfil one of the aims of this study:

- Design a thorax phantom to mimic tissue characteristics and internal motion of the CTV.

The physical properties of proposed tissue materials include:

1. Electron density;
2. Effective atomic number;
3. CT number or average Hounsfield unit (HU).

(Akhlaghi et al., 2015).

As far as the density and thickness are concerned, before any dose calculation is done, the phantom will be scanned with a CT scanner and relative electron density curve will be taken into account to convert the Hounsfield units of a CT scan to electron densities that can be used in dose calculation algorithms. Electron density (number of electrons per gram) ρ_e and effective atomic number Z_{eff} is specified by the following equations:

Equation $\rho_e = N_A \sum_i (W_i Z_i)/A_i$

Equation $Z_{eff} = \frac{\sum_i \frac{W_i Z_i}{A_i}}{\sum_i \frac{W_i}{A_i}}$

where N_A is Avogadro's number, and W_i, Z_i and A_i are the weight fraction, the atomic number and the atomic mass of each atom, respectively (Akhlaghi et al., 2015; J. Chang, Suh, & Lee, 2010).

For the outer shell, first aid mannequins were explored, which could be ideal, but the cost thereof was high. Also, some of the mannequins have internal organs that would not suit our purpose. Rubber or acrylic used as the outer shell from a mould is also a favourite material in customised phantoms (J. Chang et al., 2010; Steidl et al., 2012).

The ribs' composition or equivalent material is another challenge to overcome. In some cases, commercial artificial skeletons made from polyvinyl carbonate (PVC) are used (Steidl et al., 2012) or no skeleton or ribs were chosen.

Dosages to normal lung tissue are critical in SBRT dose prescription and dose heterogeneity corrections are needed for accurate estimation of absorbed doses within and around irradiated thorax tissues. Carefully selected materials are therefore necessary, but a lung substitute is more difficult to establish due to the low physical density (K.-P. Chang, Hung, Chie, Shiau, & Huang, 2012). Lung cavities are air in most cases, but lung phantom cavities are also filled with dampened sponges (J. Chang et al., 2010). In a paper by Akhlaghi et al. (2015) the proposed lung equivalent materials were polyurethane foam and composition cork. Reference lung material in a healthy adult lung has a physical density of 0.26g/cm^3, effective atomic number (Z_{eff}) of 3.43 and CT number between -950 and -750 (K.-P. Chang et al., 2012).

Water is the standard to be used for soft tissue in literature for a phantom (Molineu et al., 2005). But, to waterproof and keep the water fresh is a challenge. Another option is rubber, but then conversion of Hounsfield units of CT scan into water-equivalent path lengths must be considered (Steidl et al., 2012). Gelatine gels can also be used as an alternative in phantoms for soft tissue, but the chemical and morphological conditions promote degradation of the gel and this is a limiting factor as it has a shelf life and needs to be kept at a certain temperature/humidity to prolong life (Freile-Pelegrín et al., 2007).

2.7 Additive manufacturing technologies

From the middle 1980s additive manufacturing technologies have benefitted many applications from faster processing of products without the need for specific tooling or dies. In the area of biomedical devices, development has been slow due to stringent performance criteria and concerns related to reproducibility and part quality. Additive manufacturing (AM) technologies in bone tissue engineering has been growing rapidly in recent years and three-dimensional (3D) printing is becoming popular due to the ability to directly print porous scaffolds (structures) with designed shape, controlled chemistry and interconnected porosity (Bose, Vahabzadeh, & Bandyopadhyay, 2013).

3D printing was developed in the 1990s at MIT, Cambridge and is a powder based freeform fabrication method (also known as solid free form fabrication (SFF) (Chia & Wu, 2015) in which using a regular ink-jet print-head, binders are printed onto loose powders in a powder bed. 3D printing, solid free form fabrication and rapid prototyping are different AM approaches for scaffold fabrication. Fabrication of the scaffolds or complex 3D structures with tailored porosity is done from a CAD file. A CAD file is an image file format and stands for Computer Aided Design (Bose et al., 2013). The integration of CAD, advanced imaging techniques such as MRI and CT scans and rapid prototyping has improved or aided the advanced fabrication of such 3D objects (Chia & Wu, 2015). The following commercially available AM techniques all create 3D scaffolds layer-by-layer (RP technology) (Peltola, Melchels, Grijpma, & Kellomäki, 2008) without any part specific tooling or dies:

- 3D Printing;
- Fused deposition modelling;
- Selective laser sintering;
- Stereolithography;
- 3D plotting;
- Various forms of direct writing. (Bose et al., 2013).

These AM techniques can be classified as:

- Extrusion (deformation + solidification);
- Polymerisation;
- Laser-assisted sintering;
- Direct writing-based processes. (Bose et al., 2013)

Table 2.4 summarises some of the advantages and disadvantages for some of the AM techniques used towards bone tissue engineering applications which forms the basic techniques and is still appropriate.

Technique	Process details	Processed materials for bone tissue engineering	Advantages (+) and disadvantages (−)
3D Plotting/direct ink writing	→ Strands of paste/viscous material (in solution form) extrusion based on the predesigned structure → Layer by layer deposition of strands at constant rate, under specific pressure → Disruption of strands according to the tear of speed	→ PCL → Hydroxyapatite (HA) → Bioactive glasses → Mesoporous bioactive glass/alginate composite → Polylactic acid (PLA)/polyethylene glycol (PEG) → PLA/(PEG)/G5 glass → Poly(hydroxymethylglycolide-co-ε-caprolactone) (PHMGCL) → Bioactive 6P53B glass	+: → Mild condition of process allows drug and biomolecules (proteins and living cells) plotting −: → Heating/post-processing needed for some materials restricts the biomolecule incorporation
Laser-assisted bioprinting (LAB)	→ Coating the desired material on transparent quartz disk (ribbon) → Deposition control by laser pulse energy → Resolution control by distance between ribbon/substrate, spot size and stage movement	→ HA → Zirconia → HA/MG63 osteoblast-like cell → Nano HA → Human osteoprogenitor cell → Human umbilical vein endothelial cell	+: → Ambient condition → Applicable for organic, inorganic materials and cells → Quantitatively controlled → 3D stage movement −: → Homogeneous ribbons needed
SLS	→ Preparing the powder bed → Layer by layer addition of powder → Sintering each layer according to the CAD file, using laser source	→ PCL → Nano HA → Calcium phosphate (CaP)/poly (hydroxybutyrate–co-hydroxyvalerate) (PHBV) → Carbonated hydroxyapatite (CHAp)/poly(L-lactic acid) (PLLA) → PLLA → β-Tricalcium phosphate (β-TCP) → PHBV	+: → No need for support → No post processing is needed −: → Feature resolution depends on laser beam diameter
SLA	→ Immersion of platform in a photopolymer liquid → Exposure to focused light according to desired design → Polymer solidifying at focal point, non-exposed polymer remains liquid, → Layer by layer fabrication by platform moving downward	→ Poly(propylene fumarate) (PPF)/diethyl fumarate (DEF) → PPF/DEF-HA → PDLLA/HA → β-TCP	+: → Complex internal features can be obtained → Growth factors, proteins and cell patterning is possible −: → Only applicable for photopolymers
FDM	→ Strands of heated polymer/ceramics extrusion through nozzle	→ Tricalcium phosphate (TCP) → TCP/polypropylene (PP) → Alumina (Al_2O_3) → PCL → TCP/PCL	+: No need for platform/support −: → Material restriction due to need for molten phase
Robotic assisted deposition/ robocasting	→ Direct writing of liquid using a nozzle → Consolidation through liquid-to-gel transition	→ HA/PLA → HA/PCL → 6P53B glass/PCL	+: → Independent 3D nozzle movement → Precise control on thickness → No need for platform/support −: → Material restriction

Table 2.4: Advantages and disadvantages of some additive manufacturing techniques toward bone tissue engineering applications
(Bose et al., 2013)

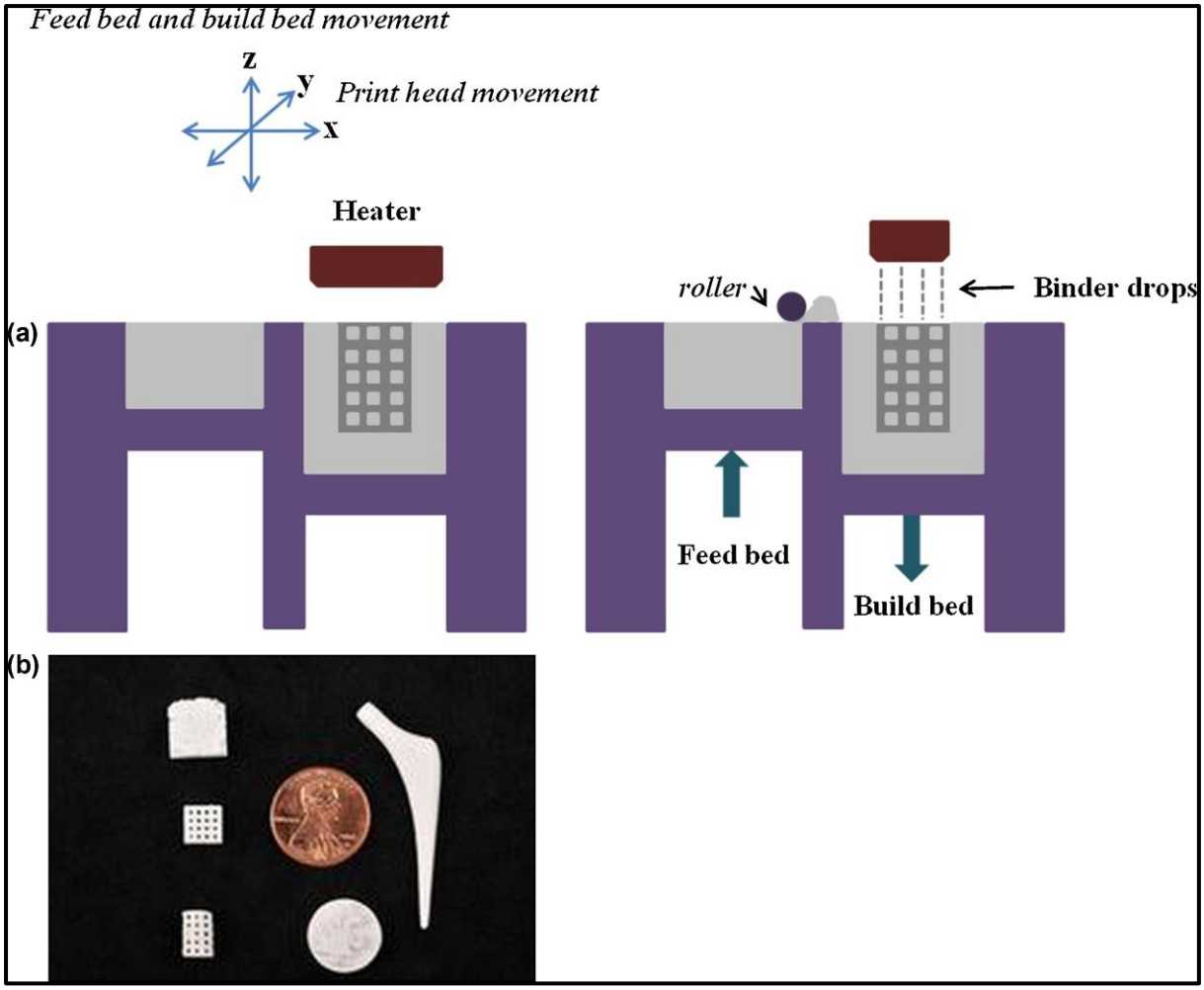

Figure 2.14: A schematic representation of the 3D print process
(Bose et al., 2013)

To establish the quality of the resultant part the following essential parameters need to be optimised:

- Powder packing;
- Density;
- Powder flowability;
- Layer thickness;
- Binder drop volume;
- Binder saturation;
- Powder wettability.

Packing density is the relative density of the powder bed after uniform spreading. To start a build, enough powder should be packed homogeneously in a feed bed. The powder bed is created by a set of rollers that spread a layer of powder evenly to a predetermined thickness.

Powder flowability determines the spreading ability and is critical in the process. Flowability again is primarily determined by particle size, size distribution, surface roughness and shape, where the layer thickness is determined by geometry and powder characteristics. The printhead sprays the binder across the build layer in several passes. This is based on the instructions in the tool path file created from the CAD file (Bose et al., 2013).

After printing, the printed layer is moved under a strip heater to allow the binder to dry and prevent spreading between layers. This is repeated until the designed part is complete. The next step involved is depowdering and involves the removal of loose powder from the printed design or body (Bose et al., 2013).

A limitation for this alternative technology is the reduced dimension available for printing (typically 20x20x20cm^3) due to the low cost for the equipment. A big 3D object could in principle be formed by assembling many smaller parts that were 3D printed. Another advantage or benefit to this entire process is that it produces much less waste than traditional manufacturing (Canessa, Fonda, & Zennaro, 2013).

As a summary and based on the background investigations and literature review discussed in the above paragraphs it was decided, therefore, to design a customised phantom that will fulfil our requirements to successfully achieve the aims of this study which are to:

- Determine the movement seen in previously treated patients from the 4D CT scan sets and used during SBRT treatment;
- Design a thorax phantom to mimic tissue characteristics and internal motion of the CTV;
- Test and compare the customised build phantom in terms of dosimetric characteristics applicable to the CT scan as well as linear accelerator, and compare the phantom motion with original 4DCT patient data in terms of lesion movement.

The inner thorax is complex with regard to realistic substructures and tumour composition and motion. So, for this study the focus was on minimum, but realistic and dosimetric important substructures in the thorax cavity that adds inhomogeneities in the phantom. This customised

build phantom consists of an outer shell, ribs, lung cavities and soft tissue. Tissue-equivalent materials used in the phantom must have similar physical properties to human tissue.

The ideal outer shell will be see-through to better visualise the target motion in the lung and have the training component as a bonus associated with it. The ability to make custom medical devices that can be tailored for patient specific needs through additive manufacturing technologies through 3D Printing was investigated and used in this study. 3D printing of the ribcage will be used since different densities or printing options can be used to match to bone or cortical bone. The lung cavities, for the purpose of this study, will remain air. A silicone gel as substitute for soft tissue was found to preserve better and have other properties that can be used in a radiotherapy environment which will be discussed at a later stage during the discussion section. Adipose tissue or fat cells, such as the yellow layer of fat beneath the skin, was not specifically considered in the design of this phantom.

3 Materials and Methods

3.1 Patient breathing cycle data collection

3.1.1 Retrospective breathing cycle data from 4D scans

After ethics approval was obtained from UCT, Human Research Ethics Committee, HREC REF number 816/2015, 7 4D datasets of patients were used retrospectively to extract the breathing cycle.

	Cancertype	Stage	Right or Left Lung	Position in Lung
Pt 1	Lung neoplasm	T1a	R	Lat, inf (1.5cm from diaphragm)
Pt 2	Squamous NSCLC	T1a	R	Post, mid (3.0cm from diaphragm)
Pt 3	Bladder	1 Lung met	L	Lat, inf (on diaphragm)
Pt 4	Squamous NSCLC	T1a	L	Post, mid (7.0cm from diaphragm)
Pt 5	NSCLC	T4	R	Mid (6.25cm from diaphragm)
Pt 6 Inf	Brongus/Oesophagus	3 Lung mets	L	Lat, inf (on diaphragm)
Pt 6 Lat	Brongus/Oesophagus	3 Lung mets	L	Lat, mid (5.4cm from diaphragm)
Pt 6 Mid	Brongus/Oesophagus	3 Lung mets	L	Post, mid (6.8cm from diaphragm)
Pt 7	Rectum	1 Lung met	L	Mid, inf (1.0cm from diaphragm)
Pt 8	Lung	T2	L	Mid, sup (12cm from diaphragm)

Table 3.1 Patient Data Sheet

Patient 3 was excluded from the study as it was not 4D scanned, but only with deep inspiration, deep expiration and normal. Therefore, three separate CT scans and not 4D CT scans were used in this study.

The following statistics could be obtained from the respiratory cycle in a 4D CT scan from each of the patients:

1. Mean breathing rate;
2. Breath rate range;
3. Average full exhalation phase;
4. Average full inhalation phase;
5. Amplitude range;
6. Amplitude standard deviation.

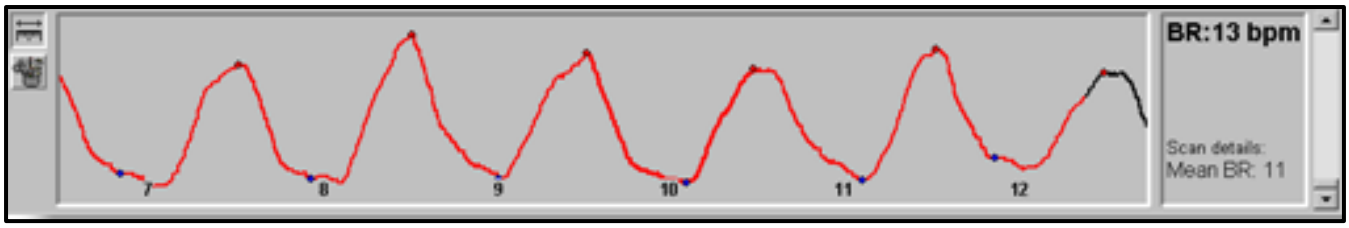

Figure (a)

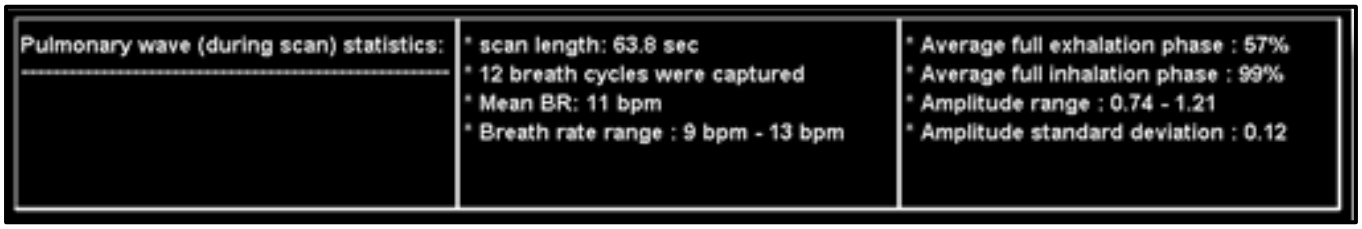

Figure (b)

Figure 3.1: Breathing rate information obtained from the 4D CT scan

3.1.2 CTV delineation

The raw 4D CT scans in DICOM format are copied onto CD from the CT scanner application where the patients were scanned. These data sets are imported into the TPS where further analysis and data extraction takes place. During the import process the scans are renamed 'Patient1' and the unique identifier, ID, also renamed to 'Patient1'. This is in accordance with the ethics rules and regulations with regard to anonymous data usage as mentioned above in 'Retrospective breathing cycle data from 4D scans'.

A CTV is contoured separately on each of the 10 phases and named to identify as such. This respiratory phase bin generation from the 4D CT scan is explained in the paragraph above under 'Acquisition of target volumes' (Rene WM Underberg, 2004). For each patient, 10 CTVs are delineated.

3.1.3 CTV coordinates

Motion of the target in the lung volume can be obtained by re-creating the movement of the CTVs in the different respiratory phase bins. When a patient is CT scanned it is placed in a coordinate system relevant to a point in the respective area to be scanned. This point can be zeroed and is called the zero coordinate or reference scan coordinate. Any movement, either for set-up purposes of the patient during treatment when considering treatment planning options or retrieving motion of organs, can then be used from this coordinate system. For the purpose of this study, the coordinates will be used to track the movement of the CTV in the lung during the 10 phases of the breathing cycle as it was 4D scanned.

An interest point or marker is added to the center of each of the 10 CTVs in the 4D CT scan set. The center is identified with the tool in the TPS, 'Jump to point' and select 'Centre of CTV'. This interest point or marker has X-, Y- and Z-coordinates (3D set of coordinates) which is relative to the CT reference scan coordinates mentioned earlier. The coordinates are recorded on the CTVs from which the motion can be extracted of the target volume moving in the lung.

3.1.4 Breathing cycle paths

The sets of coordinates obtained and explained in the above paragraph 'Coordinates of CTV' were inserted into an Excel spreadsheet.

Matlab was used in conjunction with Biomedical Engineering Department, University of Cape Town, that assisted with designing of these trajectory pathways of the respiratory cycles of the patients.

3.2 Customised phantom design

3.2.1 Phantom Dimensions

After review and extensive research on commercially available, as well as customised-made, phantoms to mimic movement and the correct density/characteristics of a human thorax, it was decided to build a customised phantom that would suit the needs and aim of this study.

From the 4D CT scan sets the following information can be obtained to assist with the design of the customised build phantom:

- Obtain average measurements of a thorax and lungs to reconstruct as part of the customised phantom;
- Convert the CT dataset of a ribcage to be 3D printed;
- Check density of the organs to evaluate the materials to be used in the customised phantom;
- Capture breathing cycles for use in this study;
- Track the path of the CTVs of the patients retrospectively.

3.2.1.1 Average measurements

Average thorax dimensions are physically measured on the patient data available in the treatment planning system. These measurements are left-right and anterior-posterior from the patient outline created on the treatment planning system in use. Superior-inferior measurement are the length of the lung OAR contour delineated on the treatment planning system. For accurate calculation of dose, should the tumour volume be located either superior or inferior in the lung, the phantom should extend 6cm beyond the superior/inferior extents of the lung, 3cm superior and 3cm inferior.

The lung measurements are the physical measurement from the treatment planning system, delineated as the left and right lung as organ at risk volumes as part of the planning process. Data are recorded for the patients and an average is calculated.

3.2.1.2 Ribcage

A ribcage has different densities that vary from bone to cartilage bone. Perspex can be used, but the density is much lower than that of bone. A suitable substitute was researched, and 3D printing investigated as discussed above under 'Additive Manufacturing Technology'. Two different compositions were explored until the correct density was found that corresponds with that of human bone on a CT scan.

The next challenge was the size of the 3D printer, as most printers in the academic environment are too small to print a complete ribcage due to cost considerations. An industrial printer was sourced and after samples were printed, scanned and analysed, the appropriate files were sent to print the ribcage. The 3D reconstruction of the ribcage is done in Mimics Materialise. This is a CAD application that uses the patient data set from the CT scan. The original CT data set is imported into the application where after a .stl file is generated. This format is derived from

the name stereolithography, the oldest of the RP technologies. This is accepted as the golden standard of this industry (Peltola et al., (2008).

The CAD data is converted into series of cross-sectional layers. The computer generated 2D layers are created as a solid model by starting at the bottom and proceeding upwards. Each layer is glued or bonded to the previous layer until a solid model is produced of the object originally imported into the programme. Three layering methods can be used, namely liquid-based, solid-based, and powder-based with a selection of material choices that range from paper to various polymers, ceramics and metals (Peltola et al., (2008). For this study the powder-based RP system was available due to agreement from the dimensions needed for printing the ribcage from the patient CT dataset.

3.2.1.3 Density of organs

To accurately determine the density of the organs to be used in the phantom, the CT dataset is used. When a patient is scanned with a CT scanner, narrow X-rays are sent through the patient in an arc motion. These x-rays are collected with detectors after it has penetrated and moved through the patient. The information collected from the detectors after the x-ray has been attenuated are converted into an 3D image due to the 360 degree rotation of the 'beam'. The CT scan application software collects the data into the CT dataset that you import into the treatment planning system. The treatment planning system converts the Hounsfield units from the CT scan to electron density values. The conversion is from a non-linear graph that is created during TPS commissioning and is conventionally named as a 'CT-to-ED. This can be used in the TPS algorithm for accurate dose calculation purposes.

3.2.1.4 Breathing Cycles/Tracking of CTV

From the 4D CT scan sets of the patients, the full breathing cycles are traced. As described in above paragraph, 'Breathing cycle paths', a map/path is plotted as to how the GTV moves during the respiratory cycle and the amount relative to its position in the lung cavity.

3.2.2 Phantom tissue equivalence

The sample 3D printed blocks that were obtained for evaluating density of bone, were used to measure and check transmission through the medium. The blocks were embedded in the soft tissue material (silicon) used in the customised phantom. Another block with only soft tissue

material was also cast to measure and check transmission. The reference set-up was 3cm Perspex for backscatter purposes and the Farmer chamber insert (also Perspex) with 5cm Perspex build-up.

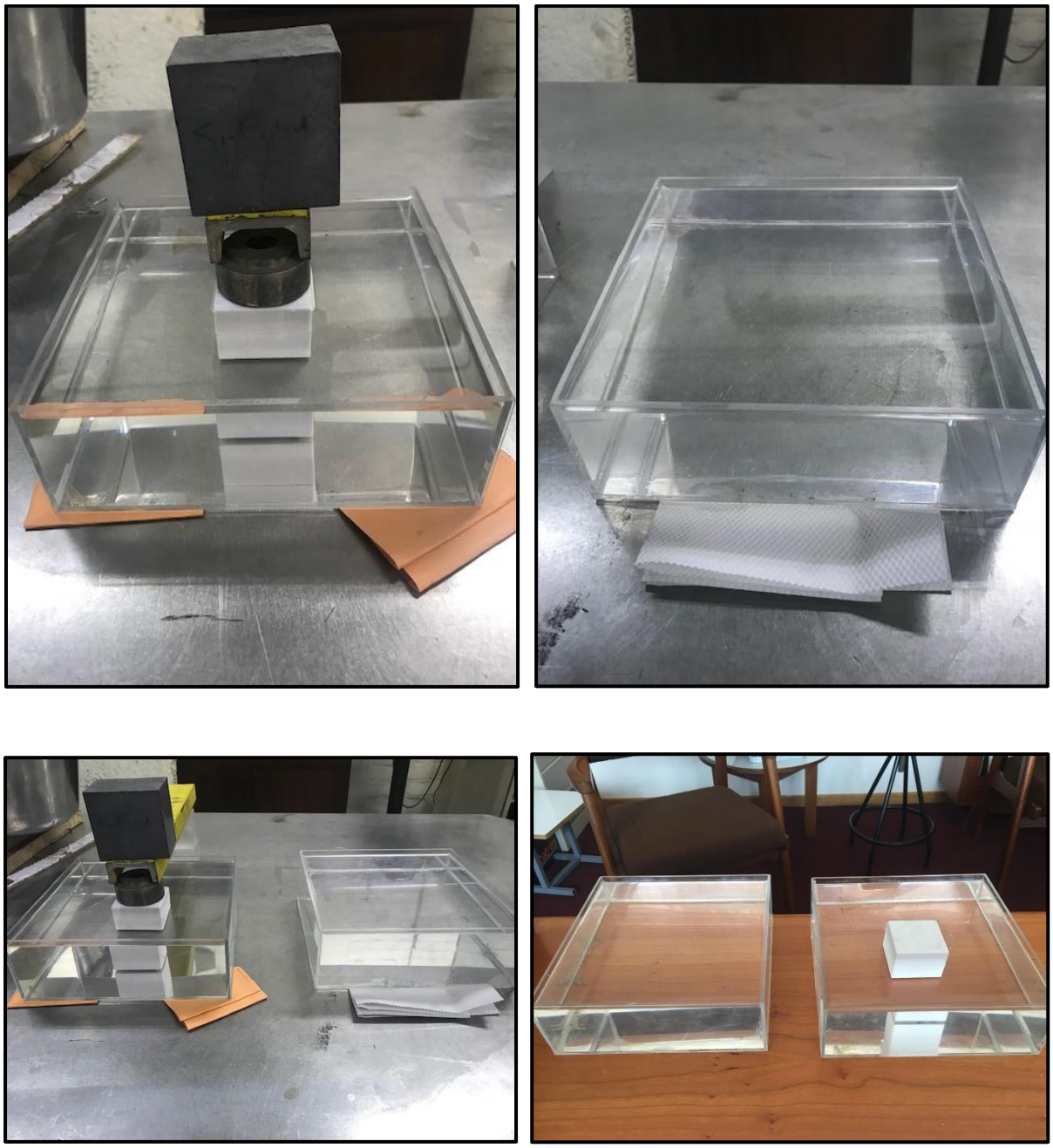

Figure 3.2: (a-d) Phantoms cast with and without 3D blocks in soft tissue material

Both these phantoms were scanned on a CT scanner and imported into the TPS. Two Treatment Planning Systems were used for calculation purposes and comparison of measured results against calculated results from the different algorithms used in both systems. The planning systems used were Monaco, version 5.11.02 from Elekta with Monte Carlo Dose calculation

and Eclipse, version 15.6 from Varian with AAA and Acuros 15.6 dose calculation models. Both these systems are currently used in the department and available for this project. For setup purposes 3cm backscatter perspex plates were used together with a 0.6cc chamber and perspex insert. The reference scan and calculation in the TPSs were only perspex, 3cm backscatter, the insert for the Farmer chamber and then 4cm build-up. For the transmission calculation or evaluation, either the 3D blocks were added on top of the chamber or the soft tissue material and scanned as such. The chambers were outlined in the TPS software and forced to perspex density. This is used when calculating the dose in medium and water at a specific point in the phantoms. An interest dose point was dropped at the depth of the ionisation chamber.

The same setup was reproduced on the linear accelerator and measurements were made with the 0.6cc chamber and each of the phantoms in place.

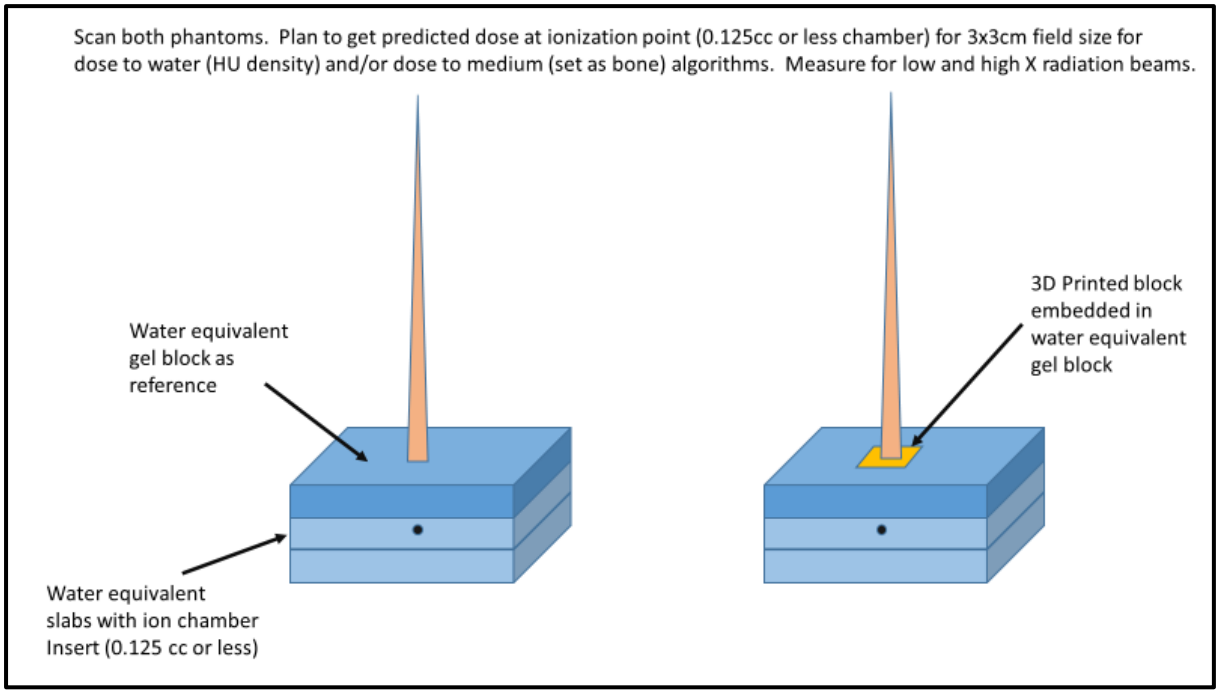

Figure 3.3: Setup for TPS planning calculation as well as Linac based measurement

PTW electrometers were used together with the chamber. Unidos was used with the 0,6cc chamber.

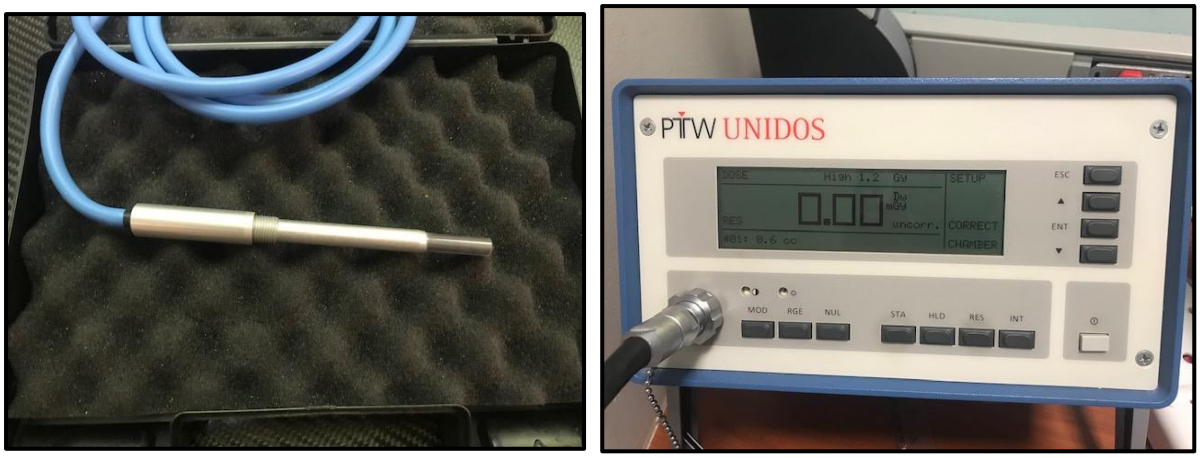

Figure 3.4: 0.6cc chamber with PTW Unidos

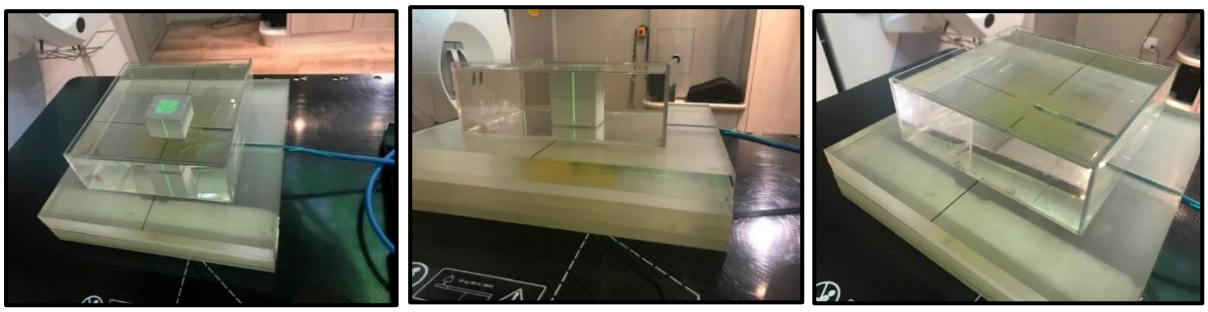

Figure 3.5: 3D sample block phantom vs reference (soft tissue) phantom

100MUs were given for all measurements and calculations as on the Treatment Planning Systems. The SSD for the silicon or soft tissue block and 3D block phantom was 89.0cm. The SSD difference between the 3D block and soft tissue block was because the 3D block was slightly higher than that of the soft tissue phantom, but this is only 2mm. The reference scan or set-up has an SSD of 95.0cm. Field sizes 10x10 and 5x5 were measured for two different energies, namely 6MV and 10MV.

3.2.3 Phantom motorisation

Simulation of tumour motions or trajectories in 3D within the lung cavity will be accomplished only with the assistance of a design of a motorised arm.

4 Results

4.1 Patient data

4.1.1 Retrospective breathing cycle data from 4D scans

The following statistics were obtained from the respiratory cycle during the 4D CT scan from each of the patients:

1. Mean breathing rate;
2. Breath rate range;
3. Average exhalation phase;
4. Average inhalation phase;
5. Amplitude range;
6. Amplitude standard deviation.

Patient	Mean Breathing Rate (bpm)	Breath Rate Range (bpm)	Average exhalation phase (%)	Average inhalation phase (%)	Amplitude Range	Amplitude Standard Deviation
1	17	16 - 20	59	99	0.66 - 1.26	0.22
2	11	9 - 13	57	99	0.74 - 1.21	0.12
4	17	5 - 24	51	85	0.75 – 1.34	0.17
5	16	8 - 23	56	99	0.64 – 1.28	0.15
6	14	11 - 19	44	98	0.84 – 1.26	0.13
7	13	12 - 15	59	98	0.82 – 1.25	0.13
8	12	9 - 14	53	97	0.84 – 1.38	0.15

Table 4.1: Statistics obtained from the respiratory cycle during the 4D CT scans

Patient 3 was excluded from the study as it was not 4D scanned, but with deep inspiration, deep expiration and a normal breathing CT scan.

4.1.2 CTV coordinates

A CTV is contoured separately on each of the 10 phases and named to identify as such, CTVnil, CTV10, etc. Thereafter an interest point or marker is added to the center of each of the 10 CTVs in the 4D CT scan set. This interest point or marker has X-, Y- and Z-coordinates (3D set of coordinates) which is relative to the CT reference scan coordinates mentioned earlier. The coordinates of the CTVs are recorded, from which the motion can be extracted of the target volume moving in the lung.

This was done for each of the patients in the study group. Refer to tables in Annexure A – CTV coordinates. Patient 3 was excluded from this study set, as the patient did not receive a 4D CT Scan, but an inhalation, exhalation and normal breathing scan.

Once these coordinates were captured (as shown in Annexure A – CTV coordinates), the non-gated CT (or free-breathing/50% phase) was used to normalise the other phases against. The actual absolute difference in distance of movement from the free-breathing or 50% phase CT was determined. This reference or normalised CT was set to (0, 0, 0) and each of the subsequent phase CTs absolute movement was calculated in each direction, X, Y, Z-axis. Again, all the patients' CTV movements were calculated as in the study group except Pt 3, as explained in above paragraph. Refer to tables in Annexure A – CTV movement.

4.1.3 Breathing cycle paths

The coordinates, depicted above from the tables, plot a path in three dimensions relative to the non-gated CT scan. Therefore, from these coordinates an attempt was made to do 3D plots or paths in Excel, but it was unsuccessful. With the assistance of Biomedical Engineering from the University of Cape Town, they could do 3D plots in MATLAB.

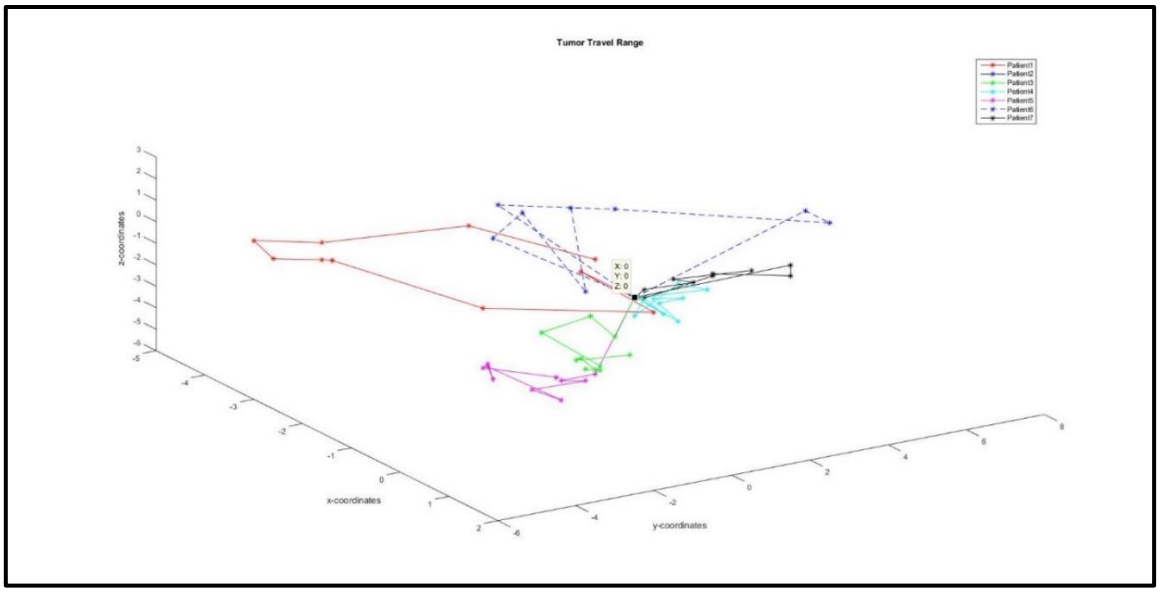

Figure 4.1: 3D plots of paths in Matlab
(Video clip Nicolene.mp4)

The intricate and complicated path of the tumour volumes, as one can see from above 3D plot, was a huge challenge. It is was even further complicated to design a 3D motorised arm to

mimic the patient movement and track the path due to the very small movements. The movements were very small, and although at a distance with an amplification factor involved, it was extremely difficult to try to replicate these submillimeter movements. An assumption was made to round any movements less than 2mm to 0. The rest of the values were rounded to 1mm. To bypass the 3D movement of the arm, and keeping it as simple as possible for this study, we selected one axis with minimal movement and assumed movement to be negligent. This axis was assumed to have 0mm movement and the plot/path can be simplified to a 2D movement or path that the tumour follows in the lung cavity.

As per in above paragraph assumption, the Z-axis in Patient 1 is to be assumed a zero movement, due to more than half of absolute movements in different phases is 0.0. In Patient 2, two of the axes were found or assumed as zero, and Patient 4 indicated no movement. But with Patients 5, 6, 7 and 8, the X-axis and Y-axis were taken as the axis with zero movement, respectively. This is atttributed to the fact of the position of the tumour in the lung.

The plots were done but not all plots completed one full cycle, and some paths crossed which could not be replicated.

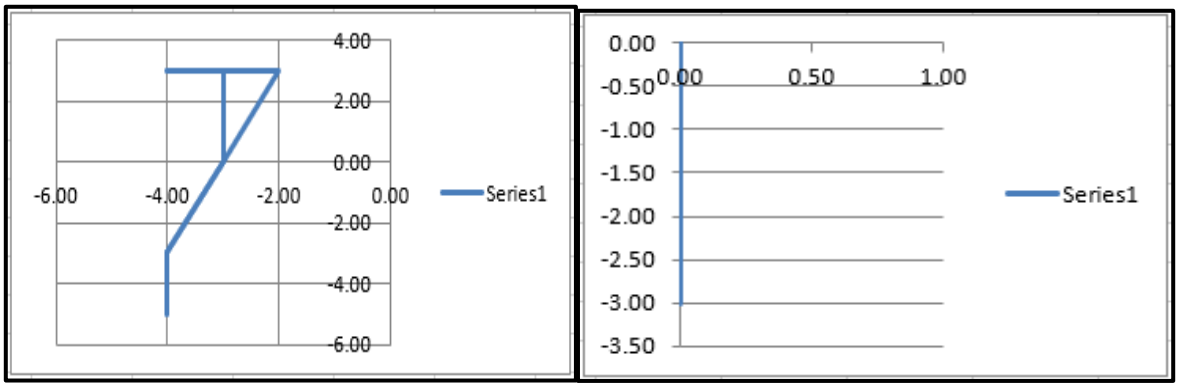

Patient 1 Patient 2

Figure 4.2: Graphs for movement of tumor in mm for Patient 1 and Patient 2

Patient 4: No movement could be calculated according to assumptions accepted for this study.

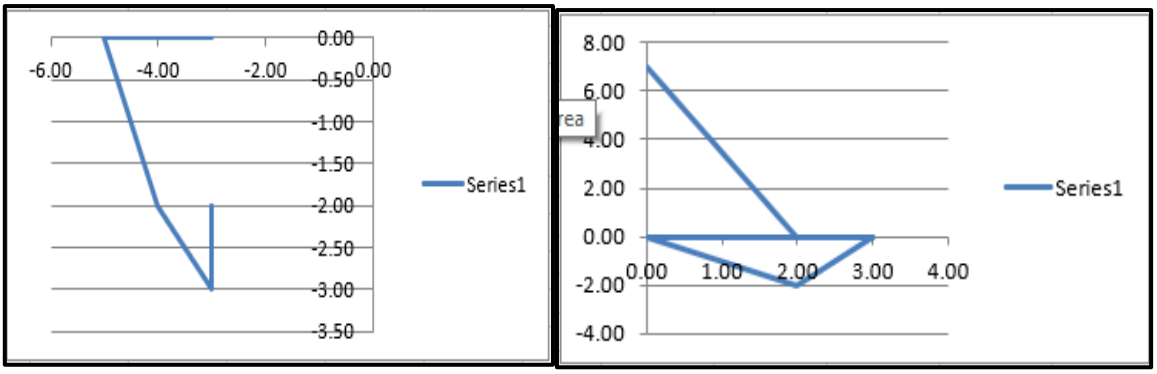

Patient 5 Patient 6 (Lat)

Figure 4.3: Graphs for movement of tumor in mm for Patient 5 and Patient 6 (Lat)

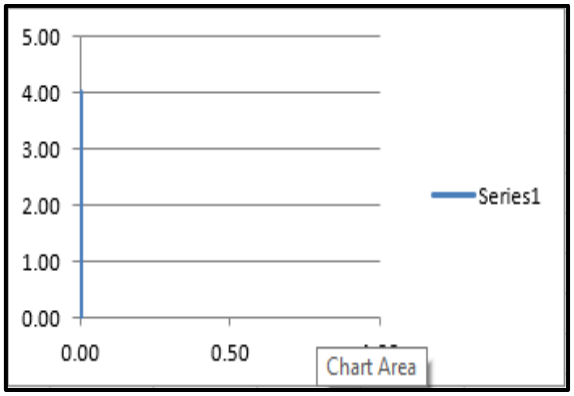

Patient 6 (Med)

Figure 4.4: Graphs for movement of tumor in mm for Patient 6 (Med)

Patient 6 (inf): No movement could be calculated according to assumptions accepted for this study.

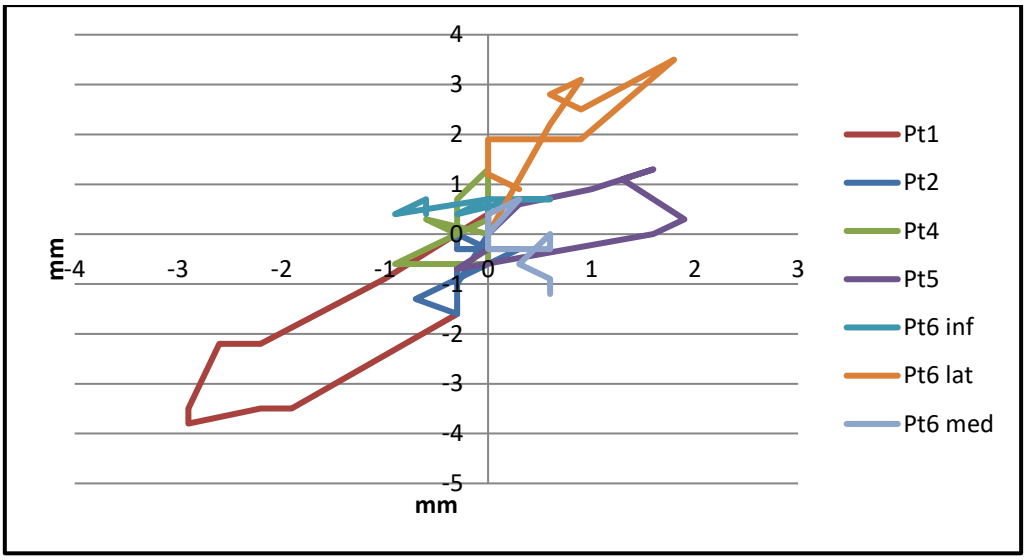

Figure 4.5: All patients 2D movements displayed on one graph

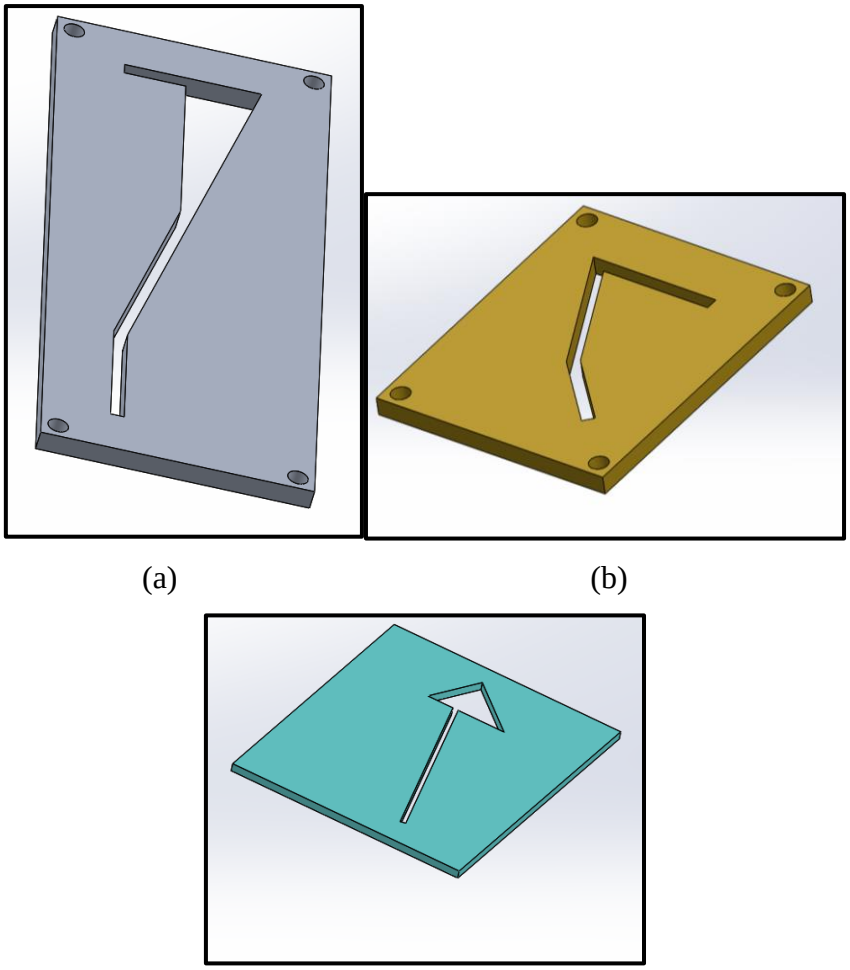

(a) (b)

(c)

Figure 4.6 (a-c) Physical templates of breathing cycle paths

Templates of the design of paths as per coordinates from 4D scans and 2D plots as shown above. An 'average' path was created from the points, as well as connecting the first and last point from the coordinates from which the plot/path was constructed. A track was re-designed for the motorised arm that could more easily follow the 2D path. This is explained in paragraph 4.2.3.4 'Fourth Design' to simply the motorised arm design that forms part of this project. Only Patient 1 and 5's paths were re-designed. This is depicted in the coloured in area on the graphs in Figure 4.7. The paths that replicated only a straight line as the plot that mimics the movement, was not simplified.

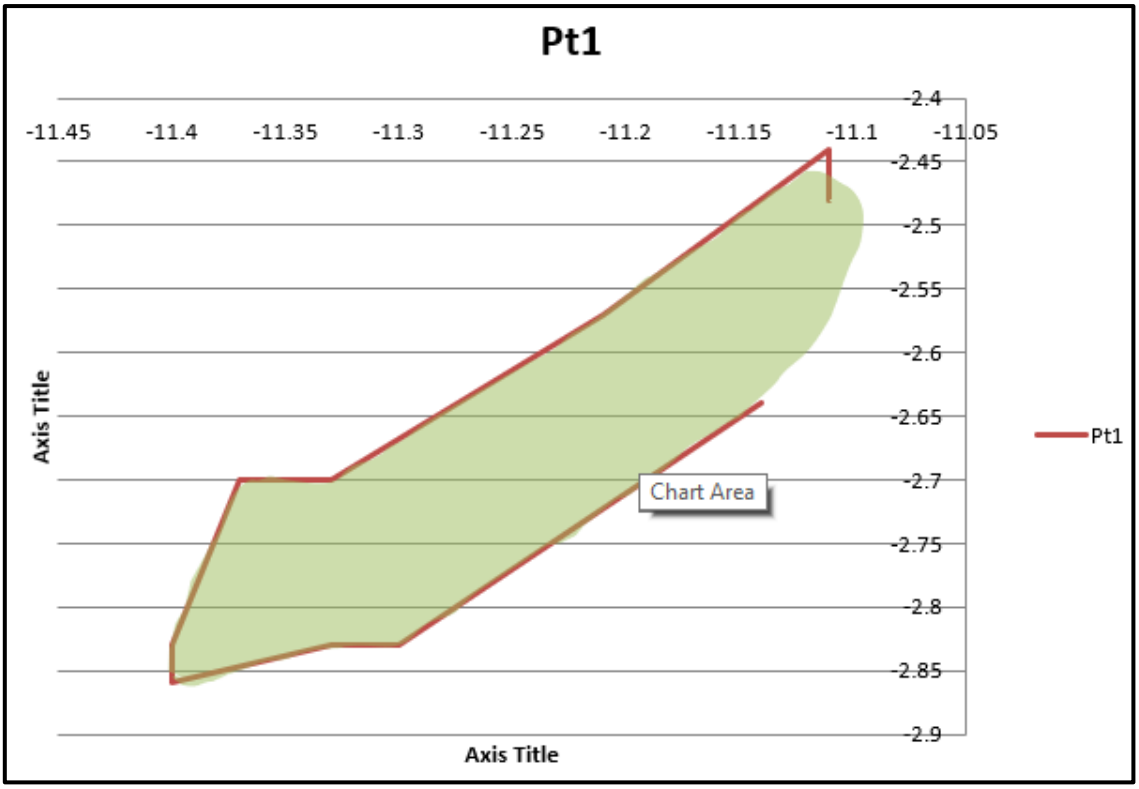

Figure (a)

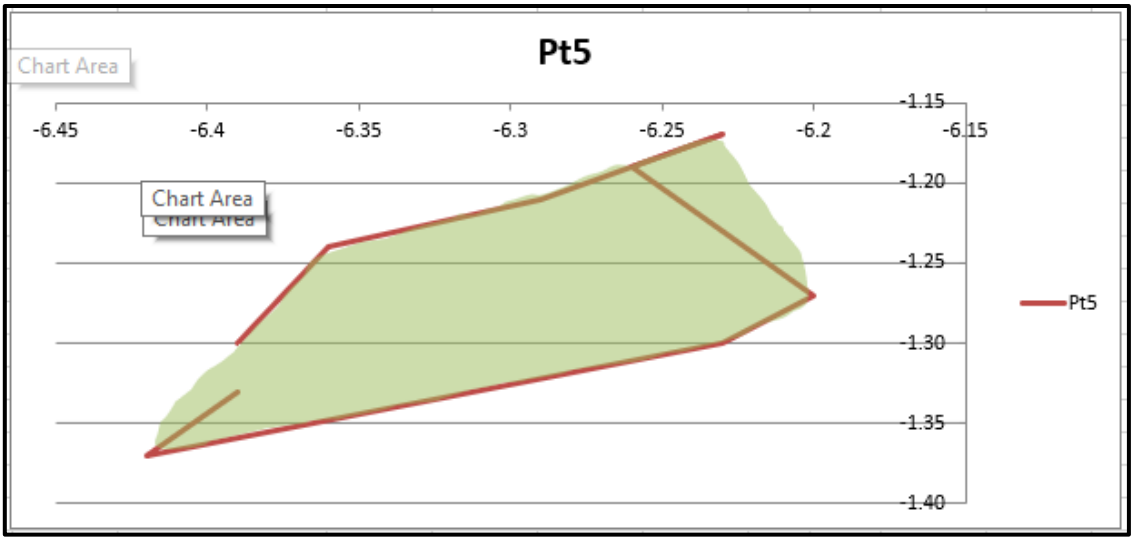

Figure (b)

Figure 4.7: Paths for Patient 1 and Patient 5

The ‘average’ paths (cm) as described in the paragraph above.

4.2 Customised phantom

4.2.1 Phantom dimensions

Below is a simplistic design of a customised phantom with a motor propelling an arm at a designated speed and cycle/path to mimic the movement of the tumour in the lung cavity.

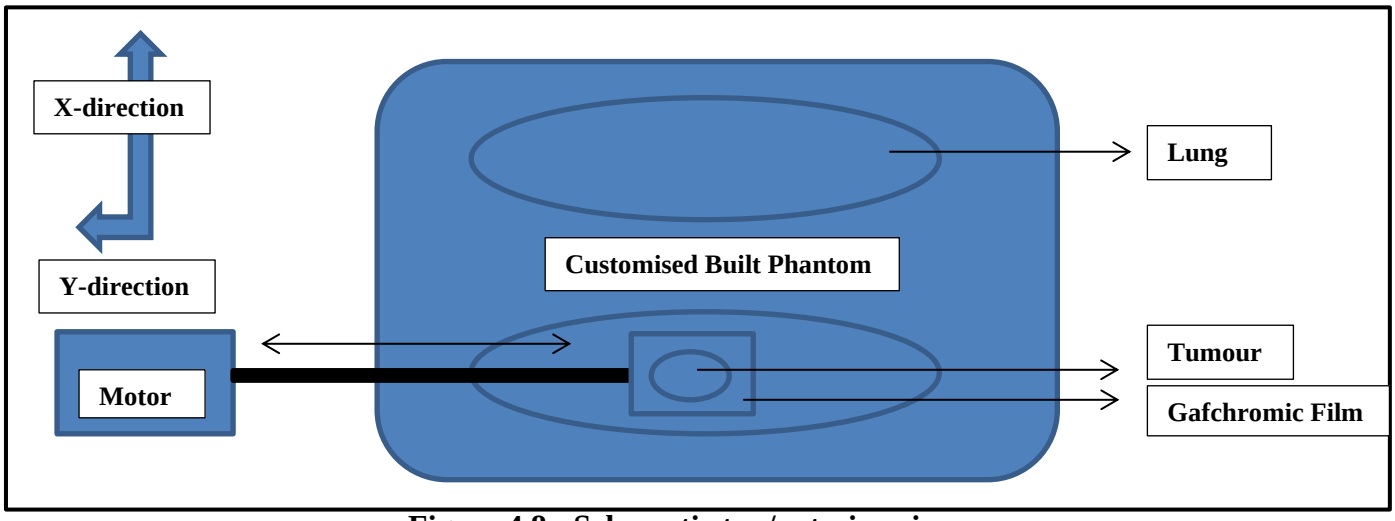

Figure 4.8: Schematic top/anterior view

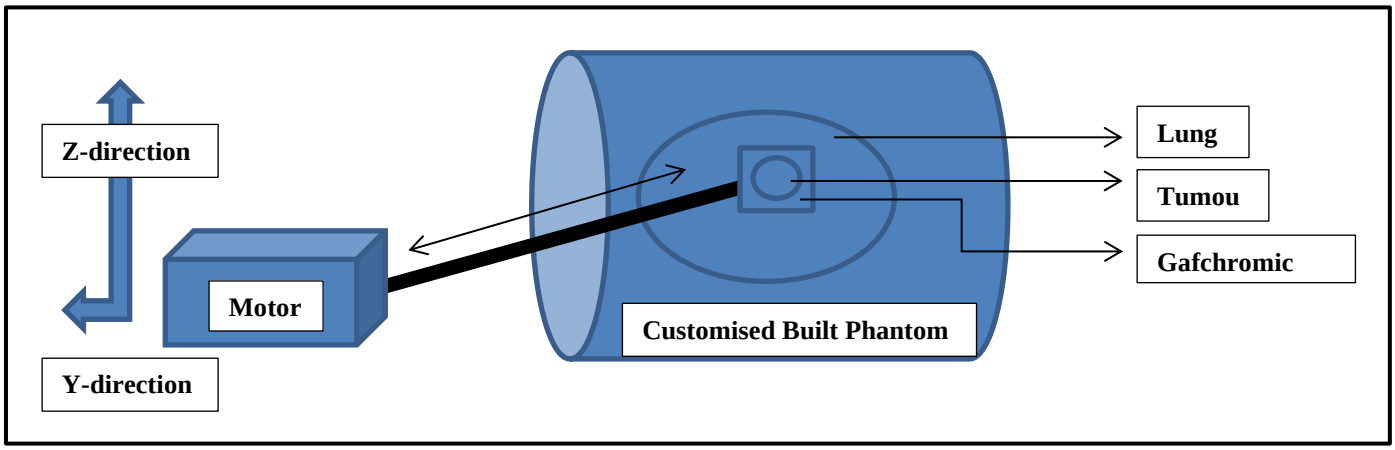

Figure 4.9: Schematic side/lateral view

As a first step to make this design a reality, the body or shell of the phantom must be created. This is all calculated from average measurements from the 4D CT scans of the retrospective patients used during this study.

4.2.1.1 Average measurements – Thorax (Shell)

The average thorax dimensions are calculated as 34.11cm, 29.42cm and 25.07cm for left to right, superior-inferior and anterior-posterior distance respectively, from the patients in the study. See Table 4.2 and for the sup-inf direction, 6cm was added, 3cm superior and 3cm

inferior, to allow for dose calculation accuracy should the CTV be located either superior or inferior in the lung cavity.

	Left-right (cm)	Superior-inferior (cm)	Anterior-posterior (cm)
Pt1	32.2	25.9	29.1
Pt2	30.6	22.7	21.2
Pt3	38.4	24.0	27.6
Pt4	34.9	23.1	24.8
Pt5	33.8	21.4	23.6
Pt6	37.1	24.3	24.0
Pt7	34.3	22.2	25.7
Pt8	31.6	23.8	24.5
Average	**34.11**	23.42	**25.07**
6cm added sup-inf		**29.42**	

Table 4.2: Average measurements for thorax dimension

A mould was reconstructed simulating a thorax to house the relevant organs at risk (OAR) from the above-mentioned average values of the retrospective patients used in the study.

A 3D model of a set of anterior and posterior ribs was presented (discussed under ribcage) so that an ultra high impact acrylic cast could be made to house the ribs, lungs and then be filled with a tissue equivalent material. A subject was chosen on the measurements taken from the superior, middle and inferior levels of the ribs. The subject was informed of the procedure and consent obtained to manufacture this two-piece Plaster of Paris impression.

See Annexure B for a full description of methodology.

Figure 4.10: Anterior mould (A)

Figure 4.11: Anterior mould (B)

Figure 4.12: Posterior mould (A)

Figure 4.13: Posterior mould (B)

(Impressions and models made by: Susan Tovey, UCT/GSH)

4.2.1.2 Average measurements – lung

The average values to reconstruct the lung moulds are 10.60cm, 23.30cm and 18.27cm for left to right, superior-inferior and anterior-posterior distance respectively, from the patients in the study.

	Left-right (cm)	Superior-inferior (cm)	Anterior-posterior (cm)
Pt1	11.1	25.9	21.4
Pt2	10.3	22.7	15.8
Pt3	10.2	24.0	18.7
Pt4	10.5	23.1	16.7
Pt5	10.5	21.4	17.7
Pt6	-	-	-
Pt7	10.3	22.2	19.4
Pt8	11.4	23.8	18.1
Average	**10.60**	**23.30**	**18.27**

Table 4.3: Average measurements for lung dimensions

Note Patient 6 is ignored in this calculation of averages as the R Lung was collapsed and L Lung over-used because of R Lung incapacity.

Screenshots from the TPS of lung 3D wire images were made, saved and used as an example of what the lung moulds must look like/represent once finished.

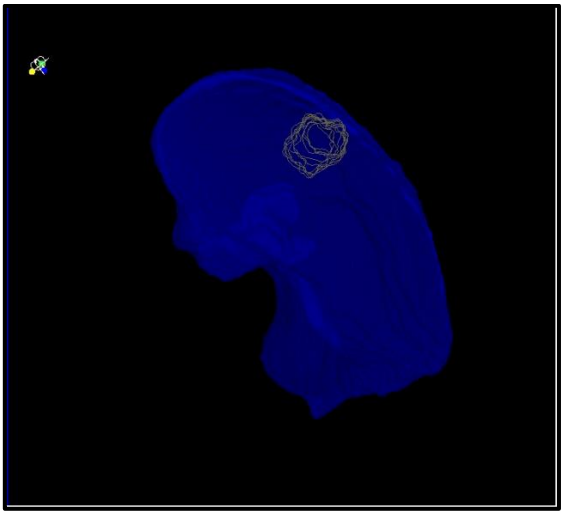

Figure (a)

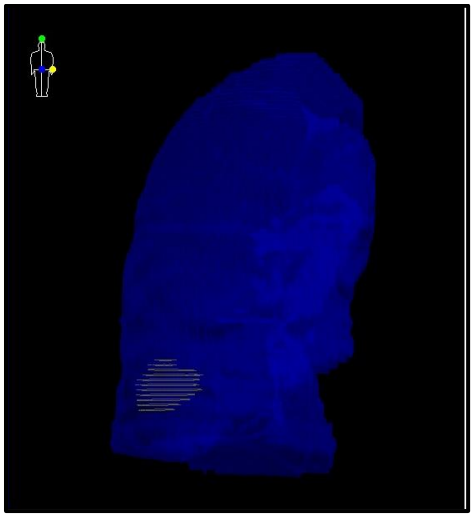

Figure (b)

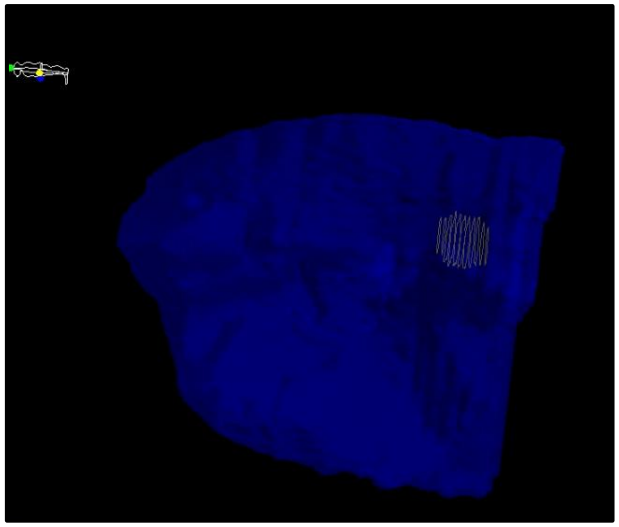

Figure (c)

Figure 4.14: 3D wire screenshots of lung from (a) feet, (b) anterior and (c) lateral view, respectively

These lung moulds were reconstructed on Stillam software, Alphacam 2016 R1. Alphacam is CAD CAM software to aid in the design and manufacturing of woodworking, metal and stone cutting.

Medium density fibreboard (MDF) was used as the material for the moulds. MDF is a high grade, composite material that performs better than solid wood in many areas. Made from recycled wood fibres, combining it with wax and resin, MDF is machine dried and applying high pressure and temperature to produce dense, stable sheets or panels. MDF is more stable than solid wood and stands up better to changes in heat and humidity.

Figure 4.15: MDF Board

A Biesse Klever 1836 G FT CNC Router with a Matrix Vacuum bed was used in the construction of the lung OARs. A CNC router is a computer controlled cutting machine related to the hand-held router used for cutting various hard materials, such as wood, composites, aluminium, steel, plastics and foams. CNC stands for computer numerical control. Slabs or sections of 30mm thick are cut/routered and glued together with an adhesive called Kleibert 501 PUR.

Figure 4.16: Biessie Klever Router

The lung moulds were formed layer by layer as described above and shown below in the photos.

Figure 4.17(a)

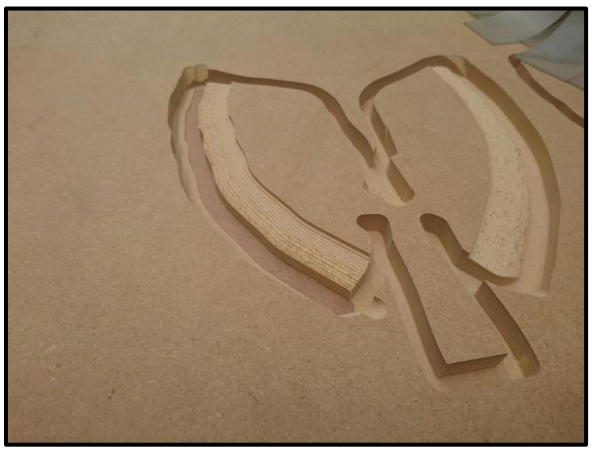

Figure 4.17 (b)

Figure 4.17 (c)

Figure 4.17: (a+b) Router cut from MDF board; (c) Final lung mould

The cast or shell reconstructed from these moulds is done with a vacuum wrap machine. A 'dummy' mould was constructed in the same manner as the lung moulds to check if the vacuum wrap of thermoplastic would succeed. Below a photo of this preliminary check.

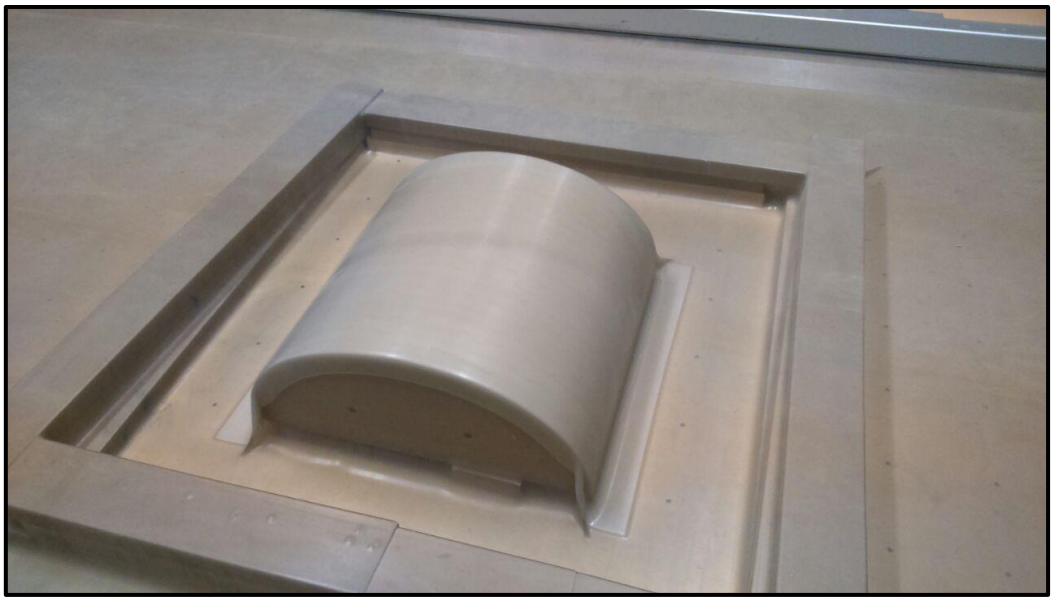

Figure 4.18: Dummy mould to investigate if wrapping process would work

It was successful and the process could continue.

4.2.1.3 Construction of thorax and lung moulds

The customised build thorax and lung moulds were vacuum wrapped with thermoplastic. Polycarbonate (PC) sheets were used to form the thorax and lungs from the mould. It was vacuumed in the desired shape. 2mm thick PC sheet was used for the thorax and 1mm for the lungs. A Woodtech Mechatronics Technowrap Plus Double Bed Vacuum Press with 2900mm bed was used for the vacuum process.

Figure 4.19: Vacuum wrapped machine - Woodtech Technowrap 2900mm bed

See Annexure C - Thorax for the full description of the process to vacuum wrap the moulds.

Figure 4.20: (a+b) Outer shell of thorax

An opening inferior of the shell will allow mimicking movement of the tumour in the lung.

The same process was followed with the lung moulds after manufacturing, explained in Annexure C - Lung. The MDF lung moulds were fitted in a jig, thermoplastic of 1mm was added and it was heated. Thereafter the vacuum process was followed, half settings for

temperature and pressure were used due to the fact of the thinner and smaller moulds used to fabricate the lung shells.

4.2.2 Patient tissue equivalence

4.2.2.1 ***Body***

As discussed under 'Construction of thorax and lung moulds' above, the material used for the body or thorax shell was 2mm thermoplastic. It is sturdy enough to keep shape for the purpose of this study. Also, the phantom will always be scanned with a CT scanner to take the density of the material involved in the phantom into account, when dosimetric calculations need to be done.

4.2.2.2 Tissue

The soft tissue surrounding the ribcage and filling the thorax shell was investigated and a workable solution for the soft tissue in the thorax shell must be, except for a density match, also non-biodegradable. This means that the phantom needs to be stored under normal circumstances and not e.g. under a certain temperature and only for a certain amount of time, and then needs replacement. This will increase cost of the phantom and use will be limited to a specified period only or 'end-by-date'.

Encapso K is a water clear encapsulation or display rubber (silicone) that looks just like water and is ideal for a variety of encapsulation and display purposes. This is ideal for the thorax phantom as the see-through property of the compound will be an added advantage. As per all previous materials, this also was checked to confirm the equivalence of soft tissue in a human body.

As one can see from the CT scan in the Figure 4.21, the Hounsfield number of the rubber compound to be used as soft tissue equivalent was indeed comparable to water. In radiotherapy, water is equivalent to soft tissue for phantom-based calculations and evaluations. This value is 0 and this clear medium indicated on the CT scanner a value of 134HU, which is comparable to water and will still be a usable material for this project.

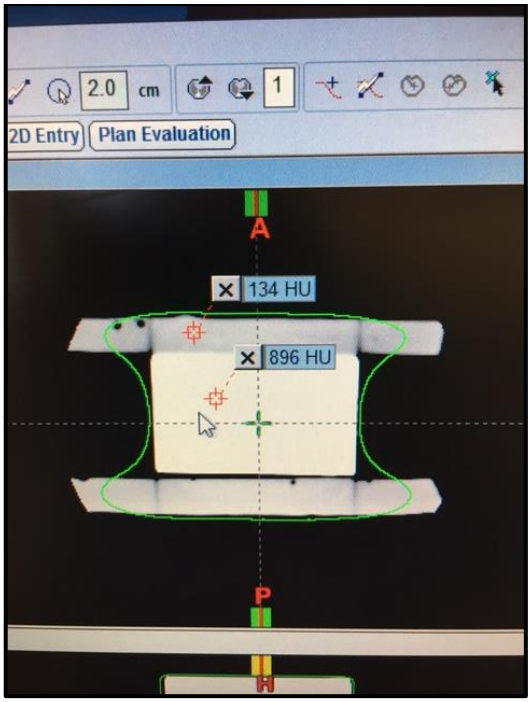

Figure 4.21: CT scan of Encapso K to verify density

Two clear liquids (part A and B) are mixed in equal amounts (parts) after vigorously shaking to mix each one separately before commencing with the mixing of the two liquids. Mix for at least five minutes, making sure that all is blended especially against the sides of the container. The mixture at first appears to be cloudy but will clear after a few minutes. Please see Addendum D for Specifications and Manual of Encapso K.

It is now ready for pouring into the thorax shell. The printed ribcage and lung shells were fixed in position with fishing line to keep it up straight while hanging in the thorax with the silicon to set around it; it was left to set over a couple of days.

Figure 4.22: Ribcage suspended in shell and fixed in frame

(a)

(b)

(c)

Figure 4.23: (a+b) lung cavities within ribcage handing down
(c) Weight bearing down in lung cavities to not float in liquid

(a+b) lung cavities within ribcage hanging upside down (c) Weight bearing down in lung cavities to not float in liquid

Refer to Addendum E for the complete pouring process and set of the Encapso K compound.

Figure 4.24: Complete thorax phantom

A CT scan was performed on the customised phantom. This was done to evaluate the phantom against the retrospective patient CT data from which the original files were extracted to use in the 3D printing process as well as organs at risk that were simulated to create and/or build this customised phantom.

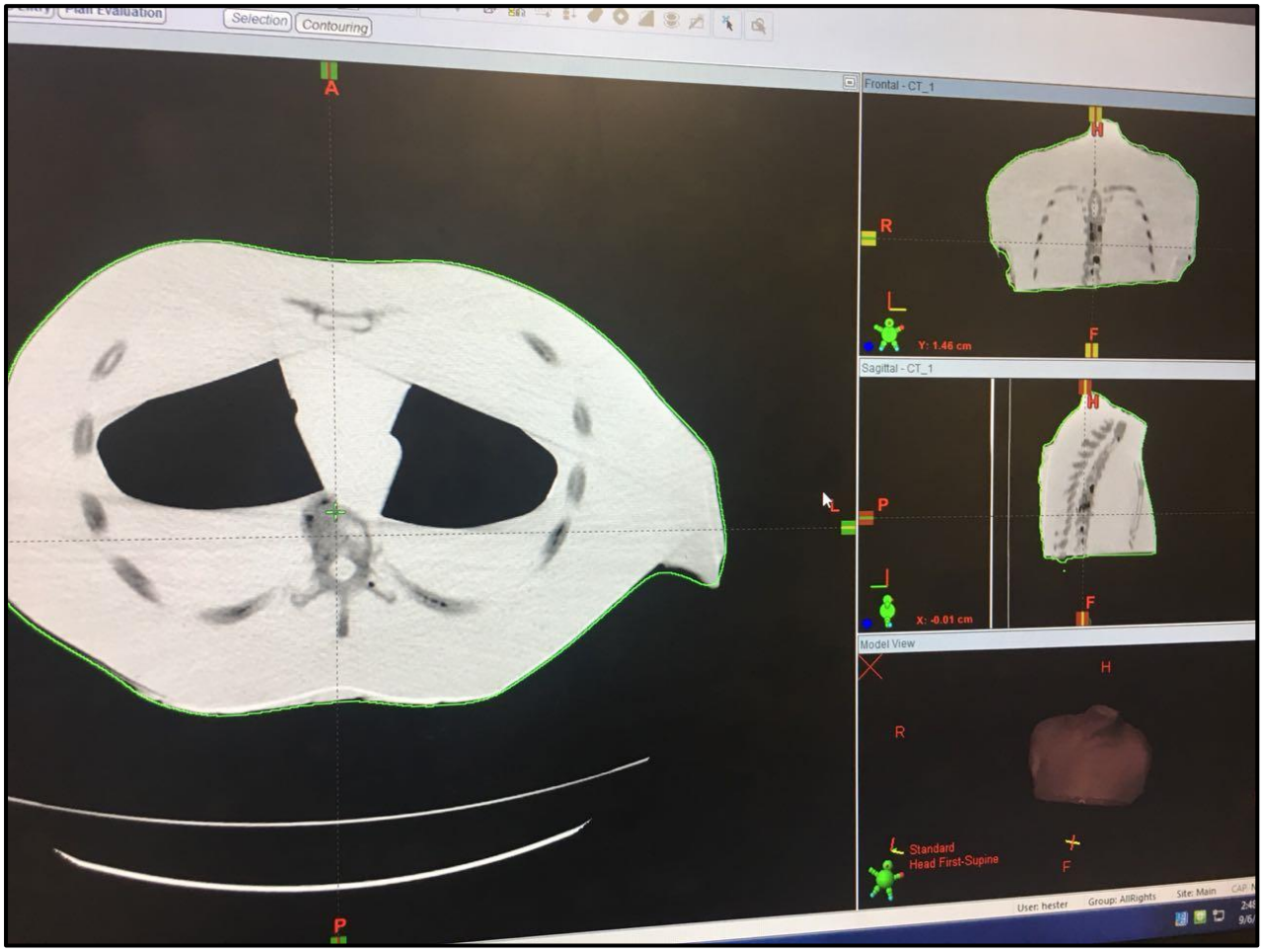

Figure 4.25: CT scan of finished phantom

4.2.2.3 Lung

The organ at risk that needs to be simulated in the phantom is the lungs. To keep the phantom simple, it was decided for this study to keep the lungs as air cavities.

4.2.2.4 Ribcage

As was previously mentioned, to find the correct match for rib bone, samples were printed, scanned and evaluated to check density.

The first 3D printer to be used in this study was from Biomedical Engineering, University of Cape Town. The 3D printer is a Zortrax M200, desktop size.

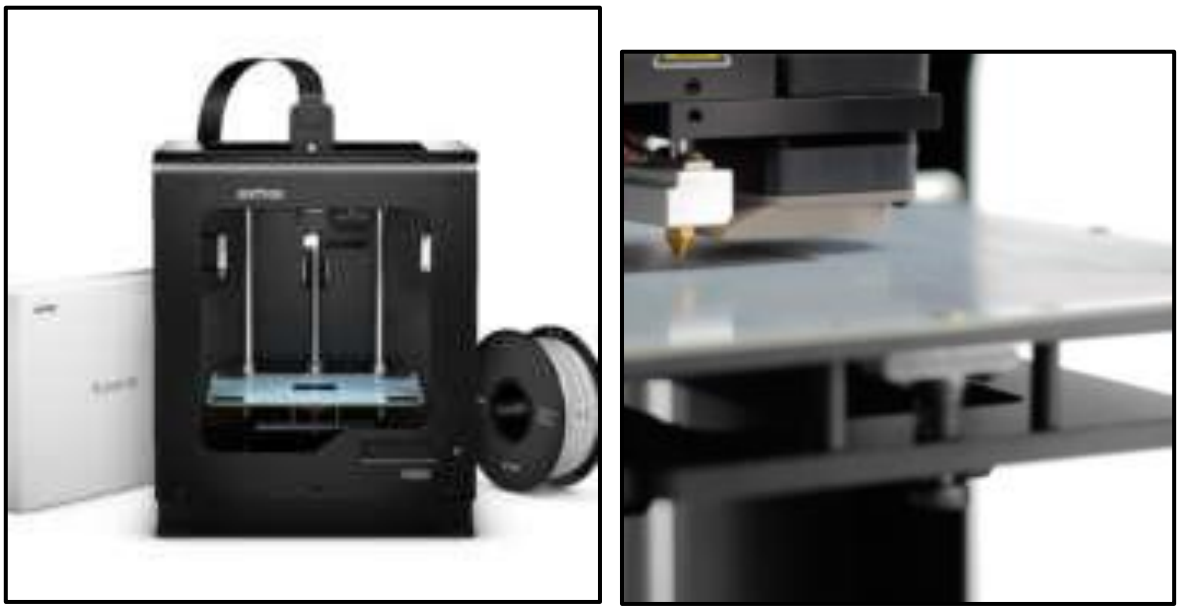

Figure 4.26: Zortrax M200 desktop 3D printer

Although we knew the printing size of the printer was a problem, the first step was to match the density and the relevant materials or components used during the printing process.

Barium powder was supplied by Groote Schuur Hospital. It is a dense powder compared to nylon. The 3D outer housing (printed in a matrix) of the sample blocks (dimensions of 10.0 x 10.0 x 1.0cm) was printed with nylon and filled with barium powder. The red sample was only partially filled with barium and the pink sample block was fully filled with barium. The powder was evenly spread with a knife, but 5% of the periphery holes were partially filled.

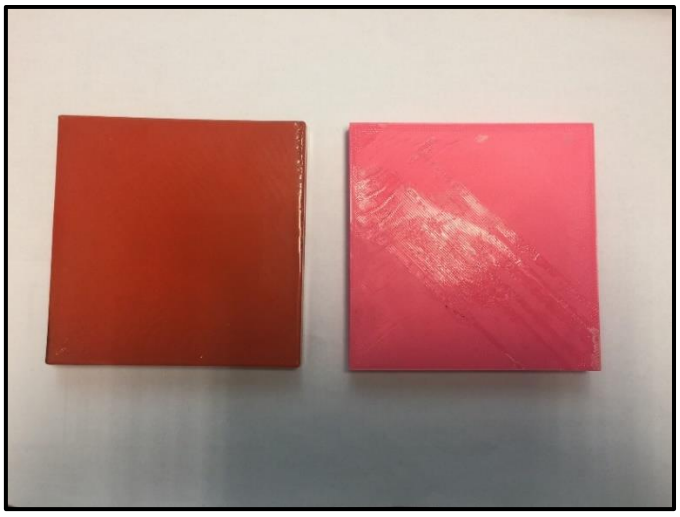

Figure 4.27: Red medium filled with barium and pink is full filled with barium powder

Alone the barium powder filled matrix did not fulfil the density requirement that we needed to replicate rib bone. This was due to not completely being able to fill the matrix that was printed on the 3D printer or housing. Also, if this was true for only a simple matrix printed, then a complex 3D print, such as a ribcage, will not be successful. A suggestion was to mix the barium powder with water to have a liquid that would fill the holes. The following concerns were raised by Biomedical Engineering:

Concern 1: The plate on which the 3D printing happens is 110 degrees, enough to evaporate water; and

Concern 2: The hot water might also eat into the material and deplete it.

Therefore, in their opinion the liquid barium technique might not work and was abandoned.

Another denser material to use in the 3D printer was sourced and the following material was suggested:

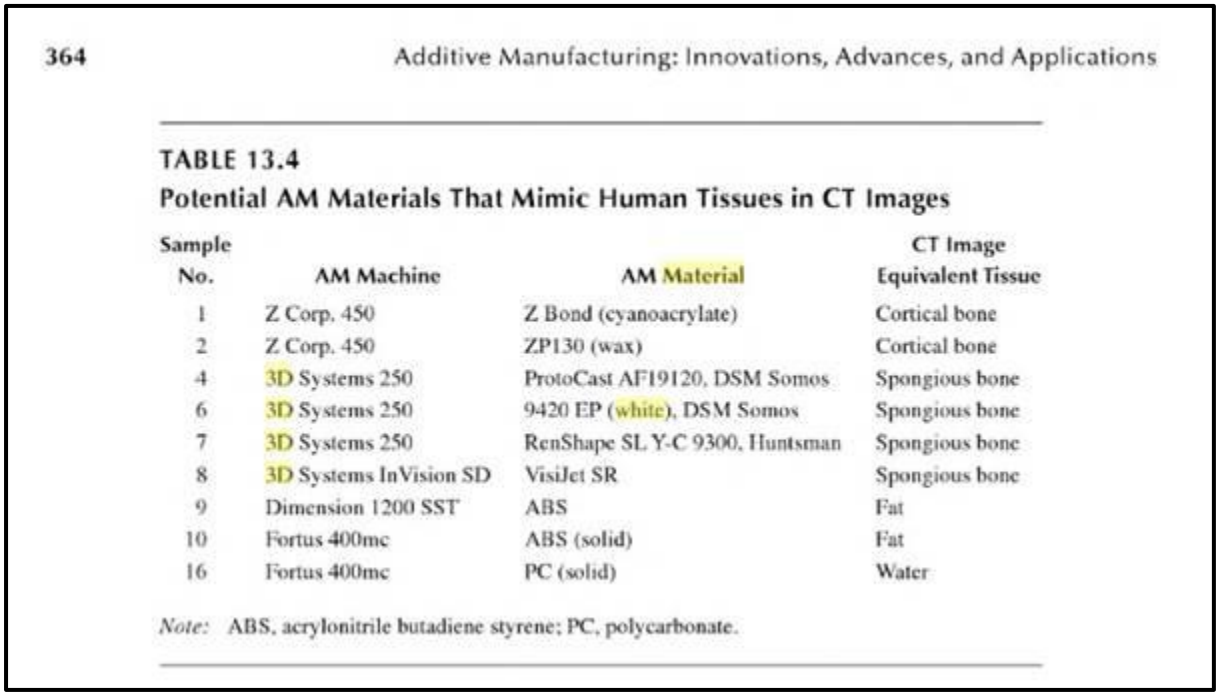

364 Additive Manufacturing: Innovations, Advances, and Applications

TABLE 13.4
Potential AM Materials That Mimic Human Tissues in CT Images

Sample No.	AM Machine	AM Material	CT Image Equivalent Tissue
1	Z Corp. 450	Z Bond (cyanoacrylate)	Cortical bone
2	Z Corp. 450	ZP130 (wax)	Cortical bone
4	3D Systems 250	ProtoCast AF19120, DSM Somos	Spongious bone
6	3D Systems 250	9420 EP (white), DSM Somos	Spongious bone
7	3D Systems 250	RenShape SL Y-C 9300, Huntsman	Spongious bone
8	3D Systems InVision SD	VisiJet SR	Spongious bone
9	Dimension 1200 SST	ABS	Fat
10	Fortus 400mc	ABS (solid)	Fat
16	Fortus 400mc	PC (solid)	Water

Note: ABS, acrylonitrile butadiene styrene; PC, polycarbonate.

Table 4.4: Potential additive manufacturing materials
(TS Srivatsan, 2015)

TABLE 13.3
CT Number, Standard Deviation of CT Numbers, and Density

Sample No.	Manufacturer and Machine	Material	CT Number	Standard Deviation	Density (g/cm³)
1	Z Corp. 450	Z Bond (cyanacrylate)	850.17	51.28	1.44
2	Z Corp. 450	ZP130 (wax)	1146.41	71.72	1.64
3	EOS P100	Nylon 12 (polyamide)	−17.80	29.88	1.00
4	3D Systems 250	ProtoCast AF19120, DSM Somos	168.50	28.57	1.20
5	3D Systems 250	Watershed XC11122, DSM Somos	320.82	27.62	1.17
6	3D Systems 250	9420 EP (white), DSM Somos	251.57	26.35	1.19
7	3D Systems 250	RenShape SL Y-C 9300, Huntsman	142.43	28.67	1.22
8	3D Systems InVision SD	VisiJet SR	126.44	26.05	1.18
9	Dimension 1200 SST	ABS	−115.74	34.43	0.96
10	Fortus 400mc	ABS	−102.86	32.61	0.97
12	Fortus 400mc	ABS+	−358.93	31.08	0.79
14	Fortus 400mc	PPSF	151.60	46.01	1.17
16	Fortus 400mc	PC	−26.37	29.88	1.11
18	Fortus 400mc	PC/ABS	−30.21	26.34	1.05
19	Fortus 400mc	PC/ABS	110.36	8.86	1.17
20	Objet500 Connex	Vero White	99.75	5.06	1.17

Table 4.5: Properties of additive manufacturing materials
(TS Srivatsan, 2015)

Unfortunately, the Z Bond (cyanacrylate) material was not compatible with the Zortrax M200 3D printer used at Biomedical Engineering Department, University of Cape Town as it uses only LPD (Liquid Plastic Deposition) technology. The Zortrax M200 is best for rapid prototyping.

Another company, Rapid 3D in Howick, KwaZulu-Natal, South Africa, was researched as their business is 3D printing and supplying of 3D printers. Again, samples were requested from the company with the printer 3D Systems ProX SLS 500 using Selective Laser sintering (SLS) and fusion Type laser.

Figure 4.28: ProX SLS 500 3D Printer

The build material used in the ProX SLS 500 Printer is DuraForm ProX PA mixed with calcium sulfate hemihydrate, both a physical appearance and state of a white powder. Specification sheets available in Specification and Manual addendum.

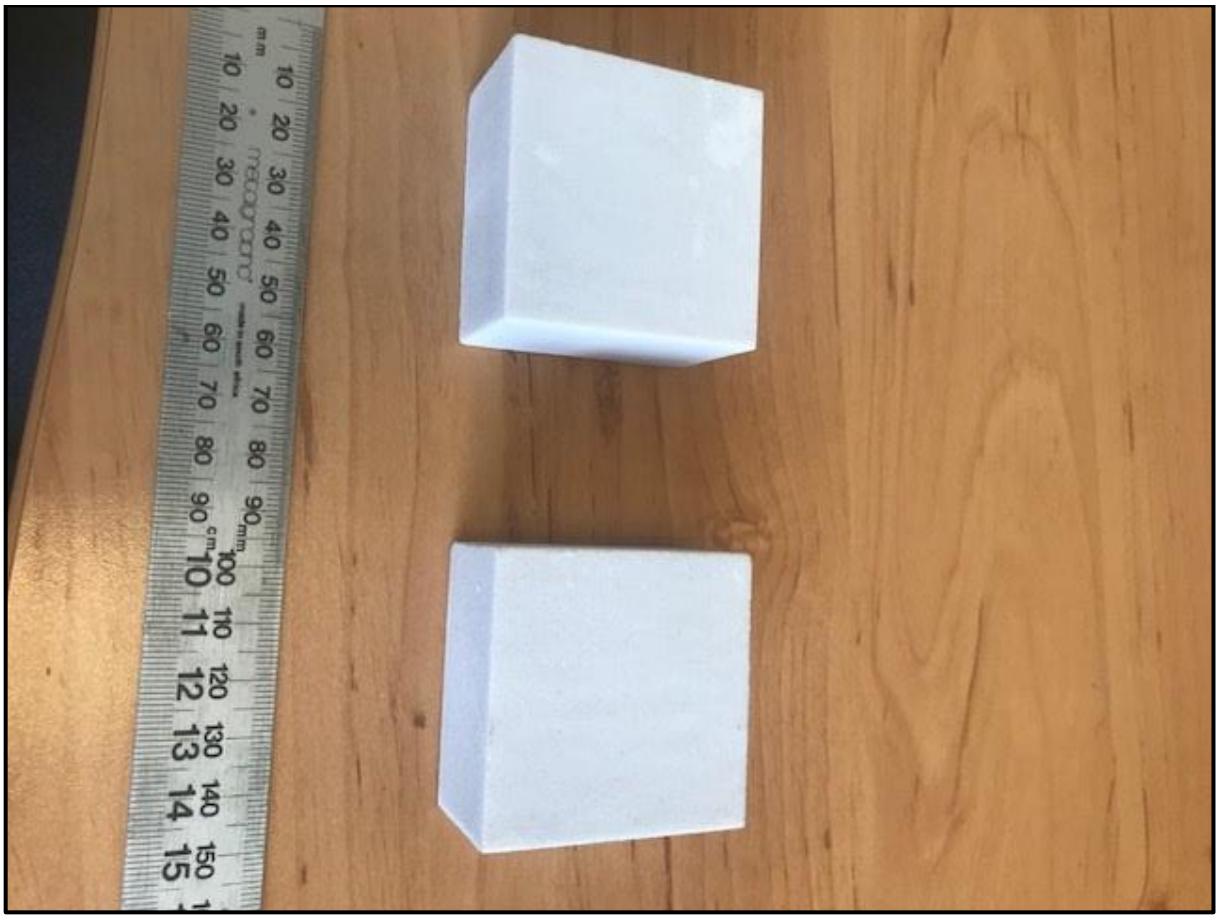

Figure 4.29: 3D blocks from Rapid 3D

To assess the density of the blocks, a CT scan was performed to extract the Hounsfield number (HU), and during conversion of CT to Electron Density (ED) values in the Treatment Planning system. It was confirmed that the density is correct and what was needed for this study. As per the previous reference in Table 4.5 for additive material, this correlates well with the values (CT number 850.17 and density 1.44g/cm^3) between 896 and 1079HU or 1.653ED from the sample blocks (TS Srivatsan, 2015).

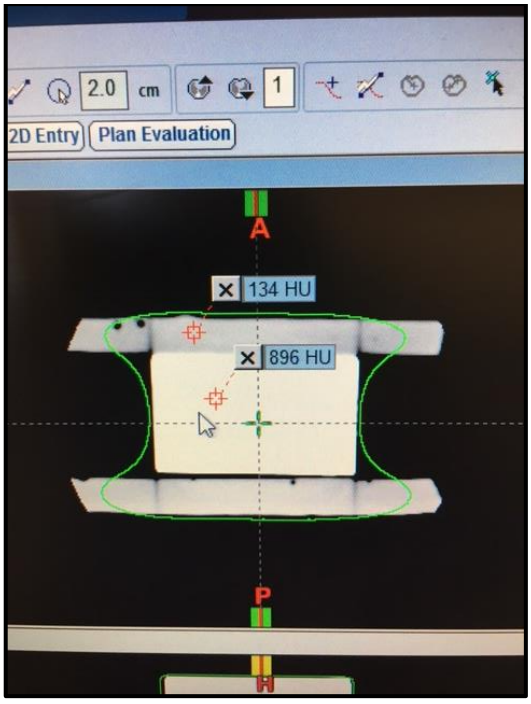

Figure 4.30 (a)

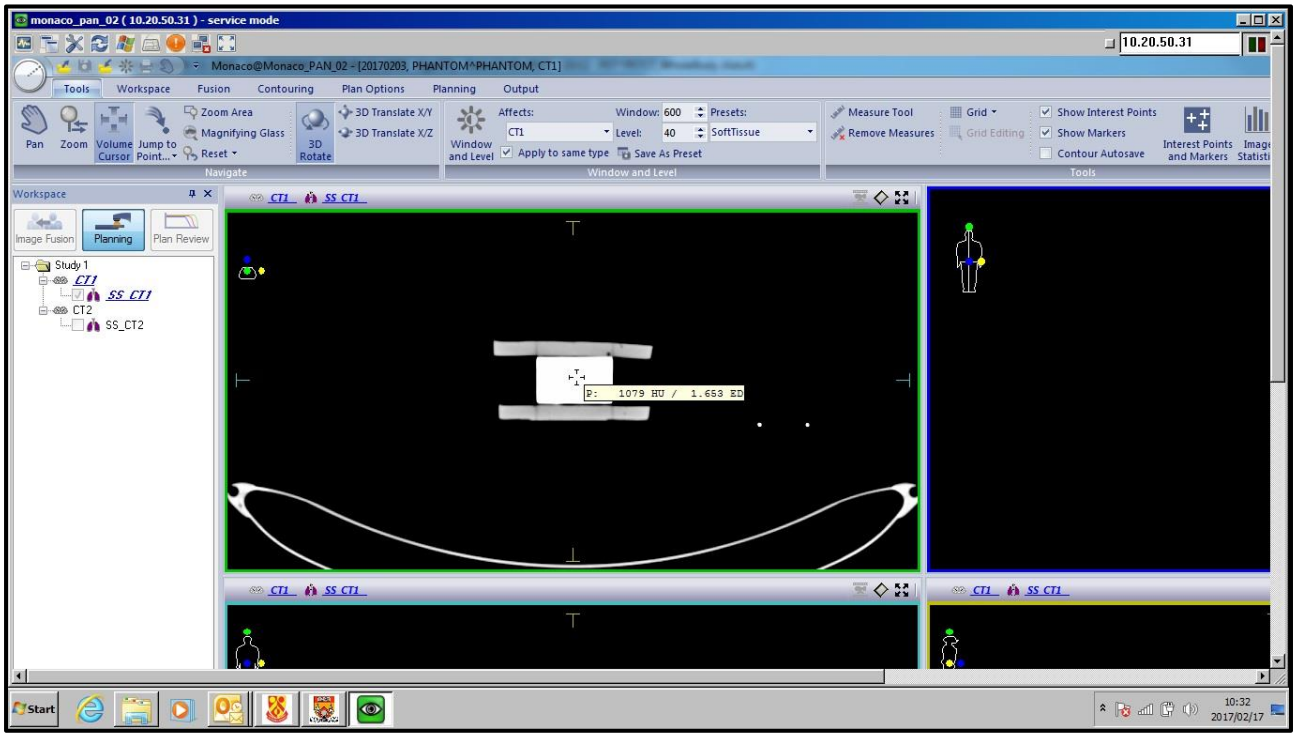

Figure 4.30 (b)

Figure 4.30: TPS evaluation of 3D sample blocks from Rapid 3D

As discussed under 'Materials and Methods – Customised Phantom design', a .stl file was generated from the CT scan and printed on a ProX SLS 500 3D printer. The measurements

and size of the ribcage were checked against the maximum printing size of the 3D printer as well as the thorax shell made.

	ProX SLS 500
Max build envelope capacity (X x Y x Z)	15 x 13 x 18 in (381 x 330 x 460 mm)
Build material	DuraForm ProX PA DuraForm ProX GF DuraForm ProX HST
Layer thickness range *(typical)*	0.003 – 0.006 in (0.08 – 0.15 mm) *(0.004 in, 0.10 mm)*
Volume build rate	1.8 l/hr
Powder recycling and handling	Fully automatic

Figure 4.31: Table ProX SLS 500 manual specifications
(Specifications and manual addendum)

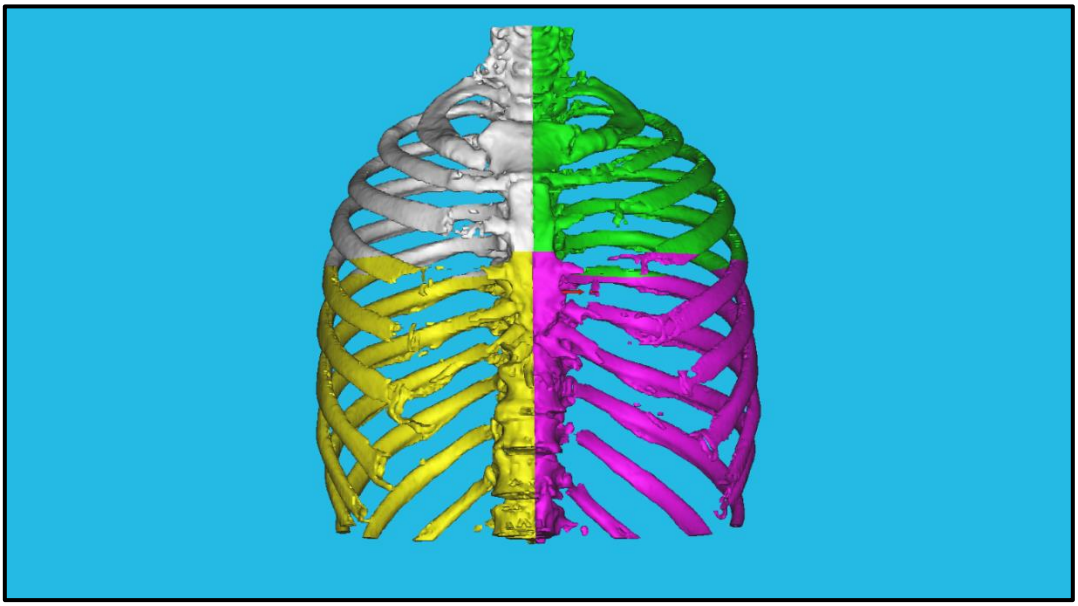

Figure 4.32: Ribcage reconstructed from CT scan in Mimics Materialise (CAD application)

The 3D print was received from Rapid 3D company and the ribcage was scanned and evaluated against the sample blocks originally tested from the company. First, during the courier process, two ribs broke off and had to be repaired. An enquiry was made as to what adhesive could be used and it was advised that a standard two-part epoxy can be used (Pratley's Quick Set Clear Epoxy). Due to the composition of the glue, a small part was first mixed and scanned on the CT scanner to ensure there are no artefacts from the glue due to possible metal or other materials that could cause 'streaky' artefacts. This would cause inaccuracies during dose calculations on the TPS. No artefacts were found when the two-part epoxy was scanned.

Figure (a) (b)

Figure 4.33: 3D print of ribcage (a) Sternum (anterior) and (b) Vertebrate (posterior)

The values obtained from the CT scan and imported into the TPS for density values were far less than the sample blocks tested before.

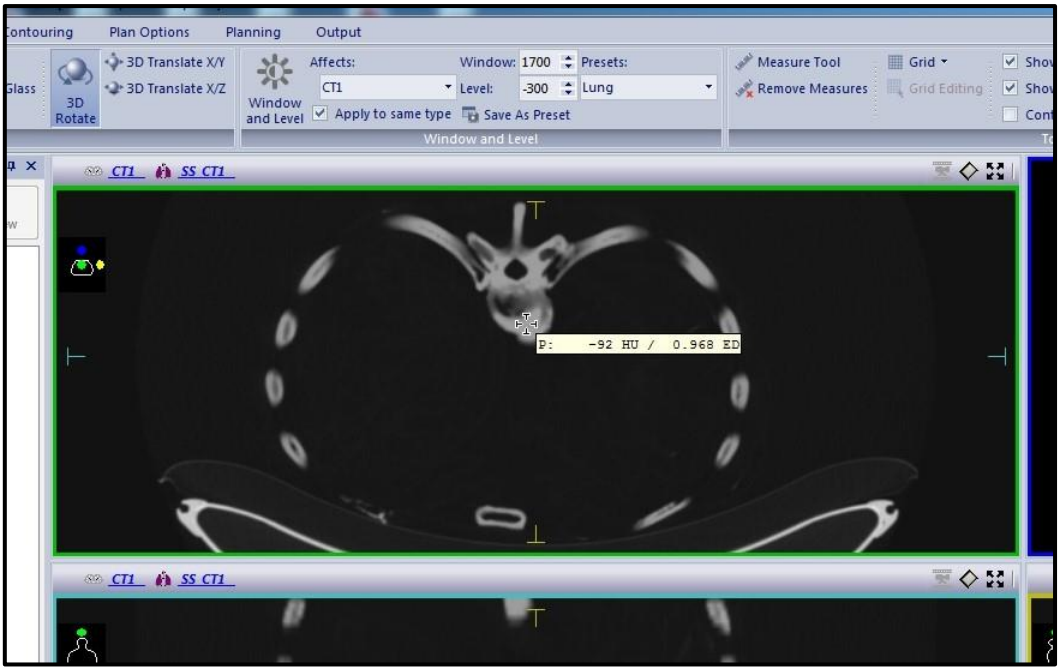

Figure 4.34: 3D printed ribcage values in TPS

A reprint was requested from the 3D printing company of only a section of the ribcage to verify that not the same material was used during the sample blocks and first print of the ribcage. This was established and confirmed by the company. This was due to two reasons (a) the original material from the sample blocks was very fragile due to the denser composition of the material and (b) the complexity of the contour or object (ribcage) that needed to be printed. Instead, the normal nylon material was used as it is much tougher and easier to work with. The reprint section was checked to make sure that sternum, vertebrae and ribs were included in the printing process to test if the denser material was true as originally speculated.

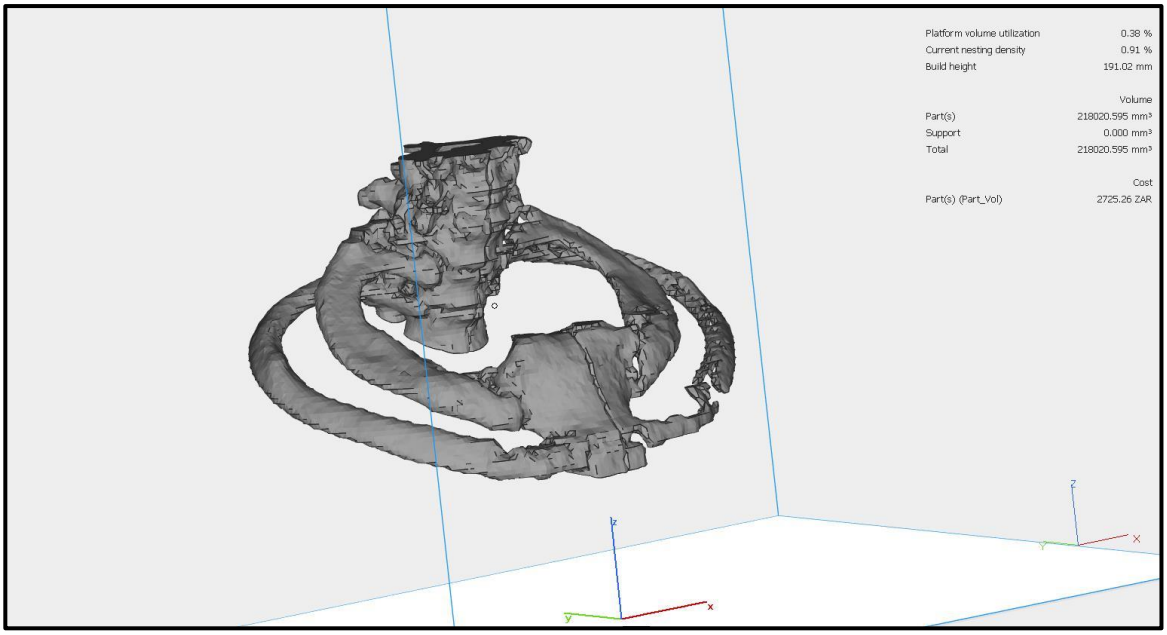

Figure 4.35: Reprint of section of ribcage done in Mimics Materialise (CAD application)

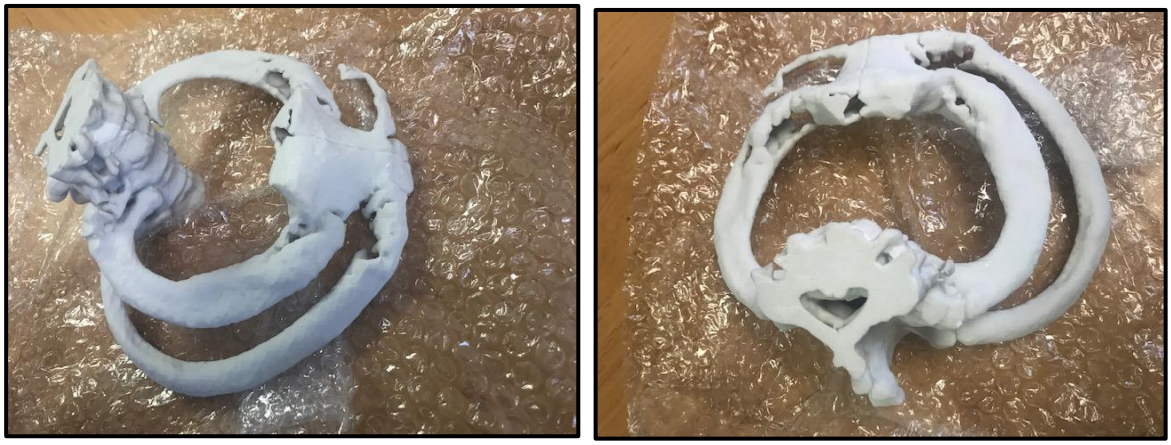

Figure 4.36: Reprint of section of ribcage with sternum, vertebrae and ribcage

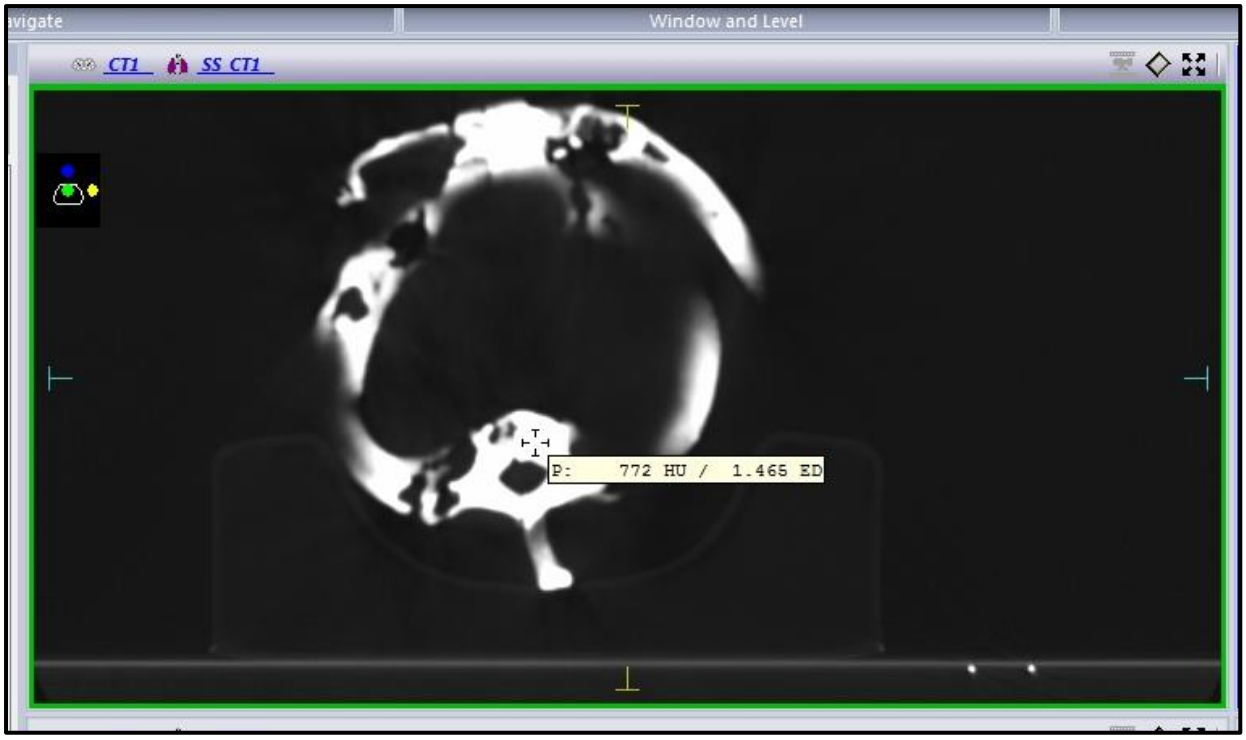

Figure 4.37: CT scan of reprint of section of ribcage

The re-print of the section of the ribcage with the denser material composition as with the sample blocks proved to have the correct density as specified for cortical bone (TS Srivatsan, 2015).

4.2.3 Phantom motorisation

To be able to replicate movement of the tumour in the lung and therefore mimic a breathing cycle or breathing path of a patient, a motorised arm needs to be designed. This motorised arm will follow the path on the template plate (see Figure 4.6, page 51) that replicates a patient's breathing cycle.

4.2.3.1 First design

As discussed before under 'Customised Phantom Design', below is a simplistic first design of a customised phantom with a motor propelling an arm at a designated speed and cycle/path to mimic the movement of the tumour in the lung cavity.

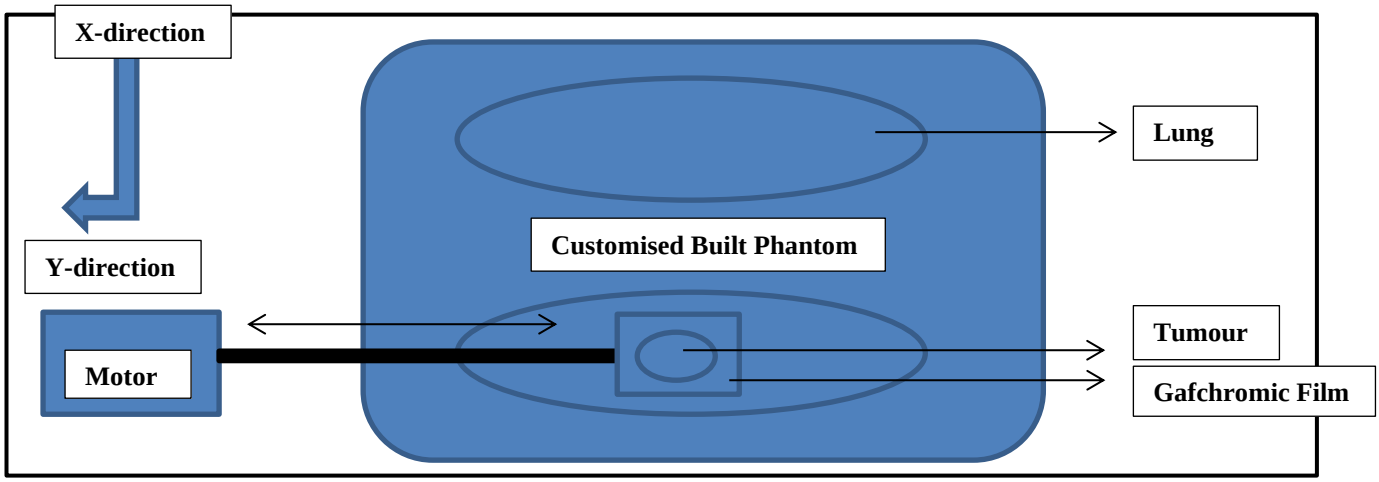

Figure 4.38: Schematic top/anterior view

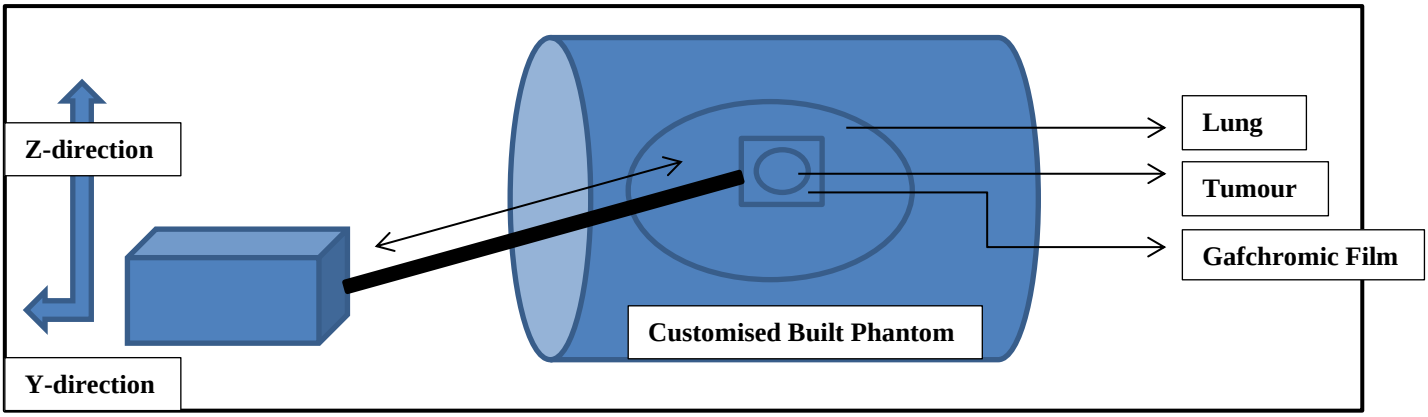

Figure 4.39: Schematic side/lateral view

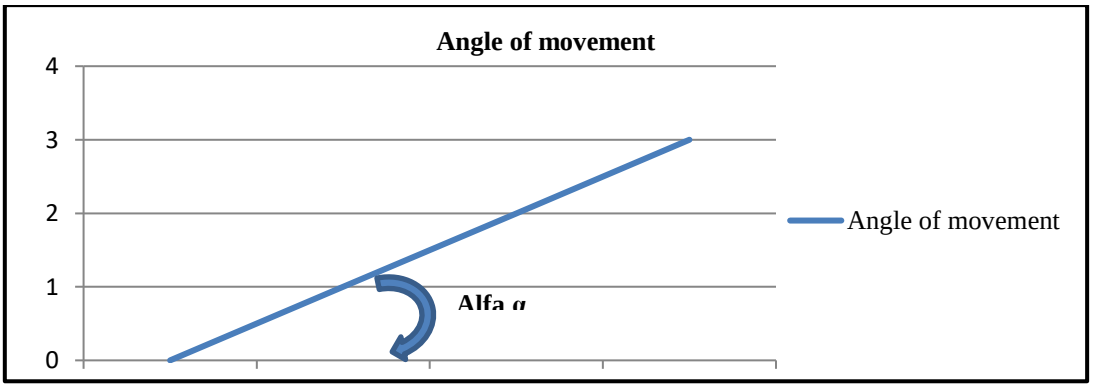

Figure 4.40: Motor angle

The fourth dimension (time) is incorporated with this motion taking place during the treatment.

4.2.3.2 Second design

An adaptation to the first design was necessary to get a practical solution for the tumour movement that the arm will mimic in the customised phantom.

A height adjustable arm on the first section of the design is for positioning in the lungs in the anterior-posterior direction as well as for lateral adjustment. Once the position in the lung has been achieved, the next section will be the tracking of the path of the tumour in the lung cavity according to the 4D CT scan set. There are two components to this section: the actual path that the arm will follow; and the motor that will drive this arm in the path at the designated speed, again according to the information extracted from the 3D CT scan set. The path was explained under 'Results – Path of the breathing cycle'. The motor is a simple design that will run against revolutions according to the breathing cycle in seconds and revolutions or completion of the path (in seconds) per minute. The motor is small and lightweight as it is fixed to the arm in the first section of the design.

The third section of the design will hold the actual target and film in a vertical and/or horizontal plane for dosimetric measurements. The template path is followed with the motorised arm in the second section. The third section of the design is in the customised phantom in the lung cavity.

The whole mechanism or design described above is positioned on a calibrated or marked plate to set and have the initial position or zero position relative to the phantom. This is necessary to monitor and record the exact movement of the tumour during the breathing cycle. This is a manual placement of the mechanism.

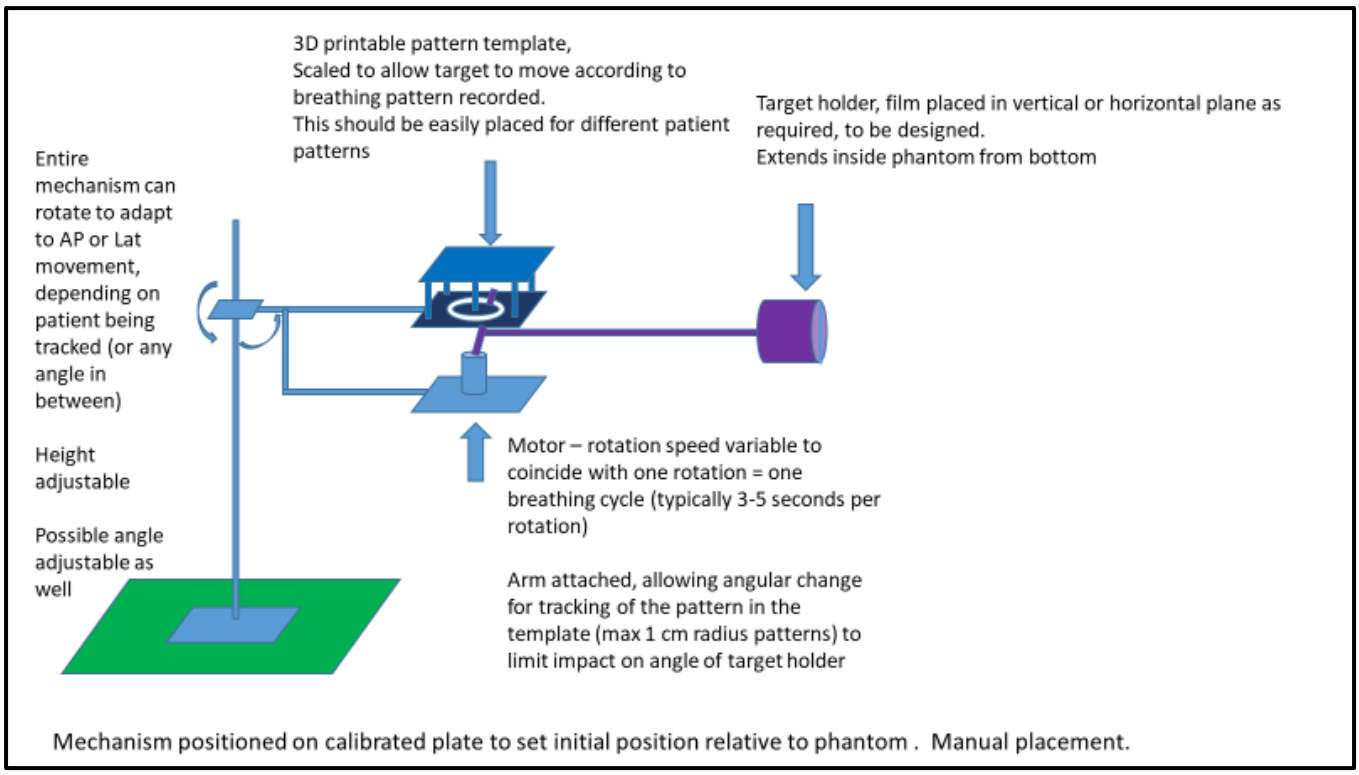

Figure 4.41: Second motorised arm design

4.2.3.3 Third design

After completion in theory of the second design, Biomedical Engineering, University of Cape Town was approached for assistance. The purpose of the customised build phantom was explained, and the third design was proposed by the Biomedical Engineering Department.

The first section is still an adjustable arm, but just more robust and stronger to hold and balance the entire ensemble.

The path template in the second section is refined in this design. Due to the small movements encountered in some of the 4D CT study sets, a one-to-one path is not possible. A scaling factor must be incorporated to assist in the motorised movement of the arm, otherwise this will be practically not a viable solution to try and follow these very small movements. This part is positioned inside the lung cavity and is scaled proportionally from the path template to the actual movement that is needed to be comparable to the 4D CT scan set. These movements are in some cases extremely small, therefore the scaling of the path from the template to the film to be able to mimic this movement realistically.

Only 2D movements are still available in this design.

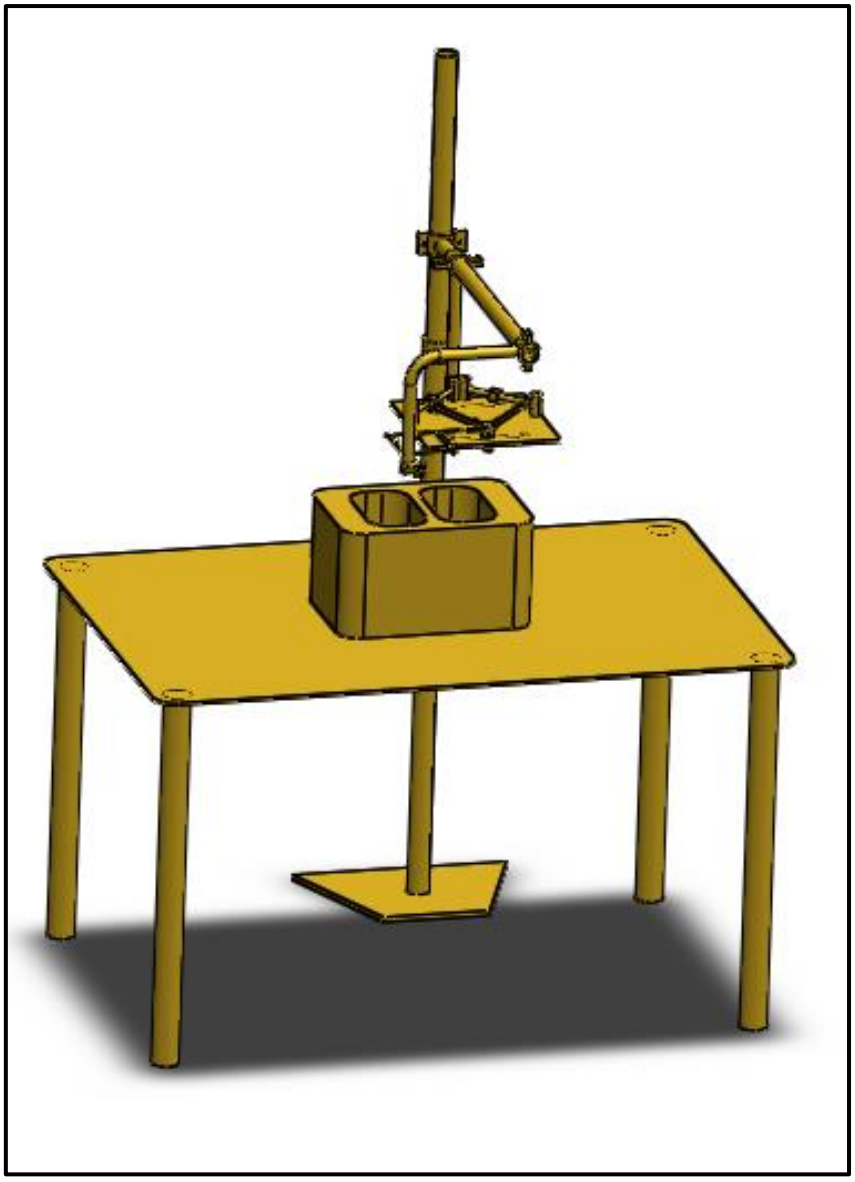

Figure 4.42: Third design of motorised arm
(Software used for 3D modelling: Solid work, version 2015)

Some parts of the assembly/motorised arm in this design can be 3D printed, but not all at this stage. The name of the 3D printer that can be used is the Zortrax M200. The expected number of components that can be printed is more than 30 components.

4.2.3.4 Fourth design

For this design a correction was made in terms of the orientation of the phantom and the placement of the motorised arm. As can be seen from the third design, the arm was moving in an anterior-to-posterior direction, which is not a realistic replication of a patient on a CT scanner bed or linear accelerator bed and treatment of the patient. So, in this design two 90° angles are incorporated to get the desired supine position of the phantom.

The arm into the customised build phantom was extended as well, as the path template was in the field of view of the CT scanner and linear accelerator. This is crucial as the template will have an influence on the imaging and attenuation on the CT scanner and linear accelerator in terms of artefacts and dosimetric calculations, respectively.

Again, only 2D motion is enabled to track the path of the breathing cycle and not 3D as originally envisaged.

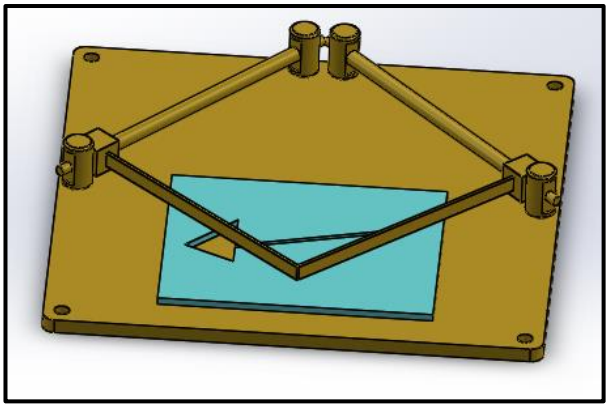

Figure 4.43 (a)

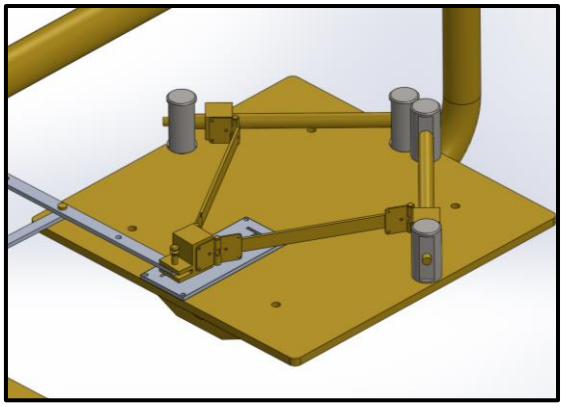

Figure 4.43 (b)

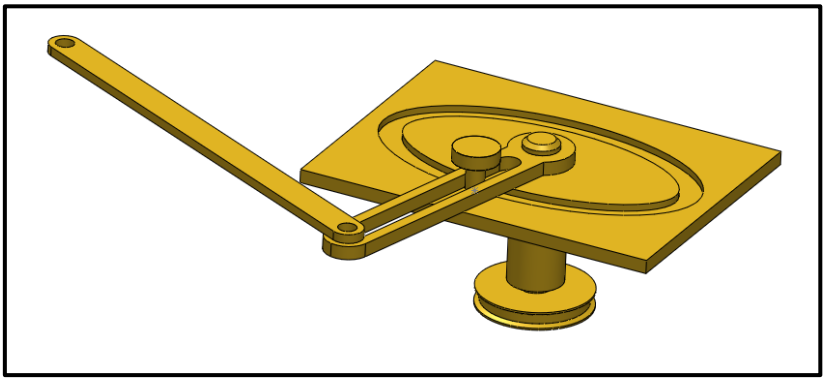

Figure 4.43 (c)

Figure 4.43: Plate seat assembly

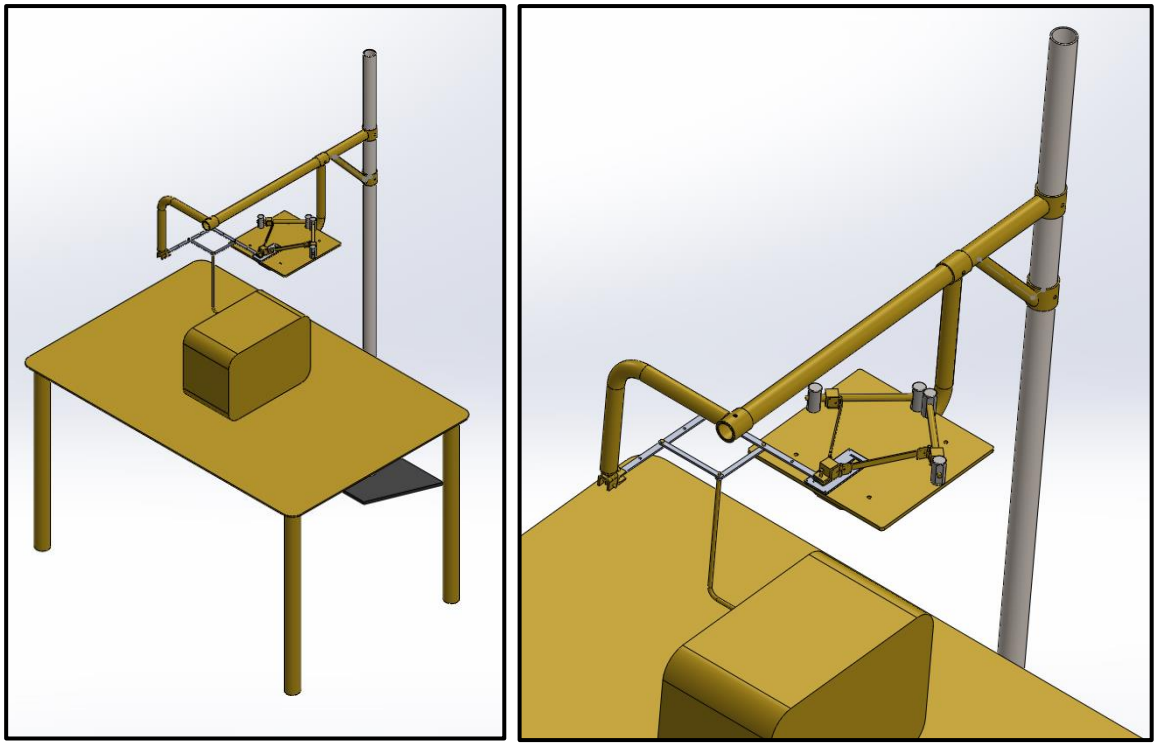

Figure 4.44 (a) Figure 4.44 (b)

Figure 4.44: Fourth design of motorised arm

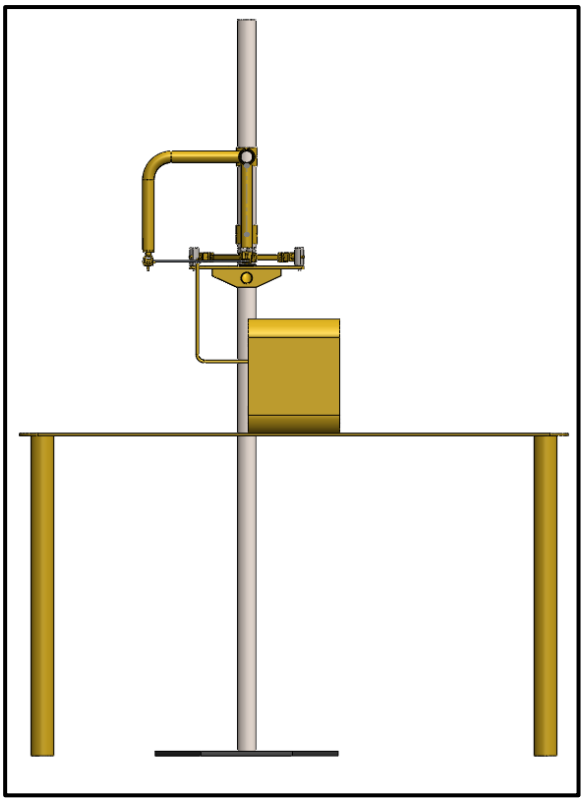

Figure 4.45 (a)

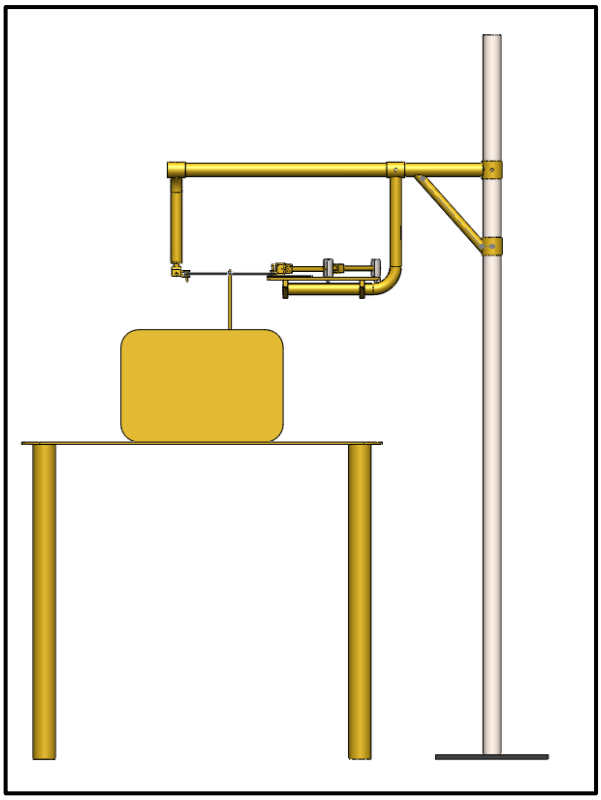

Figure 4.45 (b)

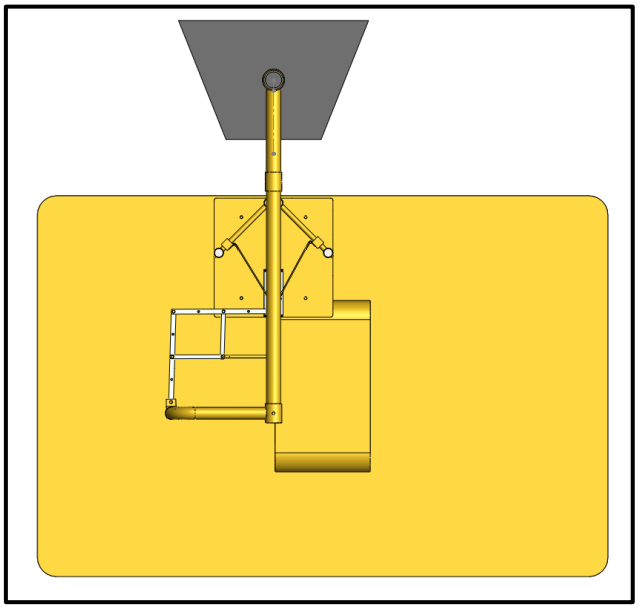

Figure 4.45 (c)

Figure 4.45: Different views of the fourth design (a+b) Side views (c) top view

4.3 Dosimetric results

4.3.1 Linac based results

The following results were obtained from the linac based measurements for 100MUs, isocentric setup – 100cm SAD, 5cm measurement depth, with a Farmer type chamber for both a 10x10cm and 5x5cm field size in terms of transmission of the silicon or tissue equivalent material and the 3D print or bone equivalent material. Detailed measurement values are given under Annexure F.

Transmission of silicon			
6MV		10MV	
10x10	5x5	10x10	5x5
0.8215	0.7896	0.8526	0.8269
Transmission of 3D prints			
6MV		10MV	
10x10	5x5	10x10	5x5
0.7791	0.7446	0.8141	0.7868

Figure 4.46: Transmission of silicon and 3D print in table format

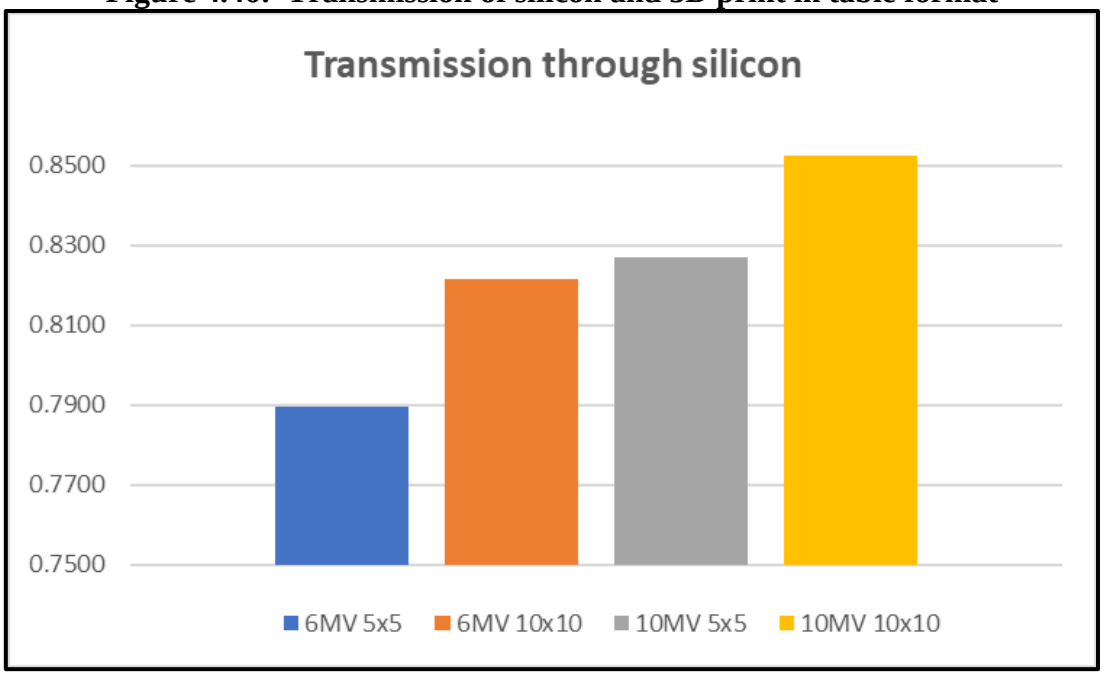

Figure 4.47: Transmission of silicon in graph format

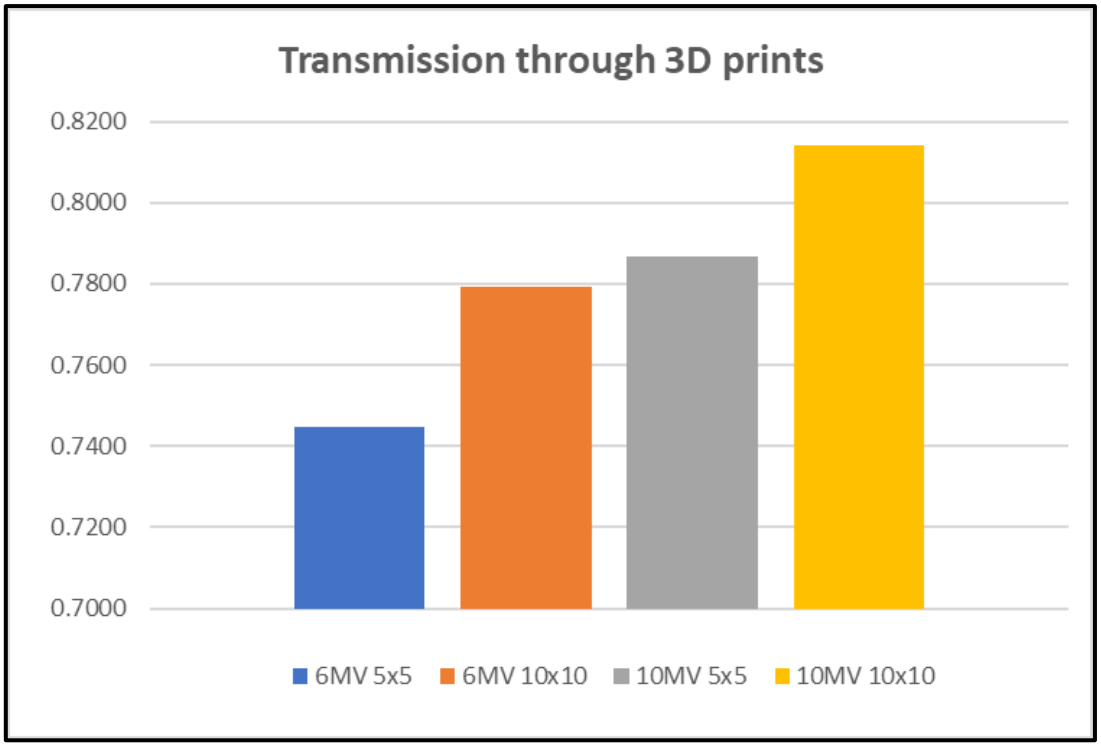

Figure 4.48: Transmission of the 3D prints in graph format

4.3.2 Treatment planning system calculation results

The results were obtained from the Treatment Planning Systems, Elekta Monaco and Varian Eclipse, at the same point of measurement as depicted in 'Customised Phantom Design' under 'Methods and Materials'.

4.3.2.1 Monaco treatment planning system

In the Monaco treatment planning system, Monte Carlo calculations are used. For tissue equivalent materials, the dose difference between the dose to medium and dose to water calculation properties is said to be 1-2%. Whereas for high density materials such as bone or metal it could be as high as 12%.

4.3.2.2 Eclipse treatment planning system

4.3.2.2.1 Anisotropic Analytical Algorithm (AAA) calculation

The Anisotropic Analytical Algorithm is based on the superposition/convolution method. Primary and scatter components are used from Monte Carlo to calculate dose by superposition of dose kernels and is done in the beamlet and lateral directions. For the beamlet direction it

includes radiologic scaling of dose deposition functions, whereas the lateral directions are based on electron density scaling of photon scatter kernels (Rana, 2014).

The calibration curve of the CT scanner is used to convert the Hounsfield Unit value to relative electron density (*Eclipse Photon and Electron Algorithms Reference Guide*).

4.3.2.2.2 Acuros External Beam Algorithm (Acuros XB) calculation

Acuros was developed as a new grid-based Boltzmann solver (GBBS) from Atilla and optimised for radiotherapy dose calculations. Atilla is a general-purpose radiation transport software that makes use of raytracing. The GBBS solves the linear Boltzmann transport equation (LBTE) that describes macroscopic behaviour of ionising particles as they travel through matter and interact with surrounding matter in each volumetric domain. There is a general trade-off between speed and accuracy, and this is the main difference between the Monte Carlo simulations (EGSnrc code) and the Acuros software. Acuros has compared well with Monte Carlo simulations when performed to tight statistical uncertainties (Vassiliev, 2010).

The calibration curve of the CT scanner is used to convert the Hounsfield Unit values to mass density. From the derived mass density, Acuros XB determines the material composition of voxels in the image (*Eclipse Photon and Electron Algorithms Reference Guide*). From the material composition or properties of the voxels, the macroscopic energy deposition cross-section and atomic density is used for Acuros Dose to medium calculations. Energy deposition for water are again then used for Dose to water calculations (Rana, 2014).

Refer to Annexure G for detailed calculated values in table format on the two different treatment planning systems and their respective calculation algorithms as mentioned in the preceding paragraphs.

For the silicon or tissue equivalent material used, the difference between the TPS calculation algorithms versus the measured values on the machine is as shown below with the largest discrepancy for the 6MV, 10x10cm field size on Acuros Dose to Medium as -3.32%.

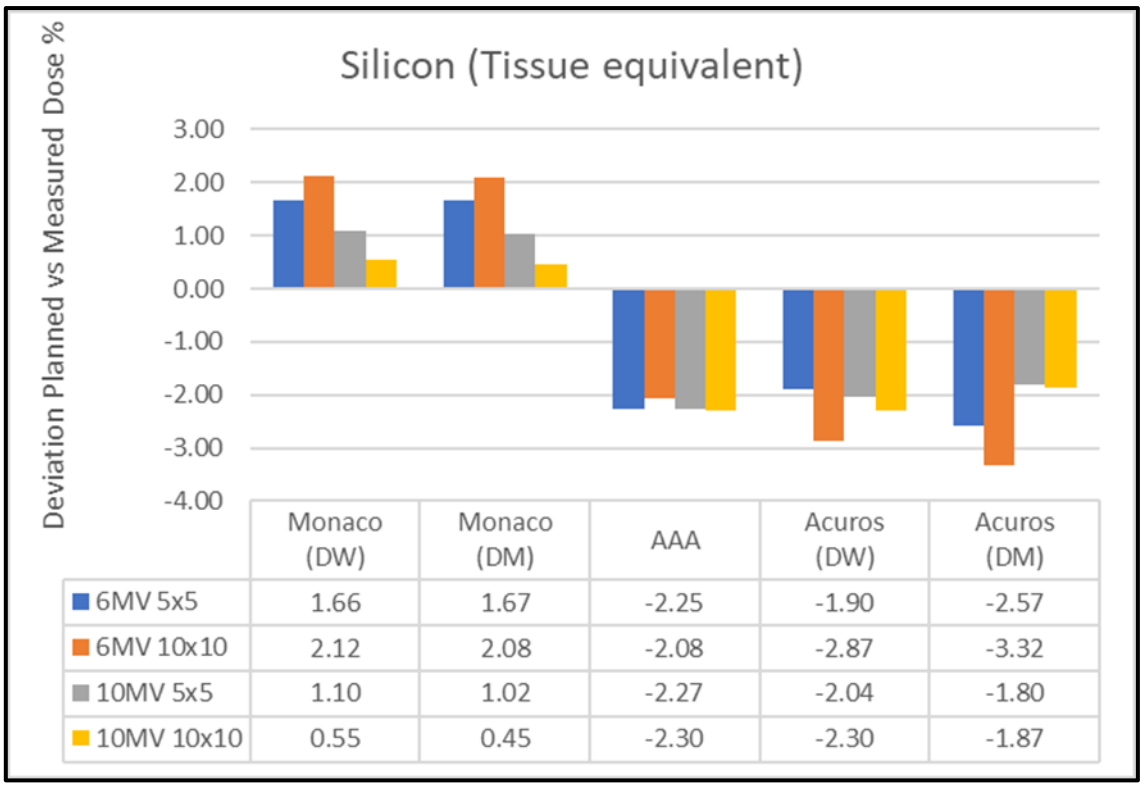

	Monaco (DW)	Monaco (DM)	AAA	Acuros (DW)	Acuros (DM)
6MV 5x5	1.66	1.67	-2.25	-1.90	-2.57
6MV 10x10	2.12	2.08	-2.08	-2.87	-3.32
10MV 5x5	1.10	1.02	-2.27	-2.04	-1.80
10MV 10x10	0.55	0.45	-2.30	-2.30	-1.87

Figure 4.49: Silicon or tissue equivalent material

In the case of the 3D printed material, which we took as equivalent to the density of bone, the biggest outlier was consistently 3.2% for the 6MV, 5x5cm field size for Monaco Dose to water and medium and Eclipse AAA.

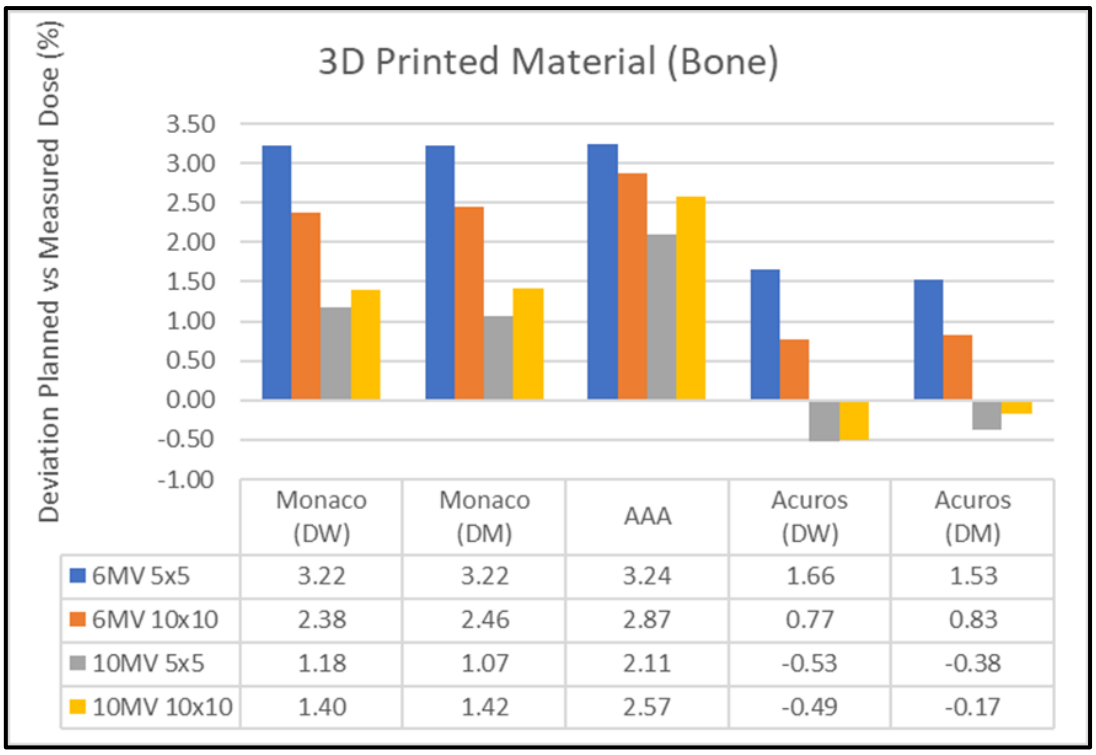

	Monaco (DW)	Monaco (DM)	AAA	Acuros (DW)	Acuros (DM)
6MV 5x5	3.22	3.22	3.24	1.66	1.53
6MV 10x10	2.38	2.46	2.87	0.77	0.83
10MV 5x5	1.18	1.07	2.11	-0.53	-0.38
10MV 10x10	1.40	1.42	2.57	-0.49	-0.17

Figure 4.50: 3D printed or bone equivalent material

5 Discussion

The three aims of this study:

1. Determine the movement seen in previously treated patients from the 4D CT scan sets and used during SBRT treatment;
2. Design a thorax phantom to mimic tissue characteristics and internal motion of the CTV; and
3. Compare the customised built phantom in terms of tissue characteristics applicable from the TPS to the linear accelerator.

5.1 Patient data collection

The breathing cycle obtained from the respiratory cycle in the 4D CT scan from each of the retrospective patients in this study indicated different paths in most of the patients. This cycle was tracked by means of an interest point that was dropped in the centre on each of the different CTVs created on each of the 10 phases from the 4D CT scan. From the 3D coordinates of the interest point, a path could be plotted to mimic the motion of the CTV in the lung in three dimensions. With this path tracked and running at the breathing rate of a patient, the fourth dimension can be included. But as discussed previously, this can be accomplished with an automated computer programme that can read the patients' breathing cycle details from the 4D CT scan, input of coordinates as depicted previously and executing the movement within the customised build thorax phantom. The result of these paths was dependent on the location of the CTV in the lung. As soon as the volume is adjacent or fixed to either the chest wall or medial wall of the lung/large vessels, the movement is restricted. When the volume is in the middle of the lung lobe or inferior, the tendency for movement is much more due to 'free' movement in the lung and/or the diaphragm that moves during inhalation or exhalation. The movement was confirmed with this study as 7mm in cranio-caudal as the most against the article (Wolthaus et al., 2008) that in the upper thorax the most movement was 3.7mm in cranio-caudal direction and in lower thorax also in cranio-caudal direction 11.6mm. The movement obtained from the 4D scans was smaller, however, to what originally was anticipated to be bigger movements.

5.2 Customised phantom design

From the eight patients used in the study only two patients had the same 2D movement, the other six patients had complicated paths that were tracked. These intricate paths had to be simplified to mimic and create desired patterns for a motorised arm that was able to be replicated on a scale for the customised phantom. Due to time constraints and resource limitations, only Patients 1, 4 and 5's paths were re-designed. This was to establish if the constraints and simplified versions of the original patient paths data could in fact be physically replicated on the motorised arm. This was indeed the case. Another constraint was the amount of movement in millimeters to try and replicate with a motor. The accuracy and detailed movement are a problem but can be accommodated in an automated computerised program to enable millimeter accuracy and movement.

As described for the fourth design, to realise and accommodate 3D movement in the motorised arm design, computerised planning of the 3D path of the tumour will need to be investigated. This falls outside the scope of this study. It can possibly be assessed for a future project to incorporate this specific design.

As for the structural design of the thorax phantom, alignment of the two halves of the body cast is very important. Fortunately, after trial and error, this could be rectified, and the manufacturing of the thorax phantom could continue. The perspex used for the outer shell as 2mm and lungs, thickness of 1mm, sufficed for the purpose of this study.

Soft tissue or water equivalent materials are always a challenge in radiotherapy and to be sustainable to be used over extended periods of time and the conditions where it is stored. Normal Apgar gel decays over a period and therefore is not useful in the making of a phantom that is supposed to last for some time. Water that is the next best solution, normally has the trouble of waterproofing and eventually the water also only lasts for a limited period. The silicone gel as a non-biological material used during this study was proven to be water equivalent or soft tissue equivalent, exactly what was needed. Even after months after manufacturing or building the thorax phantom and the use of this specific silicon material, there was only a slight discoloration of the material storing it under normal temperature and humidity conditions in an office. The photos shown in Figure 5.1 were taken more than a year after production of the thorax phantom.

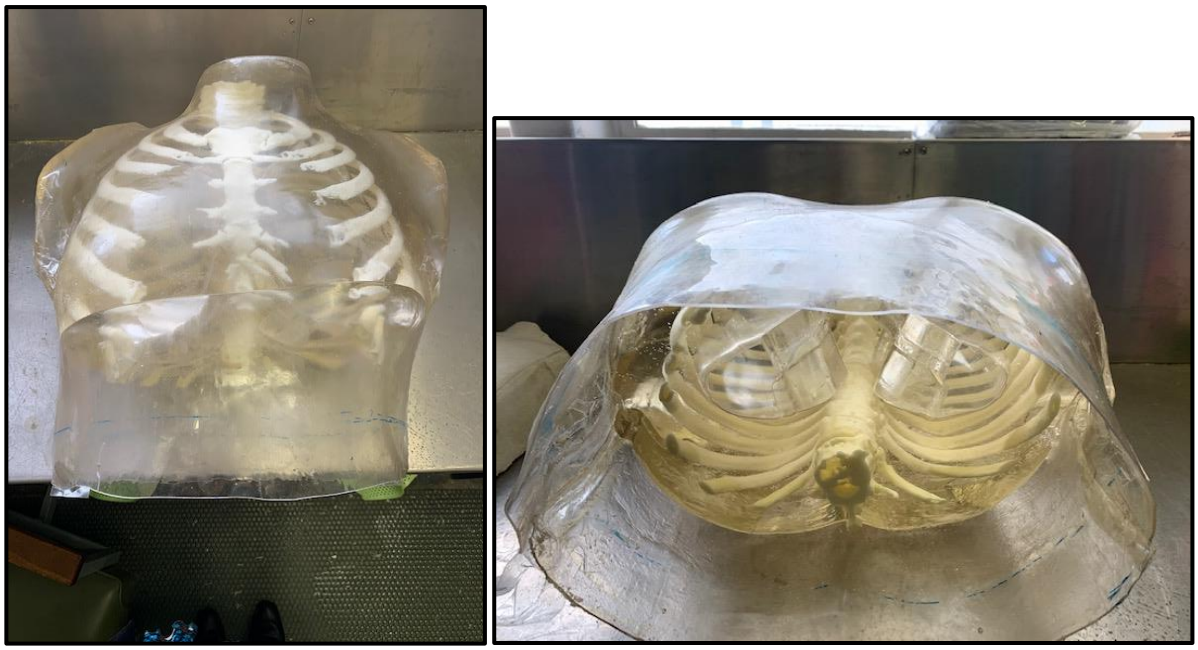

Figure 5.1: Customised made thorax phantom with only slight discolouration, but otherwise no other effects or biological decay

The only two drawbacks or negative points on this silicon is that it takes some time to set, especially the quantity that was needed to fill the outer thorax shell and during manufacturing, if spilled, it is very slippery and dangerous on the floor.

Another definite possibility of use for this silicon is to be used as a tissue equivalent material in build-up or bolus for patients with superficial lesions or separation less than 10cm. Due to the pliable capabilities of the silicon, it can be shaped and sized to any customised field size that is needed. A template mould will need to be made of the area applicable and then the silicon can be mixed and poured and set in the negative of the mould. This will then fit perfectly to the patients' anatomy and can be preferably scanned with the 'silicon bolus' material to accurately calculate the dose needed to the volume. Certain 3D printing techniques to simulate customised bolus are currently available on the market, but are extremely costly due to the printer needed, and the material used is not 100% soft tissue equivalent. This could influence the dose build-up that is needed during superficial treatment.

Bone equivalent material for testing or quality assurance purposes has always been a contentious issue. Normal practice would be to use a high-density perspex, but this does not simulate or replicate bone density that well. In this study with the 3D printing materials initially used for the test blocks and from the second 3D print, it was established and verified that a

similar material with bone density properties was successfully manufactured/3D printed and could be used in this study and for further projects in future.

The reprint requested from the 3D printing company of only a section of the ribcage to verify that not the same material was used during the sample blocks and first print of the ribcage that was established and confirmed by the company was due to two reasons: (a) The original material from the sample blocks was very fragile due to the denser composition of the material; and (b) the complexity of the contour or object (ribcage) that needed to be printed. Instead, the normal nylon material was used as it is much tougher and easier to work with.

Although there was concern for fragile components and therefore handling/breakage of 3D printed pieces from the correct materials, as mentioned above, from the company, it was noted that the ribcage was sturdy in design and as soon as it was set in the silicon material, it was protected from accidental breakage. During the design of the ribcage, the density values that was extracted from the CT scan and used in the 3D printing design software, needs to be adjusted to accommodate less dense tissue and not be printed, and rather only higher density bone structures. This could be the cause of the fragile rib bones that were printed but is in fact the costal cartilage that is a flexible connective tissue and strengthened by collagen fibres. This connects the 'true' and 'false' ribs to the sternum and is not bone as such.

5.3 Dosimetric outcome

The transmission measured on the Elekta Synergy for the silicon material on average for 6MV and 10MV is 80.6% and 84.0%, respectively. The 3D prints' transmission measured is 76.2% and 80.0% for 6MV and 10MV, respectively.

Comparing these measured values for silicon against the TPS calculated values for the different algorithms, the largest discrepancy is 3.32% for the Acuros, Dose to Medium for the 10MV, 10x10cm field size. The Monaco calculates the transmission as less through this silicon medium, whereas the Eclipse sees it as more. The same scenario is seen with the 10MV data. In the case of the 3D print material, for all the calculations it is seen as less than the measured. With the 10MV Acuros, both dose to water and dose to medium, the transmission is more with 0.53% and 0.38%, respectively. This can be assumed as equal to the measured values due to uncertainty in measurement equipment. The 3D print material has a much higher density and

could therefore be more accurately calculated with the mass density associated within the algorithms and as explained in previous paragraphs. As reasoned, this is because Acuros Dose to Medium takes mass density into account whereas the other mentioned algorithms make use of relative electron density. Although Monaco makes use of Monte Carlo which is the same principle, it leans more strongly on the attenuation coefficient and stopping power ratios.

5.4 Imaging of phantoms

Imaging sets were acquired of the only silicon and 3D print with silicon phantoms, as well as the re-print of ribs with the higher density 3D additive manufactured material. The soft tissue or silicon phantom shows up as a grainy picture as expected for a water phantom during normal MV Electronic Portal Imaging (EPI). The same as for the Cone Beam CT that was acquired with kV imaging on the Elekta Synergy machine.

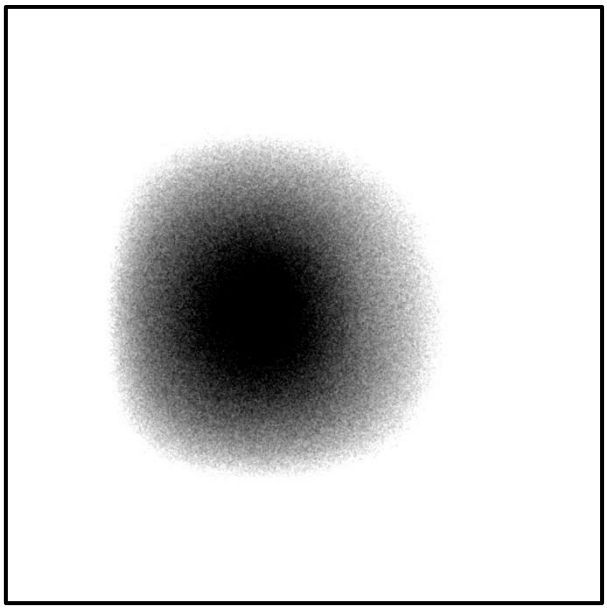

Figure 5.2: MV imaging of silicon or soft tissue equivalent material phantom

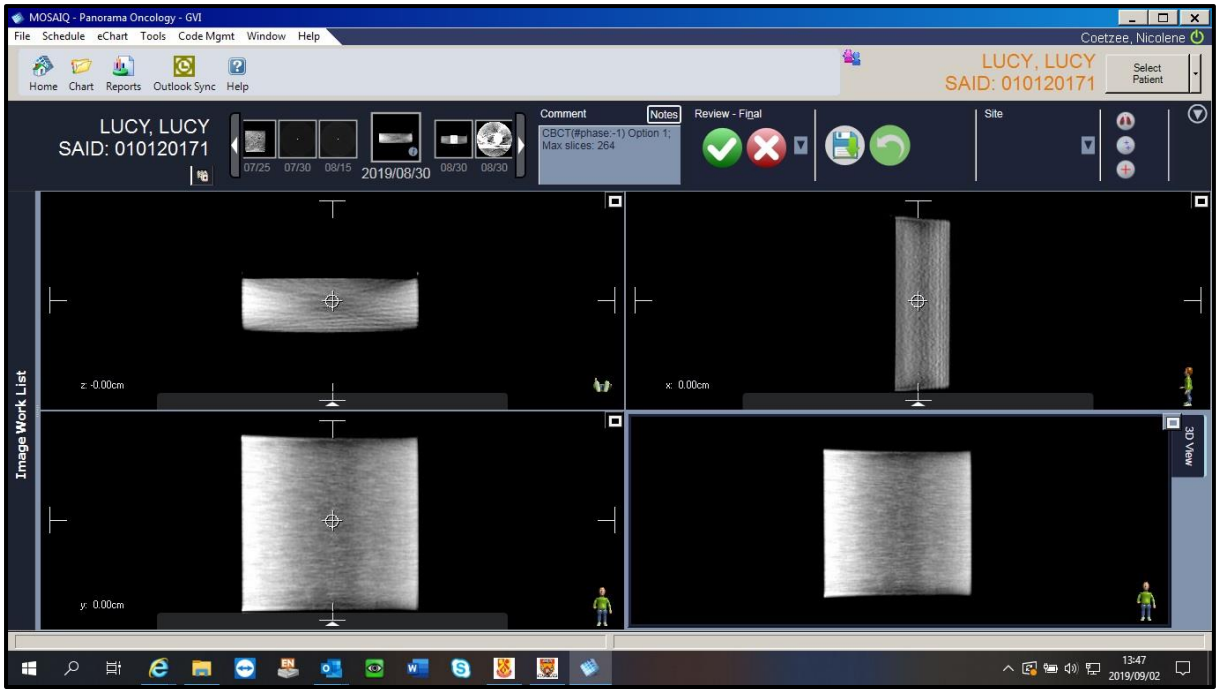

Figure 5.3: kV CBCT of silicon or soft tissue equivalent material phantom

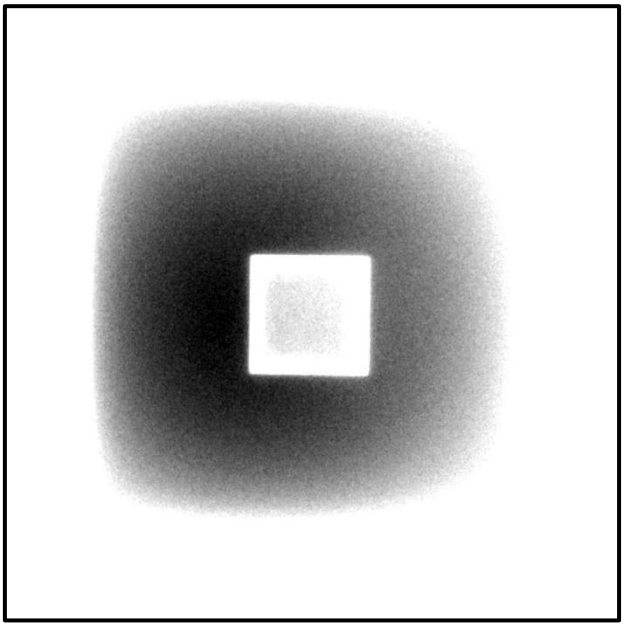

Figure 5.4: MV imaging of 3D print phantom

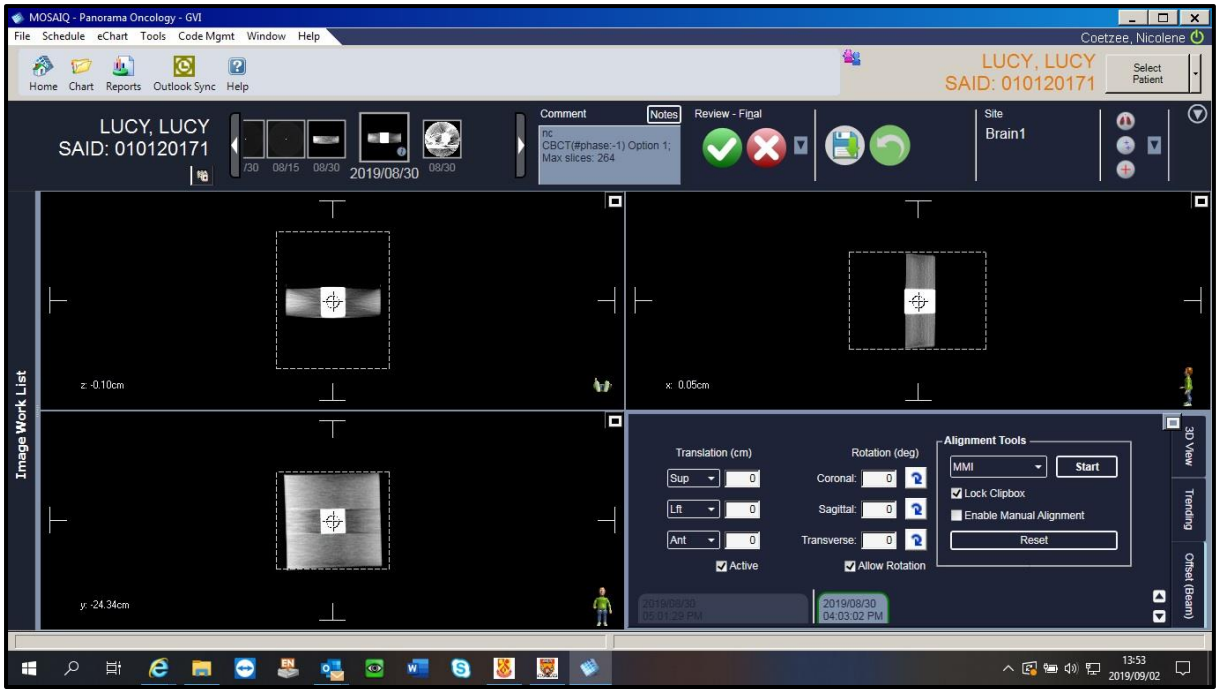

Figure 5.5: kV CBCT of 3D print phantom

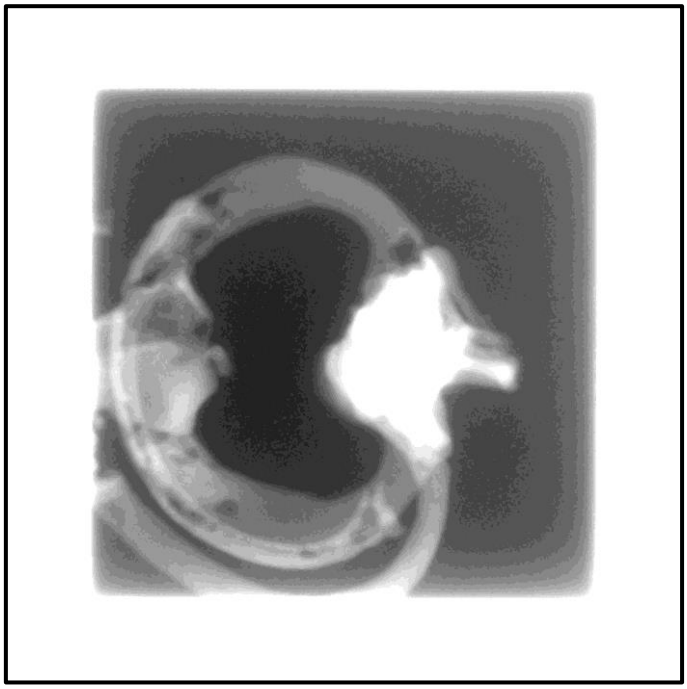

Figure 5.6: MV imaging of reprint of 3D printed ribs and sternum

Figure 5.7: kV CBCT of reprint of 3D printed ribs and sternum. Due to attenuation around the ribs there was an excess of scatter from the kV beam

5.5 Clinical radiotherapy key metrics summary

The silicon material and bone printed in 3D as with the final print version, correlates well with HU numbers for a CT scan compared to normal patient CT scans for soft tissue and cortical bone equivalent, respectively.

Comparing transmission for these materials on a linear accelerator for 6MV and 10MV energy, the deviation from planned versus measured dose varies between 1.67% to 3.32% and 0.45% to 2.30%, respectively for the silicon material and between 0.77% to 3.22% and 0.17% to 2.57% for the 3D printed bone for 6MV and 10MV, respectively. For the 3D printed material, the dose to medium algorithms compares better as to the dose to water. This could be since for dose to medium, mass density curves are taken into consideration when doing calculation, and not the electron density values or curves. Therefore, the silicon material also compares better with the dose to water in general, than the dose to medium calculations, as the silicon represents closer to water or rather soft tissue.

	Clinical Radiotherapy Key Metrics Summary					
	CT (Hounsfield nr)	**CT base value/ comparison (Hounsfield nr)**	**Treatment 6MV**	**Treatment 10MV**	**kV CBCT**	**MV Imaging**
Soft Tissue (Silicon)	~134	~60	3.32%	2.30%	✓	✓
Cortical Bone (3D Print)	~772-1079	~500-700	3.24%	2.57%	✓	✓

Table 5.1: Summary of the key metrics for clinical use in radiotherapy: CT scanning, attenuation and imaging use

6 Conclusion

The outcome of this research study is to determine the movement of tumour volumes in lung, and track the breathing cycle thereof in a customised build thorax phantom that replicates tissue equivalent organs to accurately calculate dose to the tumour volumes and surrounding organs at risk. The design of a thorax phantom and creating the breathing cycle and tracking in a 2D pathway was successfully accomplished, and further future projects can be investigated to enhance and improve on the capabilities of such a phantom. This could include extending the path from 2D to 3D movement, but this will only be possible as a robotic arm, as discussed previously, and for possible investigation in a further study or project.

In future studies the role of different and customised margins per patient and the influence on treatment outcomes and side-effects of lung volume in high-dose areas can be investigated. For this study, the design of a suitable phantom to mimic target motion in lung is the end point and was successfully accomplished.

Bibliography

Uncategorized References

Akhlaghi, P., Hakimabad, H. M., & Motavalli, L. R. (2015). Determination of tissue equivalent materials of a physical 8-year-old phantom for use in computed tomography. *Radiation Physics and Chemistry, 112*, 169-176.

Asbell, S. O., Grimm, J., Xue, J., Chew, M.-S., & LaCouture, T. A. (2016). Introduction and Clinical Overview of the DVH Risk Map. *Seminars in Radiation Oncology, 26*(2), 89-96. doi:https://doi.org/10.1016/j.semradonc.2015.11.005

Barnes, E. A., Murray, B. R., Robinson, D. M., Underwood, L. J., Hanson, J., & Roa, W. H. Y. (2001). Dosimetric evaluation of lung tumor immobilization using breath hold at deep inspiration. *International Journal of Radiation Oncology • Biology • Physics, 50*(4), 1091-1098. doi:10.1016/S0360-3016(01)01592-9

Baumann, P., Nyman, J., Hoyer, M., Wennberg, B., Gagliardi, G., Lax, I., . . . Lewensohn, R. (2009). Outcome in a prospective phase II trial of medically inoperable stage I non-small-cell lung cancer patients treated with stereotactic body radiotherapy. *J Clin Oncol, 27*(20), 3290-3296. doi:10.1200/JCO.2008.21.5681

Benedict, S. H., Yenice, K. M., Followill, D., Galvin, J. M., Hinson, W., Kavanagh, B., . . . Yin, F. F. (2010). Stereotactic body radiation therapy: the report of AAPM Task Group 101. *Med Phys, 37*(8), 4078-4101. doi:10.1118/1.3438081

Berthelsen, A. K. (2007). What's new in target volume definition for radiologists in ICRU Report 71? How can the ICRU volume definitions be integrated in clinical practice? *Cancer Imaging, 7*, 104-116.

Bose, S., Vahabzadeh, S., & Bandyopadhyay, A. (2013). Bone tissue engineering using 3D printing. *Materials Today, 16*(12), 496-504. doi:10.1016/j.mattod.2013.11.017

Bosmans, G., Buijsen, J., Dekker, A., Velders, M., Boersma, L., De Ruysscher, D., . . . Lambin, P. (2006). An “in silico” clinical trial comparing free breathing, slow and respiration correlated computed tomography in lung cancer patients. *Radiotherapy and Oncology, 81*(1), 73-80.

Buyyounouski, M. K., Balter, P., Lewis, B., D'Ambrosio, D. J., Dilling, T. J., Miller, R. C., . . . Wallner, P. E. (2010). Stereotactic Body Radiotherapy for Early-Stage Non-Small-Cell Lung Cancer: Report of the ASTRO Emerging Technology Committee. *International Journal of Radiation Oncology • Biology • Physics, 78*(1), 3-10. doi:10.1016/j.ijrobp.2010.04.010

Caldwell, C. B. (2003). Can PET provide the 3D extent of tumor motion for individualized internal target volumes? A phantom study of the limitations of CT and the promise of PET. *International Journal of Radiation Oncology* Biology* Physics, 55*(5), 1381-1393.

Canessa, E., Fonda, C., & Zennaro, M. (2013). *Low cost 3D printing for science, education and sustainable development* (Vol. 11).

Chang, J., Suh, T.-S., & Lee, D.-S. (2010). Development of a deformable lung phantom for the evaluation of deformable registration. *Journal of Applied Clinical Medical Physics, 11*(1), 281-286. doi:10.1120/jacmp.v11i1.3081

Chang, K.-P., Hung, S.-H., Chie, Y.-H., Shiau, A.-C., & Huang, R.-J. (2012). A Comparison of physical and dosimetric properties of lung substitute materials. *Medical Physics, 39*(4), 2013-2020. doi:10.1118/1.3694097

Chia, H. N., & Wu, B. M. (2015). Recent advances in 3D printing of biomaterials. *J Biol Eng, 9*, 4. doi:10.1186/s13036-015-0001-4

DE, D. (1992). Radiation therapy in the management of medically inoperable carcinoma of the lung: results and implications for future treatment strategies. *24*(1), 3-9.

Dunn, L., Kron, T., Johnston, P. N., McDermott, L. N., Taylor, M. L., Callahan, J., & Franich, R. D. (2012). A programmable motion phantom for quality assurance of motion management in radiotherapy. *Australasian Physical & Engineering Sciences in Medicine, 35*(1), 93-100. doi:10.1007/s13246-011-0114-0

Dynamic Dan. Retrieved from http://www.opraxmedical.com/Accessories/Phantoms/CT/RSD/Respiring/

Eclipse Photon and Electron Algorithms Reference Guide.

Ekstrand, K. E., & Barnes, W. H. (1990). Pitfalls in the use of high energy X rays to treat tumors in the lung. *International Journal of Radiation Oncology • Biology • Physics, 18*(1), 249-252. doi:10.1016/0360-3016(90)90290-Z

Emami. (1991). Tolerance to normal tissue to therapeutic irradiation. *International Journal Radiation Oncology Biology Physics, 21*, 109-122.

Freile-Pelegrín, Y., Madera-Santana, T., Robledo, D., Veleva, L., Quintana, P., & Azamar, J. (2007). Degradation of agar films in a humid tropical climate: Thermal, mechanical, morphological and structural changes. *Polymer Degradation and Stability, 92*(2), 244-252.

Grimm, J. (2011). Dose tolerance limits and dose volume histogram evaluation for stereotactic body radiotherapy. *Journal of Applied Clinical Medical Physics, 12*(2).

Hanley, J., Debois, M. M., Mah, D., Mageras, G. S., Raben, A., Rosenzweig, K., . . . Kutcher, G. J. (1999). Deep inspiration breath-hold technique for lung tumors: the potential value of target immobilization and reduced lung density in dose escalation. *International Journal of Radiation Oncology • Biology • Physics, 45*(3), 603-611. doi:10.1016/S0360-3016(99)00154-6

International Commission on Radiation Units and Measurements. Prescribing, recording, and reporting photon beam therapy (supplement to ICRU report 50). ICRU report 62. Bethesda, MD. (1999). *ICRU, 62*.

Lagerwaard, F. J., Van Sornsen de Koste, J. R., Nijssen-Visser, M. R. J., Schuchhard-Schipper, R. H., Oei, S. S., Munne, A., & Senan, S. (2001). Multiple 'slow' CT scans for incorporating lung tumor mobility in radiotheraphy planning. *International Journal of Radiation Oncology • Biology • Physics, 51*(4), 932-937. doi:10.1016/S0360-3016(01)01716-3

Lee, S., Yan, G., Lu, B., Kahler, D., Li, J. G., & Sanjiv, S. S. (2015). Impact of scanning parameters and breathing patterns on image quality and accuracy of tumor motion reconstruction in 4D CBCT: a phantom study. *Journal of Applied Clinical Medical Physics, 16*(6), 195-212. doi:10.1120/jacmp.v16i6.5620

Marks, L. B., Yorke, E. D., Jackson, A., Ten Haken, R. K., Constine, L. S., Eisbruch, A., . . . Deasy, J. O. (2010). Use of Normal Tissue Complication Probability Models in the Clinic. *International Journal of Radiation Oncology • Biology • Physics, 76*(3), S10-S19. doi:10.1016/j.ijrobp.2009.07.1754

Modh, A. (2014). Local Control and Toxicity in a Large Cohort of Central Lung Tumors Treated With Stereotactic Body Radiation Therapy. *International Journal of Radiation Oncology Biology Physics, 90*(5), 1168-1176.

Molineu, A., Followill, D. S., Balter, P. A., Hanson, W. F., Gillin, M. T., Huq, M. S., . . . Ibbott, G. S. (2005). Design and implementation of an anthropomorphic quality assurance phantom for intensity-modulated radiation therapy for the Radiation Therapy Oncology Group. *International Journal of Radiation Oncology* Biology* Physics, 63*(2), 577-583.

Park, C., Papiez, L., Zhang, S., Story, M., & Timmerman, R. D. (2008). Universal Survival Curve and Single Fraction Equivalent Dose: Useful Tools in Understanding Potency of

Ablative Radiotherapy. *International Journal of Radiation Oncology • Biology • Physics, 70*(3), 847-852. doi:10.1016/j.ijrobp.2007.10.059

Peltola, S. M., Melchels, F. P. W., Grijpma, D. W., & Kellomäki, M. (2008). A review of rapid prototyping techniques for tissue engineering purposes. *Annals of Medicine, 40*(4), 268-280. doi:10.1080/07853890701881788

Pogson, E. M., Begg, J., Jameson, M. G., Dempsey, C., Latty, D., Batumalai, V., . . . Holloway, L. C. (2015). A phantom assessment of achievable contouring concordance across multiple treatment planning systems. *Radiotherapy and Oncology, 117*(3), 438-441.

Quasar Phantom. Retrieved from https://modusqa.com/motion/phantom

Rana, S. (2014). Clinical dosimetric impact of Acuros XB and analytical anisotropic algorithm (AAA) on real lung cancer treatment plans : review. *International Journal of Cancer Therapy and Oncology, 2*.

Sibley, G. S. (1998). Radiotherapy alone for medically inoperable stage I non-small cell lung cancer: The Duke experience. *40*(1), 149-154.

Siemens Somatom. Retrieved from https://www.healthcare.siemens.com/computed-tomography/single-source-ct/somatom-definition-edge/technical-specifications

Slotman, B. J., Lagerwaard, F. J., & Senan, S. (2006). 4D imaging for target definition in stereotactic radiotherapy for lung cancer. *Acta Oncologica, 45*(7), 966-972. doi:10.1080/02841860600902817

Solutions, R. O. Anzai Respiratory Gating System.

Srivastava, R. (2013). Low Toxicity for Lung Tumors Near the Mediastinum Treated with Stereotactic Body Radiation Therapy (SBRT). *Practical Radiation Oncology*.

Steidl, P., Richter, D., Schuy, C., Schubert, E., Haberer, T., Durante, M., & Bert, C. (2012). A breathing thorax phantom with independently programmable 6D tumour motion for dosimetric measurements in radiation therapy. *Physics in medicine and biology, 57*(8), 2235.

Stroom, J. C., & Heijmen, B. J. M. (2002). Geometrical uncertainties, radiotherapy planning margins, and the ICRU-62 report. *Radiotherapy and Oncology, 64*(1), 75-83. doi:10.1016/S0167-8140(02)00140-8

Timmerman, D. R. (Producer). (2014, September 15). Long-term results of RTOG 0236 confirm good primary tumor control and positive five-year survival rates for lung cancer patients who received stereotactic body radiation therapy (SBRT). *ASTRO News and Media Center*.

Timmerman, R. (2010). Stereotactic Body Radiation Therapy for Inoperable Early stage lung cancer. *303*(11), 1070-1076.

Timmerman, R. (2014). Long-term Results of RTOG 0236: A Phase II Trial of Stereotactic Body Radiation Therapy (SBRT) in the Treatment of Patients with Medically Inoperable Stage I Non-Small Cell Lung Cancer. *International Journal of Radiation Oncology, Biology, Physics, 90*(1, Supplement), S30.

Timmerman, R. D. (2008). An Overview of Hypofractionation and Introduction to This Issue of Seminars in Radiation Oncology. *Seminars in Radiation Oncology, 18*(4), 215-222. doi:10.1016/j.semradonc.2008.04.001

Timmerman, R. D. (2009). *1. A Phase II Trial of Stereotactic Body Radiation Therapy (SBRT) in the Treatment of Patients with Medically Inoperable Stage I/II Non-Small Cell Lung Cancer RADIATION THERAPY ONCOLOGY GROUP, RTOG 0236*. Retrieved from

TS Srivatsan, T. S. (2015). Comparison of Additive Manufacturing Materials and Human Tissues in Computed Tomography Scanning *Additive Manufacturing: Innovations, Advances and Applications*.

Underberg, R. W. (2004). Four-dimensional CT scans for treatment planning in stereotactic radiotherapy for stage I lung cancer. *60*(4).

Underberg, R. W., Lagerwaard, F. J., Cuijpers, J. P., Slotman, B. J., van Sornsen de Koste, J. R., & Senan, S. (2004). Four-dimensional CT scans for treatment planning in stereotactic radiotherapy for stage I lung cancer. *Int J Radiat Oncol Biol Phys, 60*(4), 1283-1290. doi:10.1016/j.ijrobp.2004.07.665

Vassiliev, O. N. (2010). Validation of a new grid-based Boltzmann equation solver for dose calculation in radiotherapy with photon beams. *Phys Med Biol, 55*, 581–598.

White, P. J., Zwicker, R. D., & Huang, D. T. (1996). Comparison of dose homogeneity effects due to electron equilibrium loss in lung for 6 MV and 18 MV photons. *International Journal of Radiation Oncology • Biology • Physics, 34*(5), 1141-1146. doi:10.1016/0360-3016(95)02384-4

Wolthaus, J. W., Sonke, J.-J., van Herk, M., Belderbos, J. S., Rossi, M. M., Lebesque, J. V., & Damen, E. M. (2008). Comparison of different strategies to use four-dimensional computed tomography in treatment planning for lung cancer patients. *International Journal of Radiation Oncology• Biology• Physics, 70*(4), 1229-1238.

Annexures

Annexure A

Annexure A 1: CTV Coordinates

Patient1:

CT Phase sets	X-coordinate (cm)	Y-coordinate (cm)	Z-coordinate (cm)
CT – non-gated	-11.50	0.00	-2.90
nil	-11.15	-0.30	-2.52
10	-11.30	-0.30	-2.50
20	-11.19	0.00	-2.50
30	-11.12	0.30	-2.75
40	-11.10	0.30	-2.73
50	-11.12	0.45	-2.81
60	-11.08	0.45	-2.85
70	-11.10	0.30	-2.81
80	-11.16	0.00	-2.85
90	-11.18	-0.30	-2.61

Patient2:

CT Phase sets	X-coordinate (cm)	Y-coordinate (cm)	Z-coordinate (cm)
CT – non-gated	-7.79	19.25	-12.37
nil	-7.87	19.40	-12.33
10	-7.82	19.40	-12.37
20	-7.84	19.55	-12.37
30	-7.96	19.55	-12.35
40	-7.96	19.55	-12.33
50	-7.93	19.55	-12.30
60	-7.95	19.55	-12.32
70	-7.92	19.55	-12.34
80	-7.91	19.55	-12.32
90	-7.90	19.40	-12.28

Patient 3 was excluded from this study set, as the patient did not receive a 4D CT Scan.

Patient4:

CT Phase sets	X-coordinate (cm)	Y-coordinate (cm)	Z-coordinate (cm)
CT – non-gated	8.01	11.15	-18.24
nil	7.94	11.05	-18.32
10	8.00	11.05	-18.28
20	7.93	11.25	-18.28
30	7.99	11.15	-18.26
40	7.95	11.15	-18.23
50	8.03	11.15	-18.25
60	7.92	11.15	-18.23
70	7.96	11.15	-18.27
80	7.91	11.15	-18.35
90	7.97	11.15	-18.28

Patient5:

CT Phase sets	X-coordinate (cm)	Y-coordinate (cm)	Z-coordinate (cm)
CT – non-gated	-6.40	-36.65	-1.60
nil	-6.40	-36.55	-1.28
10	-6.33	-36.55	-1.17
20	-6.30	-36.65	-1.10
30	-6.27	-36.55	-1.06
40	-6.33	-36.55	-1.08
50	-6.26	-36.45	-1.19
60	-6.35	-36.35	-1.27
70	-6.34	-36.35	-1.33
80	-6.33	-36.35	-1.30
90	-7.90	19.40	-12.28

Patient6 (1st lesion – Lat Lung):

CT Phase sets	X-coordinate (cm)	Y-coordinate (cm)	Z-coordinate (cm)
CT – non-gated	15.08	0.35	-0.06
nil	Coordinates does not match rest of scans/phases - ignore CT set		
10	15.29	-0.35	0.02
20	15.24	-0.35	0.02
30	15.20	0.25	-0.30
40	15.28	0.45	-0.30
50	15.08	0.35	-0.06
60	15.21	0.55	-0.26
70	15.23	0.45	-0.32
80	15.10	0.45	-0.10
90	15.21	0.35	-0.33

Patient6 (2nd lesion – Med Lung):

CT Phase sets	X-coordinate (cm)	Y-coordinate (cm)	Z-coordinate (cm)
CT – non-gated	6.77	0.05	-8.74
nil	6.77	-0.35	-8.75
10	6.77	-0.35	-8.70
20	6.77	-0.15	-8.78
30	6.77	-0.15	-8.77
40	6.75	0.05	-8.76
50	6.77	0.05	-8.74
60	6.75	0.05	-8.80
70	6.73	-0.05	-8.82
80	6.77	-0.05	-8.79
90	6.77	-0.25	-8.76

Annexure A 2: CTV Movement

Patient1:

CT Phase Sets	X movement (mm)	Y movement (mm)	Z movement (mm)
Non-gated	0	0	0
nil	-3.50	3.00	-3.80
10	-2.00	3.00	-4.00
20	-3.10	0.00	-4.00
30	-3.80	-3.00	-1.50
40	-4.00	-3.00	-1.70
50	-3.80	-4.50	-0.90
60	-4.20	-4.50	-0.50
70	-4.00	-3.00	-0.90
80	-3.40	0.00	-0.50
90	-3.20	3.00	-2.90

Patient2:

CT Phase Sets	X movement (mm)	Y movement (mm)	Z movement (mm)
Non-gated	0	0	0
nil	0.80	-1.50	-0.40
10	0.30	-1.50	0.00
20	0.50	-3.00	0.00
30	1.70	-3.00	-0.20
40	1.70	-3.00	-0.40
50	1.40	-3.00	-0.70
60	1.60	-3.00	-0.50
70	1.30	-3.00	-0.30
80	1.20	-3.00	-0.50
90	1.10	-1.50	-0.90

Patient4:

CT Phase Sets	X movement (mm)	Y movement (mm)	Z movement (mm)
Non-gated	0	0	0
nil	0.70	1.00	0.80
10	0.10	1.00	0.40
20	0.80	-1.00	0.40
30	0.20	0.00	0.20
40	0.60	0.00	-0.10
50	-0.20	0.00	0.10
60	0.90	0.00	-0.10
70	0.50	0.00	0.30
80	1.00	0.00	1.10
90	0.40	0.00	0.40

Patient5:

CT Phase Sets	X movement (mm)	Y movement (mm)	Z movement (mm)
Non-gated	0	0	0
nil	0.00	-1.00	-3.20
10	-0.70	-1.00	-4.30
20	-1.00	0.00	-5.00
30	-1.30	-1.00	-5.40
40	-0.70	-1.00	-5.20
50	-1.40	-2.00	-4.10
60	-0.50	-3.00	-3.30
70	-0.60	-3.00	-2.70
80	-0.70	-3.00	-3.00
90	0.00	-2.00	-3.00

Patient6 (1st lesion – Lat Lung):

CT Phase Sets	X movement (mm)	Y movement (mm)	Z movement (mm)
Non-gated	0	0	0
nil	-2.10	7.00	-0.80
10	-1.60	7.00	-0.80
20	-1.20	1.00	2.40
30	-2.00	-1.00	2.40
40	0.00	0.00	0.00
50	-1.30	-2.00	2.00
60	-1.50	-1.00	2.60
70	-0.20	-1.00	0.40
80	-1.30	0.00	2.70
90	-2.10	7.00	-0.80

Patient6 (2nd lesion – Med Lung):

CT Phase Sets	X movement (mm)	Y movement (mm)	Z movement (mm)
Non-gated	0	0	0
nil	0.00	4.00	0.10
10	0.00	4.00	-0.40
20	0.00	2.00	0.40
30	0.00	2.00	0.30
40	0.20	0.00	0.20
50	0.00	0.00	0.00
60	0.20	0.00	0.60
70	0.40	1.00	0.80
80	0.00	1.00	0.50
90	0.00	3.00	0.20

Annexure A 3: CTV Path

Patient1:

CT Phase Sets	X movement (mm)	X - Rounded to 1mm +less than 2mm=0	Y movement (mm)	Y – Rounded to 1mm +less than 2mm=0	Z movement (mm)	Z – Rounded to 1mm +less than 2mm=0
nil	-3.50	-4.00	3.00	3.00	-3.80	-4.00
10	-2.00	-2.00	3.00	3.00	-4.00	-4.00
20	-3.10	-3.00	0.00	0.00	-4.00	-4.00
30	-3.80	-4.00	-3.00	-3.00	-1.50	0.00
40	-4.00	-4.00	-3.00	-3.00	-1.70	0.00
50	-3.80	-4.00	-4.50	-5.00	-0.90	0.00
60	-4.20	-4.00	-4.50	-5.00	-0.50	0.00
70	-4.00	-4.00	-3.00	-3.00	-0.90	0.00
80	-3.40	-3.00	0.00	0.00	-0.50	0.00
90	-3.20	-3.00	3.00	3.00	-2.90	-3.00

Patient2:

CT Phase Sets	X movement (mm)	X - Rounded to 1mm +less than 2mm=0	Y movement (mm)	Y – Rounded to 1mm +less than 2mm=0	Z movement (mm)	Z – Rounded to 1mm +less than 2mm=0
nil	0.80	0.00	-1.50	0.00	-0.40	0.00
10	0.30	0.00	-1.50	0.00	0.00	0.00
20	0.50	0.00	-3.00	-3.00	0.00	0.00
30	1.70	0.00	-3.00	-3.00	-0.20	0.00
40	1.70	0.00	-3.00	-3.00	-0.40	0.00
50	1.40	0.00	-3.00	-3.00	-0.70	0.00
60	1.60	0.00	-3.00	-3.00	-0.50	0.00
70	1.30	0.00	-3.00	-3.00	-0.30	0.00
80	1.20	0.00	-3.00	-3.00	-0.50	0.00
90	1.10	0.00	-1.50	0.00	-0.90	0.00

Patient4:

CT Phase Sets	**X movement (mm)**	**X -** Rounded to 1mm +less than 2mm=0	**Y movement (mm)**	**Y** – Rounded to 1mm +less than 2mm=0	**Z movement (mm)**	**Z** – Rounded to 1mm +less than 2mm=0
nil	0.70	0.00	1.00	0.00	0.80	0.00
10	0.10	0.00	1.00	0.00	0.40	0.00
20	0.80	0.00	-1.00	0.00	0.40	0.00
30	0.20	0.00	0.00	0.00	0.20	0.00
40	0.60	0.00	0.00	0.00	-0.10	0.00
50	-0.20	0.00	0.00	0.00	0.10	0.00
60	0.90	0.00	0.00	0.00	-0.10	0.00
70	0.50	0.00	0.00	0.00	0.30	0.00
80	1.00	0.00	0.00	0.00	1.10	0.00
90	0.40	0.00	0.00	0.00	0.40	0.00

Patient5:

CT Phase Sets	**X movement (mm)**	**X -** Rounded to 1mm +less than 2mm=0	**Y movement (mm)**	**Y** – Rounded to 1mm +less than 2mm=0	**Z movement (mm)**	**Z** – Rounded to 1mm +less than 2mm=0
nil	0.00	0.00	-1.00	0.00	-3.20	-3.00
10	-0.70	0.00	-1.00	0.00	-4.30	-4.00
20	-1.00	0.00	0.00	0.00	-5.00	-5.00
30	-1.30	0.00	-1.00	0.00	-5.40	-5.00
40	-0.70	0.00	-1.00	0.00	-5.20	-5.00
50	-1.40	0.00	-2.00	-2.00	-4.10	-4.00
60	-0.50	0.00	-3.00	-3.00	-3.30	-3.00
70	-0.60	0.00	-3.00	-3.00	-2.70	-3.00
80	-0.70	0.00	-3.00	-3.00	-3.00	-3.00
90	0.00	0.00	-2.00	-2.00	-3.00	-3.00

Patient6 (1st lesion – Lat Lung):

CT Phase Sets	**X movement (mm)**	**X -** Rounded to 1mm +less than 2mm=0	**Y movement (mm)**	**Y** – Rounded to 1mm +less than 2mm=0	**Z movement (mm)**	**Z** – Rounded to 1mm +less than 2mm=0
nil	-2.10	-2.00	7.00	7.00	-0.80	0.00
10	-1.60	0.00	7.00	7.00	-0.80	0.00
20	-1.20	0.00	1.00	0.00	2.40	2.00
30	-2.00	-2.00	-1.00	0.00	2.40	2.00
40	0.00	0.00	0.00	0.00	0.00	0.00
50	-1.30	0.00	-2.00	-2.00	2.00	2.00
60	-1.50	0.00	-1.00	0.00	2.60	3.00
70	-0.20	0.00	-1.00	0.00	0.40	0.00
80	-1.30	0.00	0.00	0.00	2.70	3.00
90	-2.10	-2.00	7.00	7.00	-0.80	0.00

Patient6 (2nd lesion – Med Lung):

CT Phase Sets	**X movement (mm)**	**X -** Rounded to 1mm +less than 2mm=0	**Y movement (mm)**	**Y** – Rounded to 1mm +less than 2mm=0	**Z movement (mm)**	**Z** – Rounded to 1mm +less than 2mm=0
nil	0.00	0.00	4.00	4.00	0.10	0.00
10	0.00	0.00	4.00	4.00	-0.40	0.00
20	0.00	0.00	2.00	2.00	0.40	0.00
30	0.00	0.00	2.00	2.00	0.30	0.00
40	0.20	0.00	0.00	0.00	0.20	0.00
50	0.00	0.00	0.00	0.00	0.00	0.00
60	0.20	0.00	0.00	0.00	0.60	0.00
70	0.40	0.00	1.00	0.00	0.80	0.00
80	0.00	0.00	1.00	0.00	0.50	0.00
90	0.00	0.00	3.00	3.00	0.20	0.00

ANNEXURE B

Manufacture of the two-piece Plaster of Paris impression:

Plaster of Paris or Gypsum is a crystalline mineral of hydrated calcium sulphate (chemical formula CaSO4 • 2H2O). Gypsum is colourless or white, is not highly water-soluble and is not at all hard. A mixture of gypsum and water can be poured; the gypsum hardens as the water evaporates. In art gypsum is mainly used in the partly dehydrated form of plaster of Paris (2CaSO4 • H2O) to make casts of objects or works of art in sculpture (moulds). The process entails making a negative form, of a sculpture, for instance, which is then coated with plaster of Paris. Plaster of Paris models of sculpture were widespread in antiquity and the practise was revived in the Renaissance. From the late 17th century plaster of Paris casts was made for art academy study and model collections (plaster cast collections), which were taken up by museums and art historical and other institutes in the 19th century.
Online search / accessed on 18 March 2019 at 12:20.
https://www.kettererkunst.com/dict/gypsum-plaster-of-paris.php

The room was prepared, and rolls of Plaster of Paris bandage were cut into 35cm strips or lengths. The subject had to have aqueous cream rubbed on the skin to prevent the plaster from sticking onto the skin. All body hair was covered with a Jelonet material to prevent adhering to the plaster.

Jelonet consists of a leno-weave fabric, of cotton or cotton and viscose, which has been impregnated with white soft paraffin (yellow soft paraffin in the case of the bulk preparations). The dressing is used as a primary wound contact layer and the paraffin is present to reduce the adherence of the product to the surface of a granulating wound.
Online search / accessed on 18 March 2019 at 12:30.
http://www.dressings.org/Dressings/jelonet.html

Warm water was used, 4 layers of Plaster of Paris bandage was moulded over the skin from the superior surface of the neck to lower than the diaphragms on the posterior surface to include the side of the chest wall. Once the plaster bandage was firm, a layer of aqueous cream was rubbed around all the edges, which will give access to loosen the posterior and anterior impressions from each other. The anterior impression was made using the same manner as

above. A 2cm overlap on the sides of the chest walls was also made from the neck down to the lower diaphragm to ensure a full two-piece impression of the thorax.

When the Plaster of Paris bandage had set, the anterior and posterior impression was removed from the subject. These two halves were then taken to the mould room laboratory. At each end of the neck and lower diaphragm level, it had to be enclosed with Plaster of Paris bandage to form a shell so that Plaster of Paris material could be poured into each one of the halves.

A separating medium was coated on the inside of the impression to prevent the Plaster of Paris model sticking to the impression bandage. The models were secured on a levelled surface and immobilized in that position. Water was poured into a bowl at 3/4 level and then gradually Plaster of Paris powder is sifted into the water until most is absorbed by the water. The mixture is mixed thoroughly using a spatula until a smooth and creamy texture is obtained. This is then poured into the negative Plaster of Paris shell. The process is repeated until the impression is filled to the edges. The second impression was filled in the same manner.

Both positive models are left to set and dry for 2 days as they were very large in size. The outer layers of Plaster of Paris bandage were removed from both models. The positive models were then smoothed and filed until perfect as a Vacuum forming technique is used to manufacture the Ultra High Impact Acrylic shell. It is important to ensure that the edge of overlap of the two-piece model, is carefully maintained so that the two halves will accurately fit together, this is to ensure a tight fit when filling the shell with tissue equivalent impression material.

Impressions and Models made by: Susan Tovey, UCT/GSH

ANNEXURE C

Annexure C 1*:* Thorax

The customised build thorax and lung moulds were vacuum wrapped with thermoplastic.

Due to a height constraint on the vacuum machine (maximum part height – 250mm) the thorax was cut in half (anterior-posterior distance). This also assisted with an opening that is needed in the thorax for the arm to move in and out of the thorax to simulate the motion of the tumour. Unfortunately, with the thorax mould the amount that was needed to decrease the fitted height into the vacuum press, the shape that was originally designed and the 2cm overlap to fit anterior and posterior halves, were lost. At the time it did not seem to be a problem.

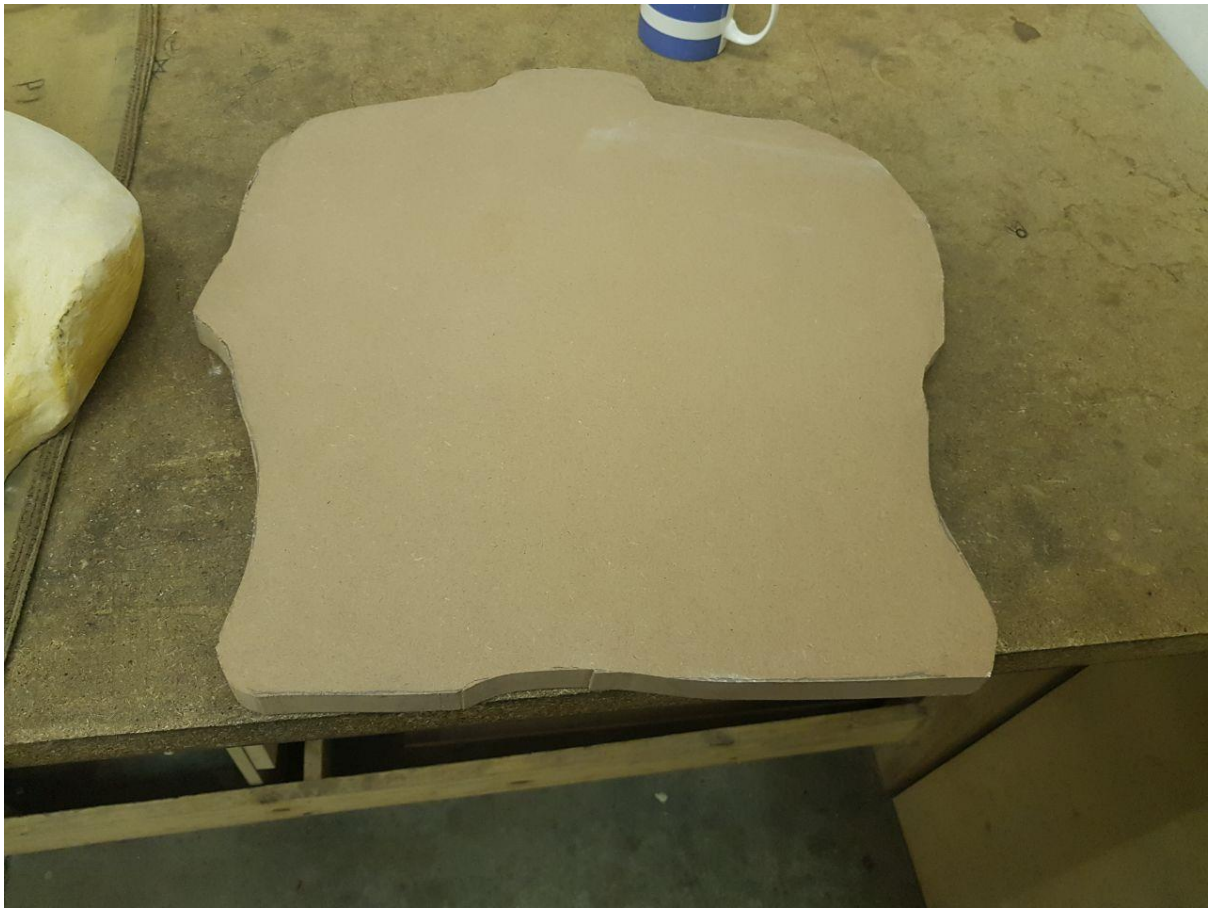

Figure Off-cut from thorax mould to fit into vacuum press

The mould had to be flattened otherwise the vacuum press will not be able to ‘couple’ or attach between the bed of the press and mould to form a proper vacuum to draw the thermoplastic

over the mould. The mould was clamped down and secured with a piece of wood and screws when the brushes run over the bottom of the mould to flatten the surface in preparation of the vacuum press to work optimally.

Figure Thorax mould clamped down

Figure Mould clamped with screws and a piece of wood

Video Clip Flattening bottom of thorax mould

Figure Flattened thorax mould

The thorax mould was laid onto the 2900mm vacuum bed.

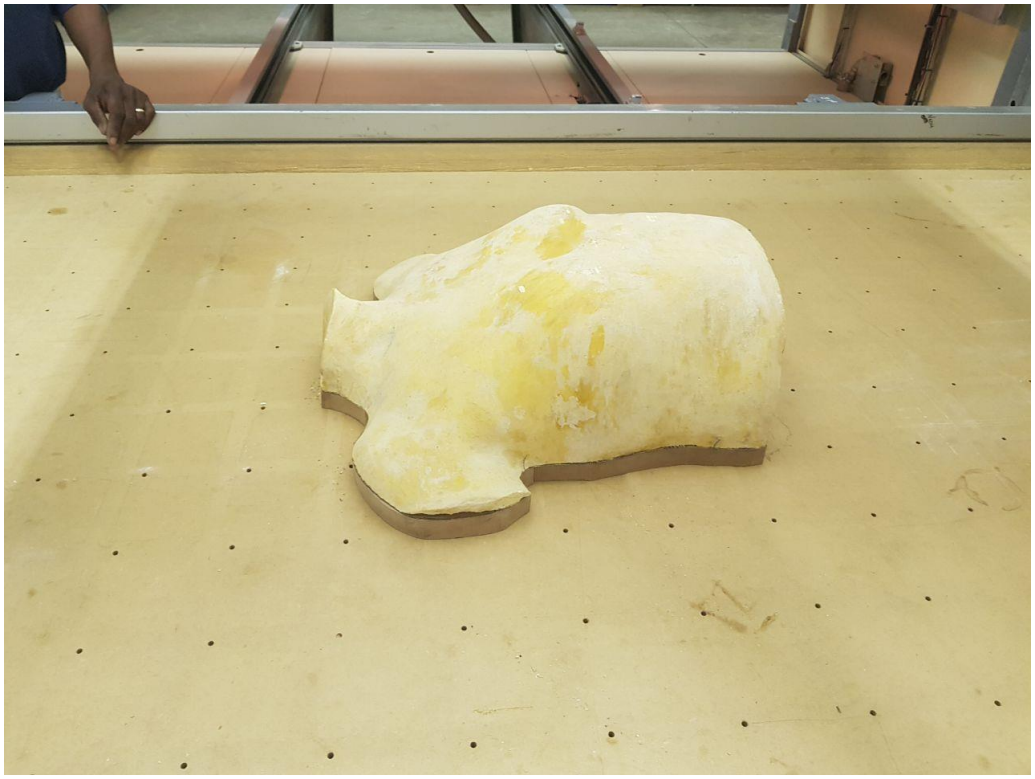

Figure Mould on bed

The 2mm thermoplastic in jig is placed over the thorax mould in preparation of heating sequence to mould or ply the thermoplastic by means of the vacuum press.

Temperature and pressure are PC controlled through the interface of the vacuum press. The technical specification of the machine is for the heaters 45kW and vacuum 65m^3/hr.

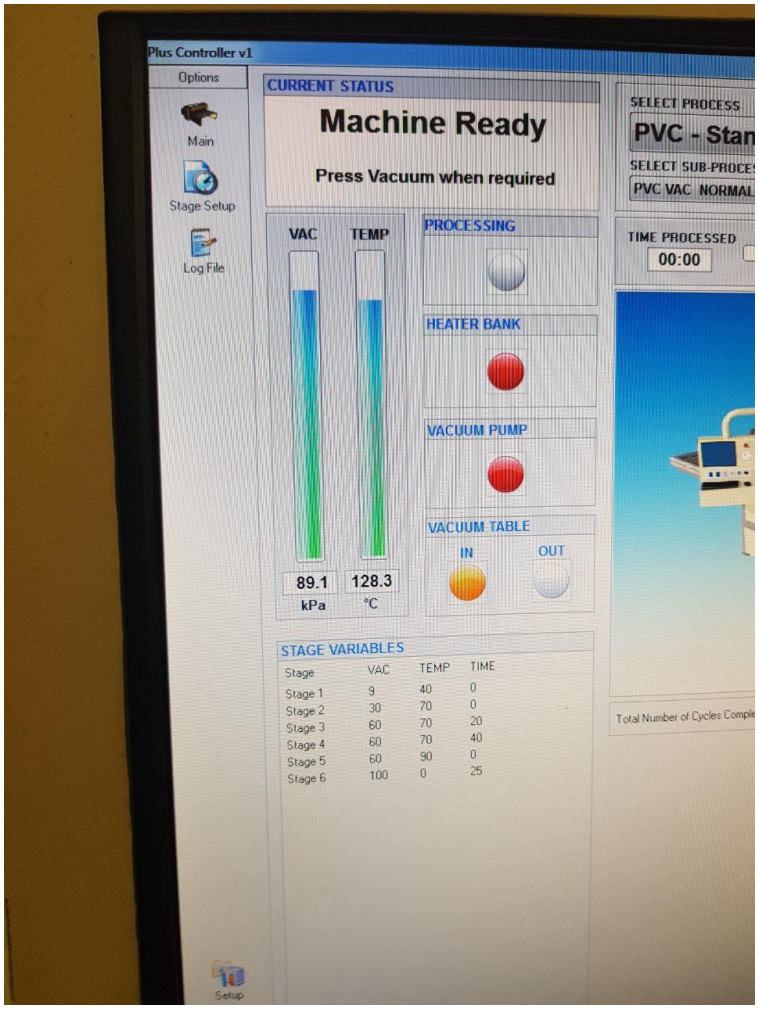

Figure Settings on vacuum press

Figure Mould in jig under heaters

When the pre-set temperature is achieved, the mould is extracted from underneath the heaters and the membrane is fitted over the mould and jig. This membrane is used in the vacuum process as can see below in the photos and video clip.


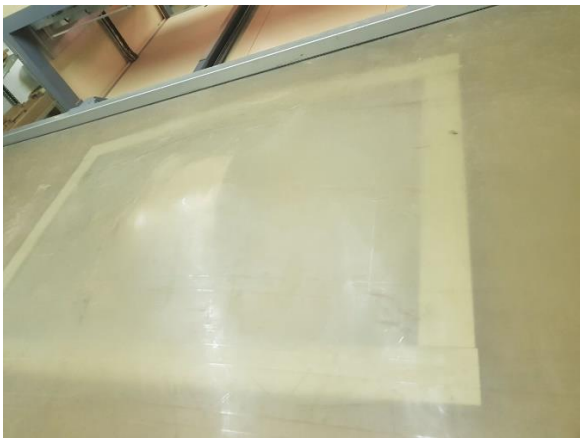


Figure (a-c) Membrane fitted over mould and heated thermoplastic

Video clip 3

This process of heating and vacuum is repeated until the desired form or shell is achieved.

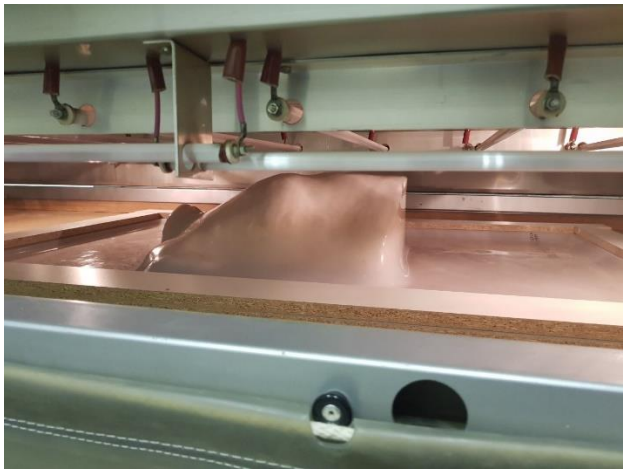

Figure Repeat process of heating and vacuum

Video clip Temp

Figure Finished vacuum wrap thorax

The outer shell comprises of 2mm Perspex sheeting vacuumed wrapped around a mould that was reconstructed from the dimensions of the patient' dataset ribcage printed.

After the plastic shell was cool enough to work with, it was cut from the jig with an overlap to secure the two halves.

Figure (a-c) The plastic mould or shell is cut from the jig

Unfortunately, the plaster of paris mould did not want to come loose from the thermoplastic and the mould was damaged trying to loosen it from the shell.

Figure (a) Mould damaged (b) plastic shell finished

It was evident now that trying to fit the two halves, it did not fit anymore as was planned, due to the limitation on the vacuum press with the maximum part height of 250mm.

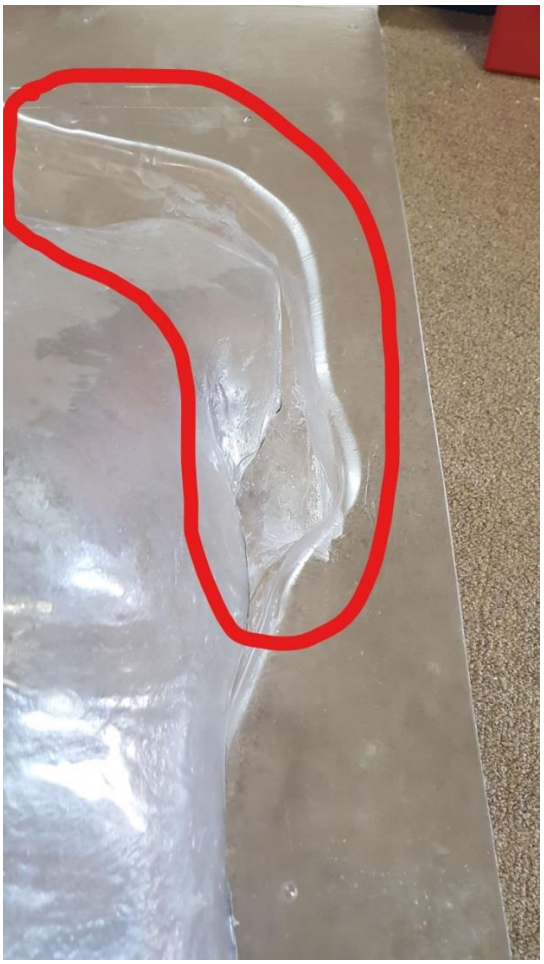

Due to this misfit of the 2 halves it was impossible to secure for no leakage of the tissue equivalent material to be used. The posterior half of the thorax had to be redone. The same process was followed with the plaster of paris except that no subject was used, but the mould room technician fabricated it from the anterior part of the thorax so that a better fit was achieved.

Annexure C 2*:* Lungs

The MDF lung moulds were fitted in a jig, thermoplastic of 1mm was added and it was heated. Thereafter the vacuum process was followed, half settings for temperature and pressure were used due to the fact of the thinner and smaller moulds used to fabricate the lung shells.

Figure (a+b) MDF moulds for lung

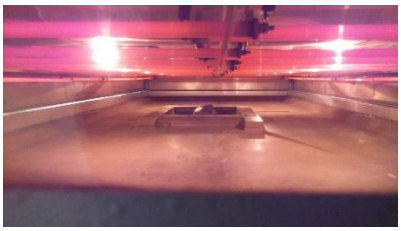

Figure (a-c) Thermoplastic heated

Figure Vacuum pressed lung mould

ANNEXURE D

Spesifications of Encapso K:

Encapso® K

Water Clear Encapsulation / Display Rubber

SMOOTH-ON

www.smooth-on.com

PRODUCT OVERVIEW

Encapso® K is a water clear encapsulation rubber that looks just like water and is ideal for a variety of encapsulation and display applications.

How Does Encapso® K Work? – Two clear liquids (Part A and Part B) are mixed together in equal amounts. The mixture is then poured around artificial flower stems or over an object. **Encapso® K** cures to a soft rubber over night depending on casting thickness and conditions (see reverse side of this technical bulletin). When cured, **Encapso® K** looks just like water and will last a long time.

Encapso® K Advantages:

- Non-Hazardous – No dangerous chemicals
- Soft, Clear Rubber Lasts A Long Time
- Easy To Use – Mix two liquids in equal amounts and pour
- UV Resistant
- Cures without generating any dangerous heat or fumes
- Minimal Bubble Entrapment
- Cures perfectly clear - Looks just like water
- Cured rubber can be removed from object

Applications for Encapso® K - This rubber is perfect for encapsulating artificial flower stems for creating lasting floral displays. You can also pour **Encapso® K** around just about any inanimate object to encapsulate for display. You can also create a variety of display props and novelty items. **Encapso® K** can be used to create water/pond effects for small scale model environments. Fully cured **Encapso® K** can also be crumbled to look like broken glass, diamonds or ice. Add color to **Encapso® K** with Silc Pig® or Ignite® liquid color pigments.

TECHNICAL OVERVIEW

Mix Ratio: 1A : 1B by volume or weight	
Mixed Viscosity, cps: 150	(ASTM D-2393)
Specific Gravity, g/cc: 0.97	(ASTM D-1475)
Specific Volume, cu. in./lb.: 28.6	
Pot Life: 120 minutes (73°F/23°C)	(ASTM D-2471)
Cure time: 16 hrs (73°F/23°C)	
Color: Clear	
Shore A Hardness: 33	(ASTM D-2240)
Dielectric Strength, volts/mil: 319	
Dielectric Constant, 100 Hz: 3.17	
Shrinkage, in./in.: <0.001	(ASTM D-2566)

All values measured after 7 days at 73°F/23°C

PROCESSING RECOMMENDATIONS

PREPARATION...Safety - Use in a properly ventilated area ("room size" ventilation). Wear safety glasses, long sleeves and rubber gloves to minimize contamination risk. Wear vinyl gloves only. Latex gloves will inhibit the cure of the rubber. **Do not apply this product to the skin.** Encapso® K may not cure over objects containing sulfur. If compatibility is in question, a small scale test is recommended.

Store and use material at room temperature (73°F/23°C). These products have a limited shelf life and should be used as soon as possible.

For Encapsulating Artificial Floral Stems - Arrange / position bedding objects (stones, glass beads, etc.) and flowers in vase prior to mixing material.

MEASURING & MIXING...

Pre-Mix Parts A and B - Shake containers vigorously before using to re-disperse material that may have separated. If material is packaged in buckets, remove lid and pre-mix aggressively with a paint stick or mixing paddle.

Dispense One Part A and One Part B by volume into mixing container (for example, 1 cup A + 1 cup B). Mix thoroughly for at least five minutes, making absolutely sure that you scrape the sides and bottom of your container several times. Material appears cloudy when first mixed, but will clear after a few minutes.

☑ GHS Compliant

Safety Data Sheet

SDS No. 823A

Section 1 - Identification

1.1 Product Identifier: Part A for: Body Double® & Body Double® SILK; Dragon Skin® Series & F/X Pro; Ecoflex® Series & Gel; Encapso® K; Equinox® Series; EZ Brush® Silicone; EZ-Spray® Silicone Series; Mold Max® Series; Mold Star® Series; OOMOO® Series; PoYo® Putty 40; Psycho Paint®; Rebound® Series; Rubber Glass®; Silicone 1515 and Silicone 3030; Skin Tite®; Smooth-Sil® Series; Solaris®; SomaFoama® Series; SORTA-Clear® Series
1.2 General Use: Silicone Elastomer
1.3 Manufacturer: Smooth-On, Inc.,
5600 Lower Macungie Rd., Macungie, PA 18062
Phone (610) 252-5800, FAX (610) 252-6200
SDS@Smooth-On.com
1.4 Emergency Contact: Chem-Tel
Domestic: 800-255-3924 International: 813-248-0585

Section 2 – Hazard(s) Identification

2.1 Classification of the substance or mixture
Not a hazardous substance or mixture according to United States Occupational Safety and Health Administration (OSHA) Hazard Communication Standard (29 CFR 1910.1200), the Canadian Workplace Hazardous Materials Information System (WHMIS) and Regulation (EC) No 1272/2008 and subsequent amendments.

2.2 GHS Label elements, including precautionary statements
Pictogram(s): none
Signal word: none
General Precautions:
P101: If medical advice is needed, have product container or label at hand.
P102: Keep out of reach of children.
P103: Read label before use.

Hazards not otherwise classified (HNOC) or not covered by GHS - none

Section 3 - Composition / Information on Ingredients

3.1 Substances

No ingredients are hazardous according to Regulation 2012 OSHA Hazard Communication Standard 29 CFR 1910.1200 criteria.

Section 4 - First Aid Measures

4.1 Description of first aid measures
Inhalation: Remove source(s) of contamination and move victim to fresh air. If breathing has stopped, give artificial respiration, then oxygen if needed. Contact physician immediately.
Eye Contact: Flush eyes with plenty of water. If irritation persists, seek medical attention.
Skin Contact: In case of skin contact, wash thoroughly with soap and water.
Ingestion: Do not induce vomiting unless instructed by a physician. Never give anything by mouth to an unconscious person.
4.2 Most important symptoms and effects, both acute and delayed
None known.
4.3 After first aid, get appropriate in-plant, paramedic, or community medical support.

Section 5 - Fire-Fighting Measures

5.1 Extinguishing Media: Water Fog, Dry Chemical, and Carbon Dioxide Foam
5.2 Special hazards arising from the substance or mixture: None known.
5.3 Advice for firefighters: Use water spray to cool fire-exposed surfaces and to protect personnel. Shut off "fuel" to fire. If a leak or spill has not ignited, use water spray to disperse the vapors. Either allow fire to burn under controlled conditions or extinguish with foam or dry chemical. Try to cover liquid spills with foam. Because fire may produce toxic thermal decomposition products, wear a self-contained breathing apparatus (SCBA) with a full face piece operated in pressure demand or positive-pressure mode.

Section 6 - Accidental Release Measures

6.1 Personal precautions, protective equipment and emergency procedures: Only properly protected personnel should remain in the spill area; dike and contain spill. Stop or reduce discharge if it can be done safely.
6.2 Environmental precautions: No special environmental precautions required.
6.3 Methods and material for containment and cleaning up: absorb or scrape up excess into suitable container for disposal; wash area with dilute ammonia solution
6.4 Reference to other sections: if appropriate Sections 8 and 13 shall be referred to.

Section 7 - Handling and Storage

7.1 Precautions for safe handling: Use good general housekeeping procedures. Wash hands after use.
7.2 Conditions for safe storage, including any incompatibilities: Keep container(s) tightly closed and properly labeled. Store in cool, dry, well ventilated place away from heat, direct sunlight, strong oxidizers and any incompatibles. Store in approved containers and protect against physical damage. Keep containers securely sealed when not in use. Indoor storage should meet OSHA standards and appropriate fire codes. Containers that have been opened must be carefully resealed to prevent leakage. Empty containers retain residue and may be dangerous. Avoid water contamination.
7.3 Specific end use(s): These precautions are for room temperature handling. Other uses including elevated temperatures or aerosol/spray applications may require added precautions.

Section 8 - Exposure Controls / Personal Protection

8.1 Control parameters: none defined
8.2 Exposure controls:
Respiratory Protection: Should a respirator be needed, follow OSHA respirator regulations 29 CFR 1910.134 and European Standards EN 141, 143 and 371; wear an MSHA/NIOSH or European Standards EN 141, 143 and 371 approved respirators equipped with organic vapor cartridges.
Hand Protection: Wear any liquid-tight gloves such as butyl rubber, neoprene or PVC.
Eye Protection: Safety glasses with side shields per OSHA eye- and face-protection regulations 29 CFR 1910.133 and European Standard EN166. Contact lenses are not eye protective devices. Appropriate eye protection must be worn instead of, or in conjunction with contact lenses.
Other Protective Clothing/Equipment: Additional protective clothing or equipment is not normally required. Provide eye bath and safety shower.
Comments: Never eat, drink, or smoke in work areas. Practice good personal hygiene after using this material, especially before eating, drinking, smoking, using the toilet, or applying cosmetics. Wash thoroughly after handling.

Section 9 - Physical and Chemical Properties

9.1 Information on basic physical and chemical properties:

Appearance : viscous liquid
Odor/Threshold: Mild to sweet odor
pH: N.A. (non-aqueous)
Melting Point/Freezing Point: N.A.
Low/High Boiling Point: N.A.
Flash Point: >300 °F
Evaporation Rate: Not available
Flammability: f.p. at or above 200 °F
UEL/LEL: Not available

Vapor Pressure: None (Polymeric Resin)
Vapor Density (Air=1): >1
Specific Gravity (H_2O=1, at 4 °C): 1.05-1.15
Water Solubility: Insoluble
Partition coefficient: Not available
Auto-ignition temperature: Not available
Decomposition temperature: Not available
Viscosity: 5,000 – 50,000 centipoise
% Volatile: Nil

Section 10 - Stability and Reactivity

10.1 Reactivity: No hazardous reactions if stored and handled as prescribed/indicated., No corrosive effect on metal. Not fire propagating.
10.2 Chemical stability: These products are stable at room temperature in closed containers under normal storage and handling conditions.
10.3 Possibility of hazardous reactions: Hazardous polymerization cannot occur.
10.4 Conditions to avoid: none known
10.5 Incompatible materials: strong bases and acids
10.6 Hazardous decomposition products: Thermal oxidative decomposition can produce carbon oxides, gasses/vapors, and traces of incompletely burned carbon compounds.

Section 11- Toxicological Information

11.1 Information on toxicological effects:
Skin Corrosion/Irritation: no data
Serious Eye Damage/Irritation: no data
Respiratory/Skin Sensitization: no data
Germ Cell Mutagenicity: no data
Carcinogenicity: No component of these products present at levels greater than or equal to 0.1% is identified as a carcinogen or potential carcinogen by IARC, ACGIH or NTP.
Reproductive Toxicity: no data
Specific Target Organ Toxicity – Single Exposure: no data
Specific Target Organ Toxicity – Repeated Exposure: no data
Aspiration Hazard: no data
Acute Toxicity: no data
Chronic Exposure: no data
Potential Health Effects – Miscellaneous: no data

Section 12 - Ecological Information

12.1 Toxicity: no data
12.2 Persistence and Degradability: no data
12.3 Bioaccumulative Potential: no data
12.4 Mobility in Soil: no data
12.5 Results of PBT and vPvB assessment: no data
12.6 Other Adverse Effects: no data

Section 13 - Disposal Considerations

13.1 Waste treatment methods: Under RCRA it is the responsibility of the user of the product to determine at the time of disposal whether the product meets RCRA criteria for hazardous waste. Waste management should be in full compliance with federal, state and local laws.
Empty containers retain product residue which may exhibit hazards of material, therefore to not pressurize, cut, glaze, weld or use for any other purposes. Return drums to reclamation centers for proper cleaning and reuse.

Section 14 - Transport Information

Not regulated by DOT, IATA or IMDG
14.1 UN number: none
14.2 UN proper shipping name: none
14.3 Transport hazard class(es): not applicable
14.4 Packing group: not applicable
14.5 Environmental hazards: none known
14.6 Special precautions for user: none known
14.7 Transport in bulk according to Annex II of MARPOL73/78 and the IBC Code: not applicable

Section 15 - Regulatory Information

15.1 Safety health and environmental regulations/legislation specific for the substance or mixture:
In the United States (EPA Regulations):
TSCA Inventory Status (40 CFR710): All components of this formulation are listed in the TSCA Inventory.
SARA 302 Components: No chemicals in this material are subject to the reporting requirements of SARA Title III, Section 302.
SARA 313 Components: No chemicals in this material are subject to the reporting requirements of SARA Title III, Section 313.
SARA 311/312 Hazards: none
California Proposition 65: This product does not intentionally contain any chemicals known to the state of California to cause cancer, birth defects or other reproductive harm.
15.2 Chemical safety assessment: No chemical safety assessment has been carried out for this substance/mixture by the supplier.

16 - Other Information

HMIS	
H	1
F	0
R	0

NFPA

Revision: 5
Date Prepared: January 4, 2017

Glossary: ACGIH-American Conference of Governmental Industrial Hygienists; ANSI-American National Standards Institute; Canadian TDG-Canadian Transportation of Dangerous Goods; CAS-Chemical Abstract Service; Chemtrec-Chemical Transportation Emergency Center (US); CHIP-Chemical Hazard Information and Packaging; DSL-Domestic Substances List; EC-Equivalent Concentration; EH40 (UK)-HSE Guidance Note EH40 Occupational Exposure Limits; EPCRA-Emergency Planning and Community Right-To-Know Act; ESL-Effects screening levels; GHS-Globally Harmonized System of Classification and Labelling of Chemicals; HMIS-Hazardous Material Information Service; IATA-International Air Transport Association; IMDG-International Maritime Dangerous Goods Code; LC-Lethal Concentration; LD-Lethal Dose; LEL-Lower Explosion Level; NFPA-National Fire Protection Association; OEL-Occupational Exposure Limit; OSHA-Occupational Safety and Health Administration, US Dept. of Labor; PEL-Permissible Exposure Limit; SARA (Title III)-Superfund Amendments and Reauthorization Act; SARA 313-Superfund Amendments and Reauthorization Act, Section 313; SCBA-Self-Contained Breathing Apparatus; STEL-Short Term Exposure Limit; TCEQ-Texas Commission on Environmental Quality; TLV-Threshold Limit Value; TSCA-Toxic Substances Control Act Public Law 94-469; TWA-Time Weighted Value; UEL-Upper Explosion Level; US DOT-US Department of Transportation; WHMIS-Workplace Hazardous Materials Information System.

Disclaimer: The information contained in this Safety Data Sheet (SDS) is considered accurate as of the version date. However, no warranty is expressed or implied regarding the accuracy of the data. Since the use of this product is not within the control of Smooth-On Inc., it is the user's obligation to determine the suitability of the product for its intended application and assumes all risk and liability for its safe use.

This SDS is prepared to comply with the Globally Harmonized System of Classification and Labelling of Chemicals (GHS) as prescribed by the United States (US) Occupational Safety and Health Administration (OSHA) Hazard Communication Standard (29 CFR 1910.1200), the Canadian Workplace Hazardous Materials Information System (WHMIS), and European Union Regulation (EC) No 1907/2006 of the European Parliament and of the Council of 18 December 2006 (REACH).

Classifications of the chemical in accordance with 29 CFR 1910.1200, signal word, hazard and precautionary statement(s), symbol(s) and other information are based on listed concentration of each hazardous ingredient. Unlisted ingredients are not "hazardous" per the OSHA Hazard Communication Standard (29 CFR 1910.1200), WHMIS and EC No 1907/2006 and are considered trade secrets under US Federal Law (29 CFR and 40 CFR), Canadian Law (Health Canada Legislation), and European Union Directives.

☑ GHS Compliant

Safety Data Sheet

SDS No. 823B

Section 1 - Identification

1.1 Product Identifier: Part B for: Body Double® & Body Double® SILK; Dragon Skin® Series & F/X Pro; Ecoflex® Series & Gel; Encapso® K; Equinox® Series; EZ Brush® Silicone; EZ-Spray® Silicone Series; Psycho Paint®; Mold Star® Series; OOMOO® Series; Rebound® Series; Rubber Glass®; Skin Tite®; Smooth-Sil® Series; Soma Foama® 15 and 25; Solaris®; SORTA-Clear® Series

1.2 General Use: Silicone Elastomer Crosslinker

1.3 Manufacturer: Smooth-On, Inc.,
5600 Lower Macungie Rd., Macungie, PA 18062
Phone (610) 252-5800, FAX (610) 252-6200
SDS@Smooth-On.com

Emergency Contact: Chem-Tel
Domestic: 800-255-3924 International: 813-248-0585

Section 2 – Hazard(s) Identification

2.1 Classification of the substance or mixture

Not a hazardous substance or mixture according to United States Occupational Safety and Health Administration (OSHA) Hazard Communication Standard (29 CFR 1910.1200), the Canadian Workplace Hazardous Materials Information System (WHMIS) and Regulation (EC) No 1272/2008 and subsequent amendments.

2.2 GHS Label elements, including precautionary statements

Pictogram(s): none

Signal word: none

General Precautions:

P101: If medical advice is needed, have product container or label at hand.
P102: Keep out of reach of children.
P103: Read label before use.

Hazards not otherwise classified (HNOC) or not covered by GHS - none

Section 3 - Composition / Information on Ingredients

3.1 Substances

No ingredients are hazardous according to Regulation 2012 OSHA Hazard Communication Standard 29 CFR 1910.1200 criteria.

Section 4 - First Aid Measures

4.1 Description of first aid measures

Inhalation: Remove source(s) of contamination and move victim to fresh air. If breathing has stopped, give artificial respiration, then oxygen if needed. Contact physician immediately.

Eye Contact: Flush eyes with plenty of water. If irritation persists, seek medical attention.

Skin Contact: In case of skin contact, wash thoroughly with soap and water.

Ingestion: Do not induce vomiting unless instructed by a physician. Never give anything by mouth to an unconscious person.

4.2 Most important symptoms and effects, both acute and delayed

None known.

4.3 After first aid, get appropriate in-plant, paramedic, or community medical support.

Section 5 - Fire-Fighting Measures

5.1 Extinguishing Media: Water Fog, Dry Chemical, and Carbon Dioxide Foam
5.2 Special hazards arising from the substance or mixture: None known.
5.3 Advice for firefighters: Use water spray to cool fire-exposed surfaces and to protect personnel. Shut off "fuel" to fire. If a leak or spill has not ignited, use water spray to disperse the vapors. Either allow fire to burn under controlled conditions or extinguish with foam or dry chemical. Try to cover liquid spills with foam. Because fire may produce toxic thermal decomposition products, wear a self-contained breathing apparatus (SCBA) with a full face piece operated in pressure demand or positive-pressure mode.

Section 6 - Accidental Release Measures

6.1 Personal precautions, protective equipment and emergency procedures: Only properly protected personnel should remain in the spill area; dike and contain spill. Stop or reduce discharge if it can be done safely.
6.2 Environmental precautions: No special environmental precautions required.
6.3 Methods and material for containment and cleaning up: absorb or scrape up excess into suitable container for disposal; wash area with dilute ammonia solution
6.4 Reference to other sections: if appropriate Sections 8 and 13 shall be referred to.

Section 7 - Handling and Storage

7.1 Precautions for safe handling: Use good general housekeeping procedures. Wash hands after use.
7.2 Conditions for safe storage, including any incompatibilities: Keep container(s) tightly closed and properly labeled. Store in cool, dry, well ventilated place away from heat, direct sunlight, strong oxidizers and any incompatibles. Store in approved containers and protect against physical damage. Keep containers securely sealed when not in use. Indoor storage should meet OSHA standards and appropriate fire codes. Containers that have been opened must be carefully resealed to prevent leakage. Empty containers retain residue and may be dangerous. Avoid water contamination.
7.3 Specific end use(s): These precautions are for room temperature handling. Other uses including elevated temperatures or aerosol/spray applications may require added precautions.

Section 8 - Exposure Controls / Personal Protection

8.1 Control parameters: none defined
8.2 Exposure controls:
Respiratory Protection: Should a respirator be needed, follow OSHA respirator regulations 29 CFR 1910.134 and European Standards EN 141, 143 and 371; wear an MSHA/NIOSH or European Standards EN 141, 143 and 371 approved respirators equipped with organic vapor cartridges.
Hand Protection: Wear any liquid-tight gloves such as butyl rubber, neoprene or PVC.
Eye Protection: Safety glasses with side shields per OSHA eye- and face-protection regulations 29 CFR 1910.133 and European Standard EN166. Contact lenses are not eye protective devices. Appropriate eye protection must be worn instead of, or in conjunction with contact lenses.
Other Protective Clothing/Equipment: Additional protective clothing or equipment is not normally required. Provide eye bath and safety shower.
Comments: Never eat, drink, or smoke in work areas. Practice good personal hygiene after using this material, especially before eating, drinking, smoking, using the toilet, or applying cosmetics. Wash thoroughly after handling.

Section 9 - Physical and Chemical Properties

9.1 Information on basic physical and chemical properties:

Appearance : viscous liquid
Odor/Threshold: Mild to sweet odor
pH: N.A. (non-aqueous)
Melting Point/Freezing Point: N.A.
Low/High Boiling Point: N.A.
Flash Point: >300 °F
Evaporation Rate: Not available
Flammability: f.p. at or above 200 °F
UEL/LEL: Not available

Vapor Pressure: None (Polymeric Resin)
Vapor Density (Air=1): >1
Specific Gravity (H_2O=1, at 4 °C): 1.07
Water Solubility: Insoluble
Partition coefficient: Not available
Auto-ignition temperature: Not available
Decomposition temperature: Not available
Viscosity: 5,000 – 50,000 centipoise
% Volatile: Nil

Section 10 - Stability and Reactivity

10.1 Reactivity: No hazardous reactions if stored and handled as prescribed/indicated., No corrosive effect on metal. Not fire propagating.
10.2 Chemical stability: These products are stable at room temperature in closed containers under normal storage and handling conditions.
10.3 Possibility of hazardous reactions: Hazardous polymerization cannot occur.
10.4 Conditions to avoid: none known
10.5 Incompatible materials: strong bases and acids
10.6 Hazardous decomposition products: Thermal oxidative decomposition can produce carbon oxides, gasses/vapors, and traces of incompletely burned carbon compounds.

Section 11- Toxicological Information

11.1 Information on toxicological effects:
Skin Corrosion/Irritation: no data
Serious Eye Damage/Irritation: no data
Respiratory/Skin Sensitization: no data
Germ Cell Mutagenicity: no data
Carcinogenicity: No component of these products present at levels greater than or equal to 0.1% is identified as a carcinogen or potential carcinogen by IARC, ACGIH or NTP.
Reproductive Toxicity: no data
Specific Target Organ Toxicity – Single Exposure: no data
Specific Target Organ Toxicity – Repeated Exposure: no data
Aspiration Hazard: no data
Acute Toxicity: no data
Chronic Exposure: no data
Potential Health Effects – Miscellaneous: no data

Section 12 - Ecological Information

12.1 Toxicity: no data
12.2 Persistence and Degradability: no data
12.3 Bioaccumulative Potential: no data
12.4 Mobility in Soil: no data
12.5 Results of PBT and vPvB assessment: no data
12.6 Other Adverse Effects: no data

Section 13 - Disposal Considerations

13.1 Waste treatment methods: Under RCRA it is the responsibility of the user of the product to determine at the time of disposal whether the product meets RCRA criteria for hazardous waste. Waste management should be in full compliance with federal, state and local laws.
Empty containers retain product residue which may exhibit hazards of material, therefore to not pressurize, cut, glaze, weld or use for any other purposes. Return drums to reclamation centers for proper cleaning and reuse.

Section 14 - Transport Information

Not regulated by DOT, IATA or IMDG
14.1 UN number: none
14.2 UN proper shipping name: none
14.3 Transport hazard class(es): not applicable
14.4 Packing group: not applicable
14.5 Environmental hazards: none known
14.6 Special precautions for user: none known
14.7 Transport in bulk according to Annex II of MARPOL73/78 and the IBC Code: not applicable

Section 15 - Regulatory Information

15.1 Safety health and environmental regulations/legislation specific for the substance or mixture:
In the United States (EPA Regulations):
TSCA Inventory Status (40 CFR710): All components of this formulation are listed in the TSCA Inventory.
SARA 302 Components: No chemicals in this material are subject to the reporting requirements of SARA Title III, Section 302.
SARA 313 Components: No chemicals in this material are subject to the reporting requirements of SARA Title III, Section 313.
SARA 311/312 Hazards: none
California Proposition 65: This product does not intentionally contain any chemicals known to the state of California to cause cancer, birth defects or other reproductive harm.
15.2 Chemical safety assessment: No chemical safety assessment has been carried out for this substance/mixture by the supplier.

16 - Other Information

HMIS	
H	1
F	0
R	0

NFPA

Revision: 6
Date Prepared: January 4, 2017

Glossary: ACGIH-American Conference of Governmental Industrial Hygienists; ANSI-American National Standards Institute; Canadian TDG-Canadian Transportation of Dangerous Goods; CAS-Chemical Abstract Service; Chemtrec-Chemical Transportation Emergency Center (US); CHIP-Chemical Hazard Information and Packaging; DSL-Domestic Substances List; EC-Equivalent Concentration; EH40 (UK)-HSE Guidance Note EH40 Occupational Exposure Limits; EPCRA-Emergency Planning and Community Right-To-Know Act; ESL-Effects screening levels; GHS-Globally Harmonized System of Classification and Labelling of Chemicals; HMIS-Hazardous Material Information Service; IATA-International Air Transport Association; IMDG-International Maritime Dangerous Goods Code; LC-Lethal Concentration; LD-Lethal Dose; LEL-Lower Explosion Level; NFPA-National Fire Protection Association; OEL-Occupational Exposure Limit; OSHA-Occupational Safety and Health Administration, US Dept. of Labor; PEL-Permissible Exposure Limit; SARA (Title III)-Superfund Amendments and Reauthorization Act; SARA 313-Superfund Amendments and Reauthorization Act, Section 313; SCBA-Self-Contained Breathing Apparatus; STEL-Short Term Exposure Limit; TCEQ-Texas Commission on Environmental Quality; TLV-Threshold Limit Value; TSCA-Toxic Substances Control Act Public Law 94-469; TWA-Time Weighted Value; UEL-Upper Explosion Level; US DOT-US Department of Transportation; WHMIS-Workplace Hazardous Materials Information System.

Disclaimer: The information contained in this Safety Data Sheet (SDS) is considered accurate as of the version date. However, no warranty is expressed or implied regarding the accuracy of the data. Since the use of this product is not within the control of Smooth-On Inc., it is the user's obligation to determine the suitability of the product for its intended application and assumes all risk and liability for its safe use.

This SDS is prepared to comply with the Globally Harmonized System of Classification and Labelling of Chemicals (GHS) as prescribed by the United States (US) Occupational Safety and Health Administration (OSHA) Hazard Communication Standard (29 CFR 1910.1200), the Canadian Workplace Hazardous Materials Information System (WHMIS), and European Union Regulation (EC) No 1907/2006 of the European Parliament and of the Council of 18 December 2006 (REACH).

Classifications of the chemical in accordance with 29 CFR 1910.1200, signal word, hazard and precautionary statement(s), symbol(s) and other information are based on listed concentration of each hazardous ingredient. Unlisted ingredients are not "hazardous" per the OSHA Hazard Communication Standard (29 CFR 1910.1200), WHMIS and EC No 1907/2006 and are considered trade secrets under US Federal Law (29 CFR and 40 CFR), Canadian Law (Health Canada Legislation), and European Union Directives.

ANNEXURE E

Mixing method for Encapso K:

Two clear liquids (part A and B) are mixed in equal amounts (parts) after vigorously shaking to mix each one separately before commencing with the mixing of the two liquids. Mix for at least 5minutes, making sure that all is blended especially against the sides of the container. The mixture at first appears to be cloudy but will clear after a few minutes. Please see Addendum D for Specifications and Manual of Encapso K.


Figure Mixing equal amounts of Encapso K Part A and B

Due to the viscosity of the liquid, it is important to fixate all parts (ribcage and lungs) in relation to the thorax as per anatomy.

The opening was at the inferior part of the thorax; therefore, all organs or parts was suspended upside down. The ribcage was fastened with fishline at multiple points due to the ribcage being fragile and not only one point can be used as fixation. The lung shells were also fixed with fishline and could be manoeuvred as with a puppet to have tilt and angle correct in the ribcage. For weight support in the 'liquid' and that the air lung cavities do not stay afloat, thick wooden

sticks were propped inside the cavities to weigh it down when the liquid is poured and curing sets in place over a period of at least 16hours or overnight preferably.

Figure (a-c) Fix thorax shell upside down (d) fish line tied to multiple parts of ribcage




Figure (a-d) Ribcage suspended in shell

(a)

(b)

Figure (a+b) lung cavities within ribcage hanging upside down (c) Weight bearing down in lung cavities to not float in liquid

As soon as all the parts were in a satisfactory position according to anatomy of the thorax, the pouring process started. A funnel with a pipe extending into the 'bottom' of the thorax shell is used to pour the liquid into the body shell. Unfortunately, as the liquid poured into the shell, where the body shell was not sealed properly due to misfit of 2 halves explained earlier, leakage was a huge problem. The pouring process was stopped immediately to first not waste any more of the rubber liquid and secondly find a solution to seal all openings.

Figure Pouring of Encapso K into thorax shell
Video clips pouring (2019-03-13-11-48-10+54)

Plaster of paris was wrapped around the thorax shell and plastic tied down 'tightly' with tape around the plaster of paris. One part of the mixture was again poured into the thorax shell and monitored for more leakage throughout the day. At the end of the day, curing started to take place and the thorax was filled to just under the edge of the lung cavities as these need to stay clear of any mixture and only air filled. Another consideration was to ensure that the ribs are as far as possibly enclosed or completely covered with the rubber compound to minimise breakage or breaking off of any ribs or part thereof at the inferior part of the ribcage. Due to the position of the lung cavities in relation to the ribcage a small part of the ribcage was left

open and not covered by the rubber compound. Care should be taken when handling the phantom.

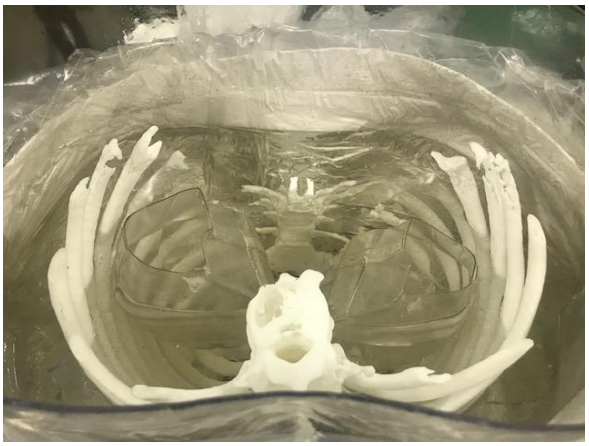

(a) (b)

Figure (a) Plaster of Paris was wrapped around the thorax shell (b) pouring to bottom of lung cavities

After overnight curing the phantom was set and the plaster of paris and plastic removed. The phantom was cleaned of any rubber at the outside of the shell and all the fish line was removed.

Figure Completed thorax phantom

ANNEXURE F

Measurements with Farmer chamber:						
Chamber with only perspex - 5cm						
100MU						
0.6cc						
95.0cm SSD	100cm SAD					
	6MV			**10MV**		
	10x10	**5x5**		**10x10**	**5x5**	
	0.9525	0.8912		0.9923	0.9349	
	0.9537	0.8904		0.9924	0.9350	
	0.9531	**0.8908**	Avg	**0.99235**	**0.93495**	Avg
With only Silicon						
100MU						
0.6cc						
89.0cm SSD	100cm SAD					
	6MV			**10MV**		
	10x10	**5x5**		**10x10**	**5x5**	
	0.7831	0.7036		0.8461	0.7734	
	0.7829	0.7032		0.846	0.7729	
	0.7830	**0.7034**	Avg	**0.8461**	**0.7732**	Avg
With 3D prints						
embedded						
100MU						
0.6cc						
89.0cm SSD	100cm SAD					
	6MV			**10MV**		
	10x10	**5x5**		**10x10**	**5x5**	
	0.7427	0.663		0.8079	0.7357	
	0.7425	0.6635		0.8078	0.7356	
	0.7426	**0.6633**	Avg	**0.8079**	**0.7357**	Avg

ANNEXURE G

0.3mm Calculation grid size was used:

Monaco TPS (Version 5.11.02)						
Calculation Dose to water						
	6MV			**10MV**		
	10x10	**5x5**		**10x10**	**5x5**	
	Gy	Gy		Gy	Gy	
Perspex	0.919	0.859		0.973	0.917	
With only Silicon	0.739	0.667		0.825	0.750	
With 3D prints	0.699	0.619		0.781	0.713	
embedded						
Transmission S	0.8041	0.7765		0.8479	0.8179	
Transmission 3D	0.7606	0.7206		0.8027	0.7775	
Attenuation coefficient and stopping power ratios are taken as those for water						

Monaco TPS (Version 5.11.02)							
Calculation Dose to medium							
	6MV			**10MV**			
	10x10	**5x5**		**10x10**	**5x5**		
	Gy	Gy		Gy	Gy		
Perspex	0.900	0.841		0.952	0.898		
With only Silicon	0.724	0.653		0.808	0.735		
With 3D prints	0.684	0.606		0.764	0.699		
embedded							
Transmission S	0.8044	0.7765		0.8487	0.8185		
Transmission 3D	0.7600	0.7206		0.8025	0.7784		
Attenuation coefficient and stopping power ratios are taken as those for in the medium							

0.25mm Calculation grid size was used:

Eclipse Version 15.6, AAA Algorithm						
	6MV			**10MV**		
	10x10	**5x5**		**10x10**	**5x5**	
	Gy	Gy		Gy	Gy	
Perspex	0.917	0.862		0.962	0.901	
With only Silicon	0.769	0.696		0.839	0.762	
With 3D prints	0.694	0.621		0.763	0.694	
embedded						
Transmission S	0.8386	0.8074		0.8721	0.8457	
Transmission 3D	0.7568	0.7204		0.7931	0.7703	
The Calibration curve of the CT scanner is used to convert the Hounsfield Unit						
value to relative electron density						

Eclipse Version 15.6, Acuros Algorithm						
Calculation Dose to water						
	6MV			**10MV**		
	10x10	**5x5**		**10x10**	**5x5**	
	Gy	Gy		Gy	Gy	
Perspex	0.917	0.87		0.962	0.909	
With only Silicon	0.775	0.7		0.839	0.767	
With 3D prints	0.709	0.637		0.787	0.719	
embedded						
Transmission S	0.8451	0.8046		0.8721	0.8438	
Transmission 3D	0.7732	0.7322		0.8181	0.7910	
The Calibration curve of the CT scanner is used to convert the Hounsfield						
Unit values to mass density						
From the derived mass density, Acuros XB determine the material composition						
of voxels in the image						

Eclipse Version 15.6, Acuros Algorithm						
Calculation Dose to medium						
	6MV			**10MV**		
	10x10	**5x5**		**10x10**	**5x5**	
	Gy	Gy		Gy	Gy	
Perspex	0.893	0.847		0.943	0.885	
With only Silicon	0.758	0.686		0.819	0.745	
With 3D prints	0.690	0.621		0.769	0.699	
embedded						
Transmssion S	0.8488	0.8099		0.8685	0.8418	
Transmission 3D	0.7727	0.7332		0.8155	0.7898	
The Calibration curve of the CT scanner is used to convert the Hounsfield						
Unit values to mass density						
From the derived mass density, Acuros XB determine the material composition						
of voxels in the image						